Core-Shell Particles and their Application for Superhydrophobic Surfaces

Dissertation

Zur Erlangung des Grades

“Doktor der Naturwissenschaften“

Im Promotionsfach Physikalische Chemie

Der Johannes Gutenberg-Universität Mainz

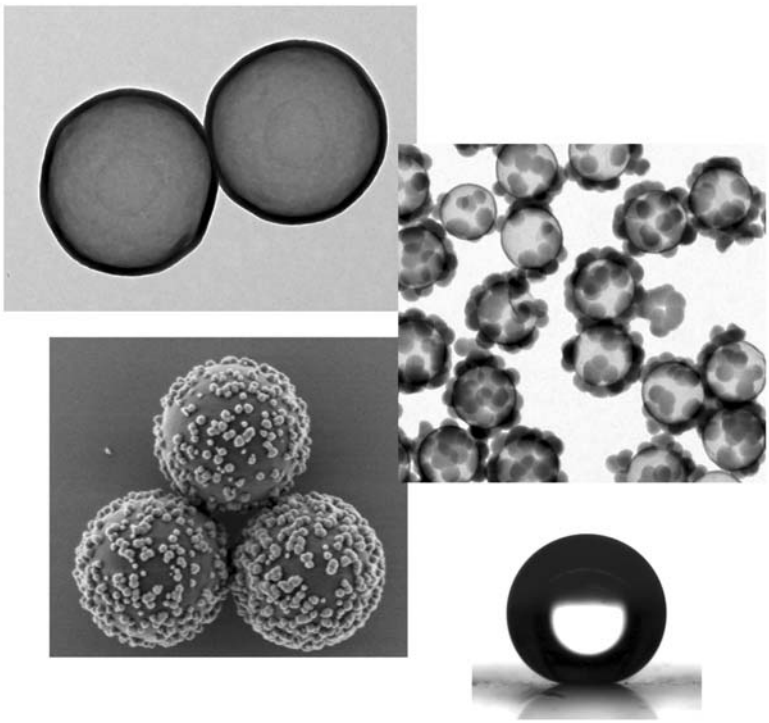

Maria D'Acunzi

Geboren in Nocera Inferiore (Salerno, Italy)

Mainz, 2010

Die vorliegende Arbeit wurde am Max-Planck-Institut für Polymerforschung in Mainz unter der Betreuung von Dr. Doris Vollmer in der Zeit von Mai 2007 bis April 2010 angefertigt.

Dekan: **Prof. Dr. Wolfgang Hofmeister**

1. Berichterstatter: PD Dr. Doris Vollmer
2. Berichterstatter: Prof. Dr. Manfred Schmidt

Tag der mündlichen Prüfung: 28/06/2010

Table of Contents:

Abbreviations:

AA	acrylic acid
AFM	atomic force microscope
APS	3-aminopropyltriethoxysilane
CLSM	confocal laser scanning microscopy
CVD	chemical vapor deposition
LS	light scattering
µm	micrometer
nm	nanometer
NMR	nuclear magnetic resonance
PAA	poly(acrylic acid)
PAH	poly(allylamine hydrochloride)
par.	paragraph
PS	polystyrene
PTEF	polytetrafluoroethylene
PVP	polyvinylpyrrolidone
rpm	round per minutes
SEM	scanning electron microscopy
TEM	transmission electron microscopy
THF	tetrahydrofuran

Abstract

During the last years great effort has been devoted to the fabrication of superhydrophobic surfaces because of their self-cleaning properties. A water drop on a superhydrophobic surface rolls off even at inclinations of only a few degrees while taking up contaminants encountered on its way.

Superhydrophobic, self-cleaning coatings are desirable for convenient and cost-effective maintenance of a variety of surfaces. Ideally, such coatings should be easy to make and apply, mechanically resistant, and long-term stable. None of the existing methods have yet mastered the challenge of meeting all of these criteria.

Superhydrophobicity is associated with surface roughness. The lotus leave, with its dual scale roughness, is one of the most efficient examples of superhydrophobic surface. This thesis work proposes a novel technique to prepare superhydrophobic surfaces that introduces the two length scale roughness by growing silica particles (~100 nm in diameter) onto micrometer-sized polystyrene particles using the well-established Stöber synthesis. Mechanical resistance is conferred to the resulting “raspberries” by the synthesis of a thin silica shell on their surface. Besides of being easy to make and handle, these particles offer the possibility for improving suitability or technical applications: since they disperse in water, multi-layers can be prepared on substrates by simple drop casting even on surfaces with grooves and slots. The solution of the main problem – stabilizing the multilayer – also lies in the design of the particles: the shells – although mechanically stable – are porous enough to allow for leakage of polystyrene from the core. Under tetrahydrofuran vapor polystyrene bridges form between the particles that render the multilayer-film stable.

Multi-layers are good candidate to design surfaces whose roughness is preserved after scratch. If the top-most layer is removed, the roughness can still be ensured by the underlying layer.

After hydrophobization by chemical vapor deposition (CVD) of a semi-fluorinated silane, the surfaces are superhydrophobic with a tilting angle of a few degrees.

1 State of the art of superhydrophobicity and thesis motivation

This chapter is intended to give an overview on the state of the art of superhydrophobicity in general and to motivate this thesis work in the light of the present status of research. It starts with the basic definitions, followed by a summary of the recent efforts in the basic understanding of superhydrophobicity. The next section is dedicated to the design of new experimental procedures to develop superhydrophobic surfaces. Special attention is given to the development of superhydrophobic surfaces by colloid assembly.

1.1 Wetting behaviour of a surface

The wetting behaviour of a surface can be experimentally characterized by the value of the contact angle of a liquid drop deposited on it.

In case of water drops (Figure 1.1), a surface is commonly defined as hydrophilic when the contact angle is lower than 90°. The extreme limit of hydrophilicity is complete wetting; water forms a film on the surface and the contact angle is zero.

When the contact angle is higher than 90°, the surface is called hydrophobic. The extreme limit of hydrophobicity is complete drying; the water drop remains spherical on the surface without any contact and the corresponding contact angle is 180˚.

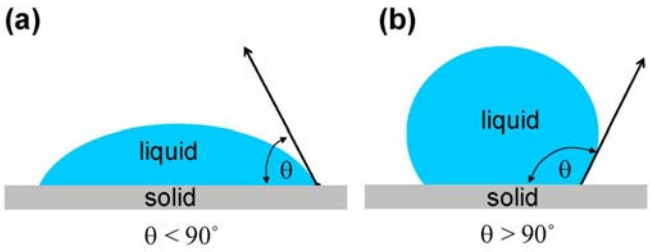

Figure 1.1. Contact angle of a water drop on a hydrophilic (a), and on a hydrophobic surface (b).

1.1.1 Smooth surface

For a smooth surface, the contact angle of a liquid drop on a solid surface in thermodynamic equilibrium can be calculated theoretically by the Young's equation[1]:

$$\gamma_{LV}\cos\theta = \gamma_{SV} - \gamma_{SL} \qquad (1)$$

where γ_{SV}, γ_{SL} and γ_{LV} are the solid-vapour, solid-liquid and liquid-vapour interfacial tensions, respectively. The three-phase contact line is schematically illustrated in Figure 1.2.

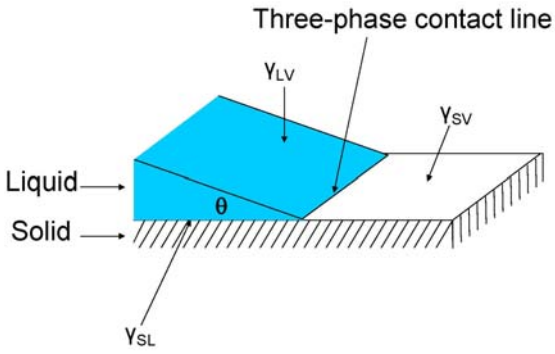

Figure 1.2. Sketch of the three phase contact line at the rim of a water drop on a solid surface (Image reproduced from ref[2]).

The wettability depends on the chemical nature of the two components.

If the interfacial tension of the solid-vapour interface is higher than that of the solid-liquid interface ($\gamma_{SV} > \gamma_{SL}$), the right side of the Young equation is positive. As a consequence, $\cos\theta$ is also positive, corresponding to a contact angle between 0 and 90°; the surface is hydrophilic.

When the right side of the Young equation is negative ($\gamma_{SV} < \gamma_{SL}$), $\cos\theta$ is negative; this corresponds to a contact angle higher than 90°and the surface is hydrophobic.

Here, the derivation of the Young's equation[2] is omitted, but it is important to point out that it can be obtained by mere energetic balances. In short, the change of the Gibbs free energy (ΔG) for a drop which moves by an infinitesimal amount can be expressed as a function of its geometrical parameters and the solid-liquid, liquid-gas and solid-gas interfacial tensions before and after the infinitesimal movement. By imposing the condition of thermodynamic equilibrium ($\Delta G = 0$), equation (1) is obtained.

In the case of smooth surfaces, the highest contact angle experimentally reported so far is about 120° for fluorinated materials[3].

1.1.2 Rough surface: Wenzel's and Cassie's models

The situation changes dramatically when the surface is textured. The contact angle can exceed the value of 150° and, as already mentioned, in some cases the drop can roll off the surface at small tilting angles.

The fact that roughness can strongly affect the wetting of a surface was already observed a long time ago. The first model to describe this phenomenon was proposed by Wenzel in 1936[4] and extended by Cassie and Baxter in 1944[5].

- Wenzel's model

Wenzel described the wettability of a rough surface compared to a smooth surface with the same chemical composition.

He considered the case of a drop deposited on a surface when water penetrates the asperities (Figure 1.3).

Then the contact angle on a rough surface (θ_0) is given by the following equation:

$$\cos \theta_0 = r \cos \theta \qquad (2)$$

where θ is the contact angle of the corresponding smooth surface obtained by the Young equation, and r is the roughness factor. Roughness factor is the ratio between the actual surface area beneath the drop and the geometric area (solid-liquid contact area in the assumption of smooth surface). The roughness factor is always bigger than 1 in case of surfaces with asperities, and it is equal to 1 when the surface is smooth (in this case the Wenzel angle coincides with the Young angle).

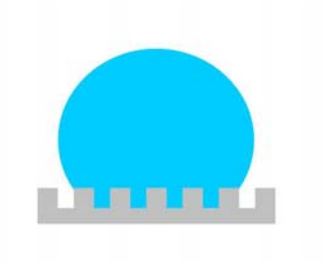

Figure 1.3. Sketch of a water drop on a rough surface in case water penetrates the asperities (Wenzel model).

Wenzel proposed this equation by simply assuming that wetting is a thermodynamic process. *" It is only necessary to apply the fact that, within a measured unit area on a rough surface, there is actually more surface, and in that sense therefore a greater intensity of surface energy, than in the same measured unit area on a smooth surface"*[4].

The influence of the increased solid-liquid contact area is given by the roughness factor. So, roughness increases both hydrophilicity and hydrophobicity.

For a given hydrophilic surface (CA ‹ 90°), a rough surface has a lower contact angle than the corresponding smooth one.
If we consider a hydrophobic surface (CA › 90°), the contact angle of a rough surface is higher than the corresponding smooth one.

- Cassie's Model

With the same thermodynamic argument, Cassie proposed an extension of Wenzel's model to a composite surface. If we consider, for example, a surface composed of two different materials, the apparent contact angle can be predicted by keeping into account the contributions of the fractional areas of the two materials:

$$\cos\theta_c = f_1\cos\theta_1 + f_2\cos\theta_2 \qquad (3)$$

where θ_C is the apparent CA, f_1 and f_2 the surface fractions of materials 1 and 2, respectively; θ_1 and θ_2 the contact angles given by the Young equation for material 1 and material 2, respectively.
This equation can represent the case of a drop suspended on a rough surface, in which the liquid does not penetrate the asperities (Figure 1.4).
In fact, this configuration can be seen as a composite material in which the second component is the air trapped in the asperities.
Since $\theta_2 = 180°$ for air [$\cos(180^\circ) = -1$] and $f_2 = (1 - f_1)$, equation 3 becomes:

$$\cos\theta_c = f(1+\cos\theta_0) - 1 \qquad (4)$$

where $f \equiv f_1$ is the solid fraction and $\theta \equiv \theta_1$.
For very small value of *f*, the contact angle approaches 180°. It only depends on the solid fraction for a given surface with Young angle θ.

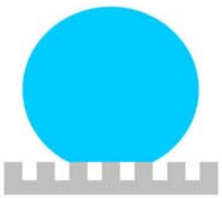

Figure 1.4. A water drop suspended on a rough surface, with air trapped between the water and the asperities (Cassie model).

1.1.3 Contact angle hysteresis

Both Young's and Cassie/Wenzel's models predict one contact angle for a given material and surface topography. In case of real surfaces, the measured value of the contact angle depends on the method of deposition of the drop on the surface, time scales etc. This phenomenon is known as contact angle hysteresis and can easily be seen and quantified by performing a "dynamic contact angle" measurement. It consists of measuring the contact angle while the drop volume is increasing; in practice the value just before the contact line starts to advance is called advancing contact angle θ_A. Then the contact angle is measured while the drop volume is decreasing; the angle just before the contact line starts to recede is called receding contact angle θ_R. In general θ_A is higher than θ_R and the difference between these two values is called contact angle hysteresis.

Hysteresis can also be visualized by tilting the plane where the drop is deposited.

Let us consider a drop on a smooth surface with a given contact angle θ. If the surface is tilted, typically the right and left contact angles slightly change as illustrated in Figure 1.5.

One contact angle becomes smaller (receding, θ_R) and the other one larger (advancing, θ_A) than the Young angle. Hysteresis is generally attributed to the pinning of the contact line due to chemical and/or geometrical heterogeneities.

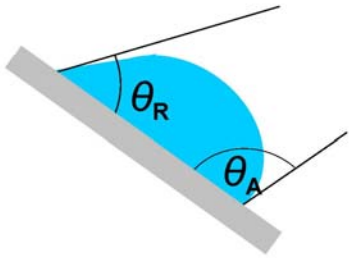

Figure 1.5. Representation of advancing (θ_A) and receding (θ_R) contact angles by tilting the plane where the drop is deposited.

In the case of textured surfaces, the roll-off of the water drop depends on the contact angle hysteresis.

For drops in Wenzel's state, hysteresis is generally high (it can be > 30˚) and no roll-off is seen.

Due to the low surface contact for drops in Cassie state, hysteresis can be as low as few degrees (< 10˚) and the roll-off happens at small tilting angles.

1.2 The last 10 year's "boom"

The idea that surface roughness modifies the wettability of a solid surface is not a recent discovery. What is new instead is the interest of the scientific community in this topic. The attention increased considerably when Shibuichi et al[6, 7], from the Kao Corporation in Japan, published 2 papers in which they described that high contact angles can be obtained on rough fluorinated surfaces. They compared the contact angle θ of a smooth fluorinated surface with the contact angle θ* of a rough surface with the same chemical composition. In order to obtain different values of θ, they used liquids with different affinity for the surface.
They plotted the values of cos θ* versus cos θ in order to deduce the influence of surface roughness on the contact angle. The graph so obtained is shown in Figure 1.6.

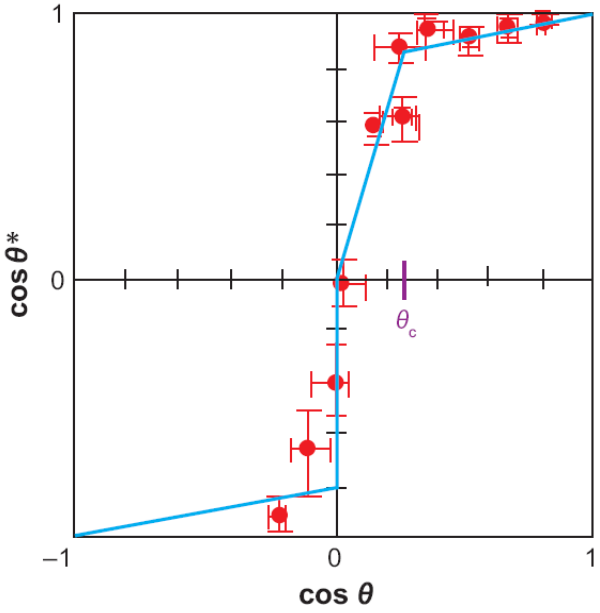

Figure 1.6. Plot of the contact angle θ of a fluorinated smooth surface versus the contact angle θ* of the surface with the same chemical composition but rough morphology (image taken from ref. [3]).

In the hydrophilic regime (cos θ > 0) it is possible to see two linear dependences with different slopes. For $\theta \geq \theta_c$, the surface roughness increases strongly the hydrophilicity. This effect can be explained with the Wenzel's model. For $\theta < \theta_c$ the effect is less pronounced; for very hydrophilic material with contact angle tending toward zero, the influence of the surface roughness is very small.
In the hydrophobic regime it was not possible (on the smooth surface) to go beyond cos θ = -0.3 that corresponds to a contact angle of 110° for a water drop (the highest contact angle

reported on a smooth surface is 120° for water on a smooth surface[3]). Nevertheless, the effect of roughness on the contact angle is impressive.

For contact angles θ on the smooth surface in the range from 90° to 110°, it was possible to obtain contact angles for the corresponding rough surface θ^* as large as 170°.

The resonance of this work was amplified by the publications of Bartlett and Neinhuis [8, 9] who systematically investigated the correlation between surface morphology and wettability for a large number of plant leaves.

They showed by scanning electron microscopy that leaves with rough surface, especially those showing hierarchical structures with micro- and nano- asperities, possess the property of water repellence and self-cleaning.

Since then, the number of papers published on superhydrophobicity has increased enormously. The contributions space from fundamental understanding to new procedures for developing superhydrophobic materials.

Experiments aimed for fundamental understanding were also encouraged by the development of very sensitive lithographic techniques[10-12], suitable for the preparation of hydrophobic surfaces with regular patterns at micrometer scale. The roughness on these surfaces can be calculated precisely by means of geometrical relations, giving the possibility to compare the predicted contact angles with the experimental ones.

Despite the widespread interest, there are still several unresolved questions.

One of the open issues is how to predict the wetting behaviour given a certain surface roughness.

In fact, both Wenzel and Cassie's models present some limitations.

Wenzel's equation, for example, is not fulfilled in the whole range of possible Young angles as shown in the experiments of Shibuiki et al.[6, 7] (Figure 1.6).

Wenzel and Cassie's equations only predict one contact angle, i.e. they do not take the contact angle hysteresis into account (par. 1.1.3).

Furthermore, Cassie and Wenzel's equations are derived by means of thermodynamic assumptions and the contact angle they predict should be "the most stable". Nevertheless it has been found that drops in Cassie state can switch to Wenzel state if energy is supplied by pressing the drop[13] or by an impact [14] (i.e. depositing it from a given height), with consequent reduction of the contact angle and increase in hysteresis. This has been explained by assuming that drops in Cassie state are often metastable[15] and the system switches to the energetically more favoured Wenzel state if energy is delivered.

Recently, McCarthy et al. questioned the whole thermodynamic approach which had so far been largely accepted. They reported experimental results which demonstrated that the contact angle is determined by the surface properties in the close vicinity of the three phase contact line and not on the contact area beneath the drop[16, 17].

In short, by means of lithography they prepared “special” textured surfaces (Figure 1.7): a hydrophilic spot in a hydrophobic field (a), a rough spot in a smooth field (both hydrophobized, b) and a smooth spot in a rough field (both hydrophobized, c). Then, they measured the contact angle within and outside the spot and found that its value only depends on the area in close proximity of the contact line. For example, the contact angle for a drop with a contact area larger than the smooth spot in Figure 1.7c gave contact angles θ_A/θ_R = 167/132. These are identical to those obtained on a completely rough surface.

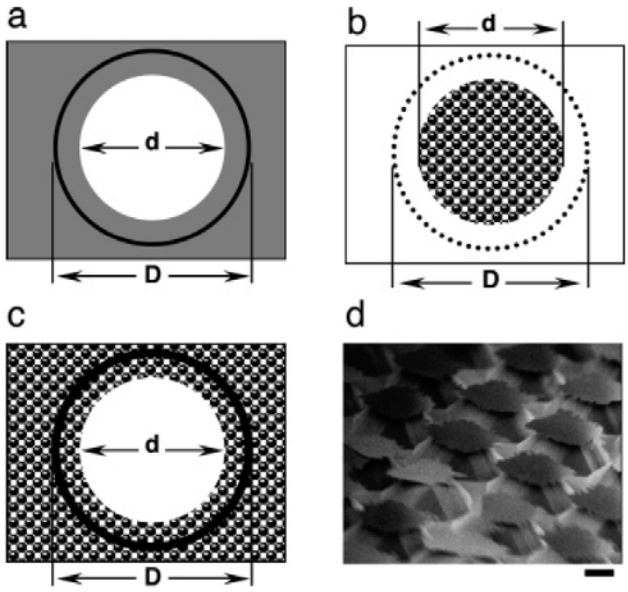

Figure 1.7. Illustration of (**a**) a hydrophilic spot in a hydrophobic field, (**b**) a rough spot in a smooth field, and (**c**) a smooth spot in a rough field. (**d**) SEM indicating the topography of the rough regions in **b** and **c**. The scale bar in **d** is 10 µm (image taken from ref.[16]).

The independence of θ on the contact area beneath the drop can also be visualized by frames taken from movies (Figure 1.8) of a drop advancing on the above illustrated spots (Figure 1.7b and c). For a drop advancing from a rough spot onto a smooth field (Figure 1.7b) the drop shows a high contact angle within the spot (Figure 1.8, 1a-d). It immediately decreases when the contact line reaches the smooth field (Figure 1.8-1e-f). The same behaviour is found for a smooth spot in a rough field (Figure 1.7c). The contact angle increases abruptly as the contact line exceeds the smooth spot (Figure 1.8-2c-f). These results are in disagreement with the values of contact angles predicted by the Cassie equation.

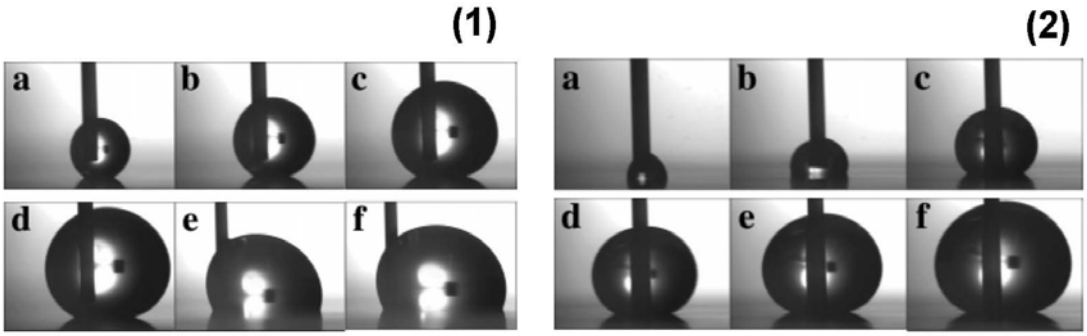

Figure 1.8. Selected frames of a videotape of a drop advancing from a rough spot onto a smooth field (1) and frames of a videotape of a drop advancing from a smooth spot onto a rough field (images taken from ref.[16].

Mc Carthy et al. concluded that the surface topography and its chemical composition in proximity of the contact line and not over the liquid-solid interfacial area control the contact angle.

In summary, the issue of predicting the contact angle is still open and under discussion.

The thermodynamic models do not give an adequate description of the wetting phenomena and values of the contact angles predicted are often only qualitative.

The contact line approach seems to be consistent with the experimental observation but it does not provide any equation able to predict the wetting behavior of a given surface.

1.3 Experimental approaches to get superhydrophobic surfaces

Many methods have been proposed to build up superhydrophobic surfaces[18, 19], like lithography [10-12], electrochemical deposition [20, 21], chemical deposition [22, 23], plasma etching [24, 25], sol-gel methods [26, 27], layer by layer (LbL) deposition [28, 29], templating [30] etc.

So far, the methods listed offer some advantages as well as limitations. Lithography, for example, produces well defined patterns. Sol-gel processing are good candidates for the fabrication of transparent coatings. Electrochemical methods and LbL deposition are effective in the coating of surfaces with shapes other than planar. Unfortunately, most of these approaches are still limited to laboratory research because they do not satisfy all the requirements for large scale production, such as easy and low-cost fabrication, large scale homogeneity and mechanical and thermal stability.

Independently of the technique used, one of the most popular approaches is mimicking the morphology of the lotus leaf. The double size roughness present on its surface is believed to

be the main reason of its extraordinary hydrophobicity. This hierarchical structure is visible in the SEM images shown in Figure 1.9.

The surface of the lotus leaf is formed by a regular pattern of micrometer sized hills (Figure 1.9a). This structure is not smooth but it shows further nano sized asperities from which a hydrophobic wax is excreted (Figure 1.9b).

Such a wax has a contact angle for the smooth surface of about 110° and the combination of its hydrophobicity and the rough structure confers the superhydrophobic behavior to the leaf.

Among the various approaches to mimic the lotus leaf morphology, layer by layer (LbL) deposition, colloid assembly and the combination of the two have been reported. These approaches have also been followed in this thesis work.

Layer-by-layer assembly of oppositely charged polyelectrolytes is a well established method[31] to coat surfaces with an organic thin film with controllable thickness at molecular level. The idea behind it is to make use of the electrostatic attraction between negatively and positively charged polyelectrolytes. The preparation is also easy. It consists of subsequent coating steps by alternate dipping of the substrate in water solutions of oppositely charged polyelectrolytes.

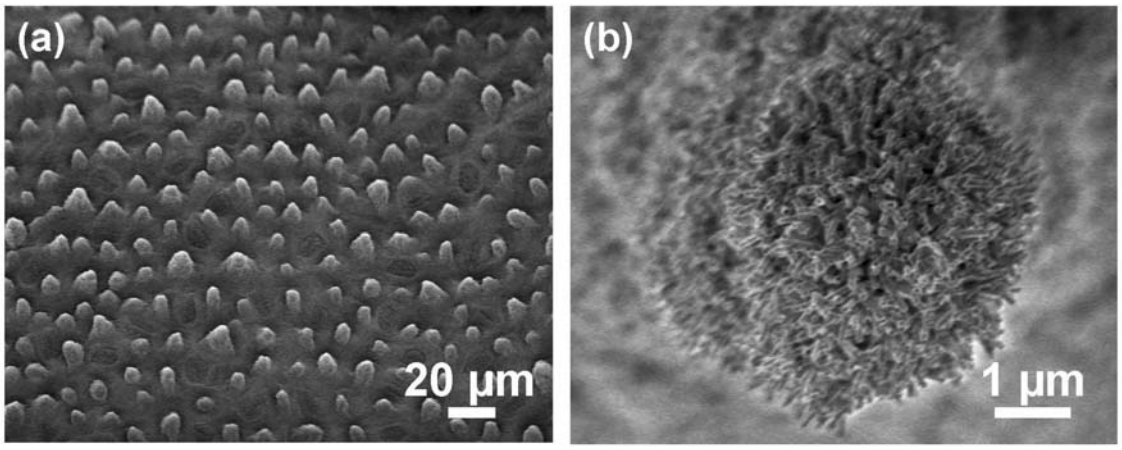

Figure 1.9. SEM images of lotus leaf surface at different magnifications. At lower magnification the micrometer size roughness is visible (a) whereas the image at higher magnification highlights the nano sized asperities. (The lotus leaf was kindly provided by the Botanical garden of Mainz University).

By means of this technique, different kinds of surfaces for different purposes have been successfully coated. One example is the coating of colloids[32-34]; after the removal of the cores by dissolution it is possible to obtain polyelectrolyte capsules.

Besides of that, layer by layer assembly has been proposed as a valid alternative to prepare superhydrophobic coatings.

In 2004 Rubner[28] and co-workers managed to mimic the lotus leaf topography by polyelectrolyte multilayers. They assembled a film of poly(allylamine hydrochloride) (PAH) and poly(acrylic acid) and immersed it in a low pH solution to get porous structures at micrometer level. After thermal treatment at 180˚ to improve the mechanical resistance of the film, they deposited two layers of 50 nm silica nanoparticles following the same principle as the polyelectrolyte deposition. The difference was in the substitution of the negative layer of poly(acrylic acid) with silica nanoparticles. After hydrophobization with chemical vapor deposition of a semifluorinated silane, they report advancing contact angle for water drops of 172˚ and a tilting angle of 2˚.

In 2007 Rubner et al. [29] also reported the preparation of transparent superhydrophobic coatings by assembling silica nanoparticles and poly(allylamine hydrochloride). The desired roughness was obtained by depositing alternating layers of nanoparticles of different size (50 and 20 nm). The disadvantage of this approach is the poor mechanical stability. Particles are assembled together only by electrostatic interactions at the points where they are in contact.

Recently, it has been shown that raspberry-like particles are suitable to make superhydrophobic surfaces[35-37]. Mimicking the lotus leaf structure, the overall diameter of the raspberry particles is in the 1 μm range, while the surface roughness is in the order of 20-100 nm (Figure 1.10).

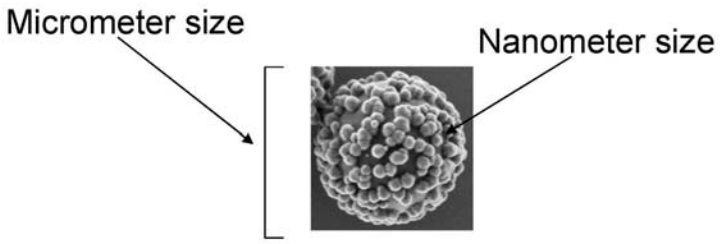

Figure 1.10. SEM image of a raspberry-like particle with emphasis on its double-scale size.

Ming et al.[35] reported a procedure to get superhydrophobic surfaces by covalently binding a monolayer of silica raspberry particles to an epoxy-based polymer matrix. The monolayer was partially embedded in the polymer matrix by a film forming reaction to improve the mechanical properties of the surface. However, the whole procedure was complicated and time-consuming. They prepared amino-functionalized silica nanoparticles and epoxy-functionalized silica microparticles and performed a reaction between them to obtain the raspberry morphology. Furthermore, the procedure was limited to only one layer of particles.

In 2007 Lee[36] and co-workers described the fabrication of superhydrophobic surfaces with raspberry-like particles. They got the raspberry-like morphology directly during the preparation of the surface, by assembling big and small silica particles (500 nm and 20-90

nm, respectively). Instead of using positive polyelectrolyte as counterpart for the silica particles, they turned (when needed) the charge of the silica from negative to positive by chemical modification with an aminosilane. They showed the results of 1, 2 and 3 layers of raspberry-like particles. They measured in all cases a contact angle higher than 160° and the lowest hysteresis for the samples with 3 layers. Although the surfaces survived an immersion in water, the mechanical stability of these surfaces was poor, as attachment of the particles is achieved via physical adhesion instead of chemical forces.

In 2009, Quian et al.[37] reported the preparation of superhydrophobic surfaces with raspberry-like particles made of a polystyrene core and small silica particles attached to its surface. These particles and their preparation are similar to the "composite particles" reported in this thesis work (discussed in chapter 4). Superhydrophobic surfaces were prepared by vertical lifting a glass substrate immersed in a mixture of particles dispersed in ethanol. After hydrophobization of the surface by a fluorosilane, the samples proved to be superhydrophobic. Again, mechanical stability needs to be improved. The glass substrate was partially covered by a fragile layer of particles that can come off if force is applied.

1.4 Thesis contribution and outline

- Superhydrophobic surfaces by hybrid raspberry-like particles

As summary of the state of art, it can be said that raspberry particles have been proven to be suitable to build up superhydrophobic surfaces but their mechanical stability is still an issue. So far, the surfaces reported are assembled only by means of weak interaction and in 1-3 layers. Upon removal of the particles from the surface due to mechanical stress, the superhydrophobicity of the surface is lost. The problem of the mechanical stability concerns also the other preparation techniques[18, 19] (e.g. lithography, chemical deposition, sol-gel method, etc.); upon scratching the surfaces become locally smooth and the superhydrophobicity is gone.

Thick layers of superhydrophobic surfaces have not been reported yet.

Superhydrophobic surfaces built up by many layers of particles offer the possibility to go one step further in the construction of scratch resistant surfaces. If the top-most layer is removed, superhydrophobicity can still be ensured by the underlying layer.

The raspberry-like particles synthesized in this work[38] are hybrid materials formed of a polystyrene core and rough silica shell that completely covers the polystyrene surface.

Multi-layers of particles are prepared by evaporation of the water dispersant, an inexpensive and simple procedure.

The sample is exposed to tetrahydrofuran (THF) vapor. This treatment induces leakage of polystyrene from the core and formation of polymer bridges between the raspberry particles. This procedure improves the cohesion between the particles and hence the mechanical stability of the surface (chapter 6). This improved mechanical stability gives the possibility to assemble multi-layers of particles. These latter are good candidate to design surfaces whose roughness is preserved after scratch.
After hydrophobization by chemical vapor deposition (CVD) with a semi-fluorinated silane, the surfaces resulted to be superhydrophobic. The surfaces can posses contact angles higher than 160° and low hysteresis.

- Mechanical stability of hollow silica shells

For good mechanical stability of superhydrophobic surfaces, several requirements are needed. First of all, the particle itself has to be stable. This means mainly that the particles do not deform, unless they undergo a “reasonable” stress. Secondly, the large scale surfaces prepared with raspberry particles have to be durable in the sense that the particle connections within the assembled film prevail over the mechanical stress suffered during usage.
Here, attention is focused on the quantitative characterization of the mechanical properties of single hollow particles. The polystyrene cores are removed in analogy with the fact that the raspberry particles are partially empty after THF leakage. Mechanical characterization is performed on hollow silica particles with smooth surface, a simplified system with respect to raspberry particles. The reason of this choice is due to the fact that raspberry particles do not represent a geometrically well defined model. The “shell theory” described later, which is necessary to get a quantitative characterization, can be utilized only if the shell thickness is known. Hence, it can be applied only to hollow spheres of spherical shape and smooth surface.
For this reason, effort was put on the synthesis of well defined silica hollow particles (chapter 3). Both silica shells (rough and smooth) are synthesized by Stöber method and expected to have similar properties.
Apart from the interest related to the stability of superhydrophobic surface, hollow spheres[32, 33] have recently attracted the attention of the scientific community as promising route for encapsulation and release of different kinds of substances, like drugs, cosmetics, fragrances etc.
To perform the function of carriers, wall permeability and mechanical stability are crucial as they have a large influence on transport properties. Hence, characterization of such materials is important.

With regards to mechanical properties, some capsules have been investigated by AFM[39], in order to get information about their stability. Coating a colloidal template with alternating layers of oppositely charged polyelectrolyte [32] followed by removal of the core is an established method to get hollow capsules. Additionally, it represents the most characterized system from a mechanical point of view.

Fery et al.[34, 39] reported on the mechanical properties of polyelectrolyte multilayer made of poly(styrene-sulfonate)/poly(allylamine). The technique used was a combination of atomic-force-microscopy (AFM) and reflection interference contrast microscopy (RICM). By analyzing force vs. deformation in a small deformation regime, they could study the elastic response of the material. The AFM experiments were performed using tip-less contact cantilever with a colloidal particle glued on its extremity. By RICM, the shape of the hollow particles could be reconstructed during the AFM measurement.

By applying the shell theory, they calculated values of Young modulus between 100 and 400 MPa.

Imhof[40] et al. published a synthesis of hollow particles by emulsion templating. They obtained shells consisting of a cross-linked network of siloxane and silica grown on an oil drop as template. The mechanical properties were also investigated by AFM. The experiment was performed by indenting the hollow sphere with a sharp tip instead of a colloidal probe.

They obtained a Young modulus of ~ 200 MPa, along with the chemical nature of their shells (organo-silica network of silicate and dimethylsiloxane units).

In the present work[41], the synthesis of core-shell polystyrene-silica particles is described. The polystyrene in the core was removed by heating the particles at 500 ˚C, leaving hollow silica particles. The elastic response of hollow silica particles of different size and shell thickness was investigated by AFM. A point load was applied on top of the particle by means of a sharp tip. For deformations below 1/10 of the particle diameter the hollow particles behaved elastically. The Young modulus was found to be ~ 36 GPa, about half of that of of fused silica but still two orders of magnitude larger than those of the polymer capsules previously reported.

The Young modulus was also measured after annealing at temperature from 20˚ to 1100˚[42]. It was found that it moderately increases after annealing at temperatures above 500°C; however, temperatures over 850°C result in a much stronger increase. The Young modulus was close to that of fused silica[43] (72 GPa) after annealing at 1100°C.

NMR analysis revealed that in untreated microcapsules synthesized by the Stöber method only 55% of the silicon atoms form siloxane bonds with four neighbors, whereas the remaining ones only form three or less siloxane bonds each and, thus, a large number of ethoxy and silanol groups still exist. During annealing at 500°C, these are successively transformed into siloxane bonds. This process correlates with a slow increase in Young's

modulus. The strong increase at temperatures above 850°C was associated with shell smoothening and a decrease in capsule size and shell thickness while the shells remained homogenous. This effect is thus mainly due to compaction by sintering.

- Outline

The present thesis is divided as follow:

- In chapter 2 the synthesis and characterization of the polystyrene cores used for subsequent silica coating is described.
- Chapter 3 deals with synthesis and characterization of silica hollow spheres.
- Chapter 4 reports the preparation of the hybrid raspberry particles used to build up superhydrophobic surfaces.
- In chapter 5 the preparation of superhydrophobic surfaces by layer by layer assembly and by Langmuir-Blodgett technique is described.
- In chapter 6, superhydrophobic surfaces composed of multilayer of particles are discussed. Polystyrene leakage which improves the mechanical stability is shown.
- In chapter 7 the procedure to get fluorescently labeled core-shell particles (both smooth and raspberry) is summarized. They will be used for a future project on superhydrophobic surfaces.
- In chapter 8 the experimental techniques used in this thesis work are explained. Furthermore, the detailed recipes of the synthesis performed are given, in order to give the possibility to reproduce the experiments to the readers who are interested.

2 Synthesis of polystyrene particles

The present chapter deals with the synthesis of polystyrene particles used as cores for subsequent silica coating.
They were prepared by soap-less emulsion polymerization or dispersion polymerization. Both polymerization techniques are described and the motivations behind the choice of one approach rather than the other are given.

2.1 Emulsion polymerization

In order to understand the reaction mechanism of soap-free emulsion polymerization, it is necessary to describe the previously developed emulsion polymerization.
In a classic emulsion polymerization[44, 45] the initial reaction mixture is a hetero-phase system composed mainly by the reaction medium and a monomer that is scarcely soluble in the medium. A surfactant is also present, with the function of emulsifying the two components. The initiator is soluble in the medium.
Since emulsion polymerization of styrene in water is one of the most widely investigated systems, hereafter it is directly referred to it.
The reaction mixture is typically stirred at room temperature and, due to the presence of surfactant, an emulsion is formed. Polydisperse, micrometer-sized styrene droplets in the order of 1-10 μm are stabilized by the surfactant. If the concentration of surfactant is above the c.m.c (critical micellar concentration), styrene-swollen micelles (5-10 nm) are also present. The reaction starts upon heating, when the radical initiator is activated and can attack the double bond of the styrene molecules (Figure 2.1a). Monomeric styrene and water are almost immiscible and form a two-phase system; nevertheless, a small amount of styrene is soluble in water (i.e. at reaction temperature of 70°C, the amount of styrene which is soluble in water is about 4 g/L[44]).
A radical polymerization starts and the radical polymer chain grows in water phase until it reaches a critical size at which it is no longer water soluble. At this point it collapses forming a polymer nucleus stabilized by the surfactant molecules. This polymer nucleus becomes the main locus of polymerization. It grows by taking up styrene and oligoradicals from the water medium. The micrometer-sized styrene droplets act as a reservoir of reagents keeping the styrene concentration in water constant (at least until they are consumed).
The polymerization goes on until all the styrene is consumed. At the end of the reaction, monodisperse polystyrene colloids are obtained (Figure 2.1b). Emulsion polymerization presents a fast and convenient method to obtain nanometer-sized particles. The diameter of

the particles thus produced is usually in the range of 100-500 nm in dependence of the reaction parameters (this aspect is discussed in the next paragraph).

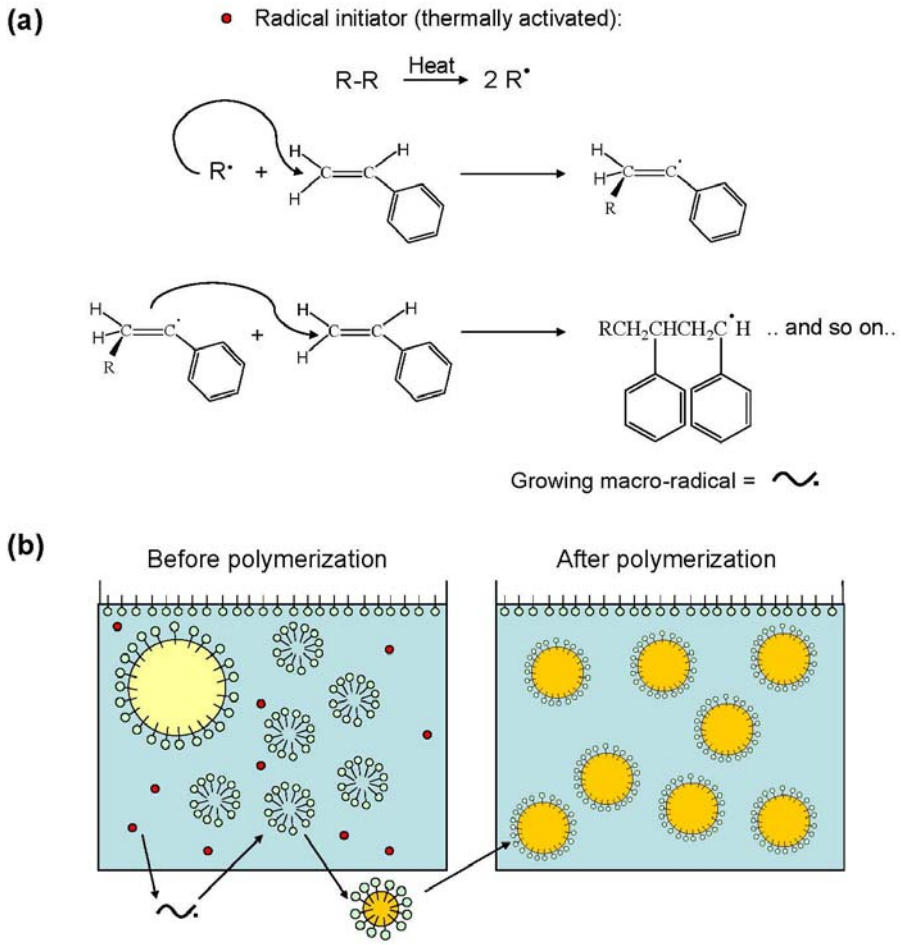

Figure 2.1. Reaction scheme of the radical polymerization of styrene(a), and illustration of the initial and final state of the reaction mixture of emulsion polymerization(b). Before polymerization: micrometer-sized styrene droplets and micelles stabilized by surfactant, and water soluble initiator (red point). After polymerization: monodisperse polystyrene particles stabilized by surfactant. (Figure partially reproduced from Antonietti et al[46]).

Nevertheless, they do not represent a well defined system in terms of surface properties. As an example, one of the most studied systems is the emulsion polymerization of styrene in water using a persulfate as initiator (potassium persulfate or ammonium persulfate) and sodium dodecyl sulfate as surfactant. The formulas of these chemicals are:

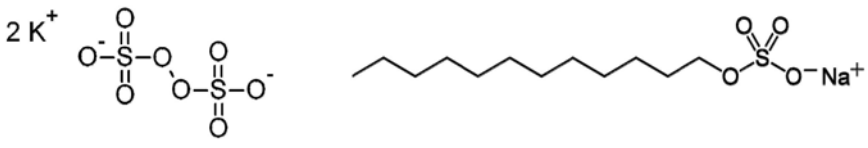

Potassium persulfate

Sodium dodecyl sulfate

The surface of the particles is covered by sulphate groups coming from both the initiator and the surfactant. These negative charges are useful to confer colloidal stability. Because the particles are negatively charged in water, they repel each other and do not aggregate (electrostatic stabilization). The sulphate groups coming from the initiator are chemically bonded to polystyrene, forming the ends of the polymer chains.

On the other hand, the sulphate groups coming from the surfactant are only physically adsorbed on the particle surface. In principle, they can be removed by repeated washing steps but in practice their complete removal is hard.

Hence, surface charge on the particles can change over time because of desorption of surfactant from the surface. As a consequence, the stability of the particles can decrease with time.

2.2 Soap-less emulsion polymerization

The term “soap-less” means that no surfactant is used. Performing emulsion polymerization without surfactant allows overcoming the inconvenience of its desorption from the particle surface with time.

Soap-less emulsion polymerization[47, 48] is performed in the same way as classical emulsion polymerization, with the only difference that no surfactant is used. Therefore the initial state of the reaction is not an emulsion. Unstable, large styrene droplets can form upon strong stirring (Figure 2.2).

After the water-soluble initiator is thermally activated, it attacks the styrene molecules that are solved in water and macro-radicals grow.

When they reach their solubility limit (at which they are no longer soluble in water), they collapse and form polymer nuclei. Because the polymer nuclei are not stabilized by surfactant, they collide and merge, forming larger and larger particles as the polymerization goes on taking up styrene from the water medium.

Most emulsion polymerizations in water are carried out using a peroxydisulfate-based initiator, which implies that each polymer chain has a sulphate end-group (negatively charged).

The surface charge increases as the particles grow, and at a certain size they become stabilized by the sulphate end-groups coming from the initiator (and eventually by the charges coming from a co-monomer, e. g. acrylic acid, discussed later in this paragraph).

They hardly merge anymore and the number of particles in the polymerization medium remains constant; hence they can only grow until all the styrene is consumed. A schematic illustration of the mechanism of soap-free emulsion polymerization is given in Figure 2.2.

Compared to the classical emulsion polymerization, soap-less polymerization is more sensitive to the styrene concentration that generally has to be < 10 % with respect to water. In the case of emulsion polymerization, this value can be as high as 30 % of styrene with respect to water because of the stabilization conferred by surfactant molecules. For the same reason (the stronger electrostatic repulsion due to the surfactant molecules during nucleation and growth stages), classical emulsion polymerization tends to produce smaller particles with the respect to soap-less emulsion polymerization.

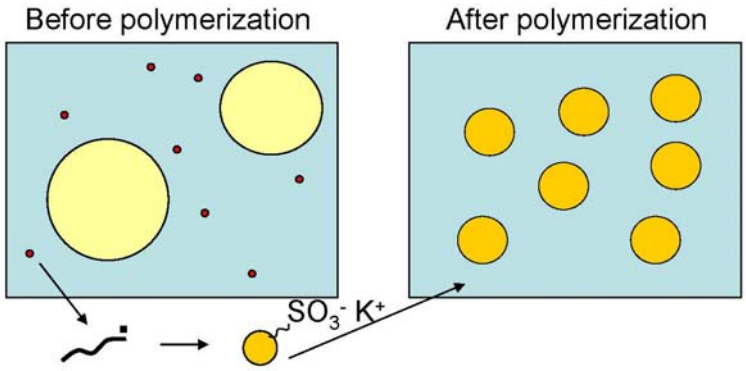

Figure 2.2. Illustration of the initial and final state of the reaction mixture of soap-less emulsion polymerization. Before polymerization: unstable styrene droplet and initiator (red dots) in water. The macroradical (black rod) grows until it collapses to form a polymer nucleus. This latter is stabilised by the sulphate groups coming from the initiator. Polymer nuclei grow until all the styrene is consumed. After polymerization: polystyrene particles (stabilized by the sulphate groups from the initiator).

2.2.1 Results

After this introductive part, the rest of this section is dedicated to the experimental work performed for this thesis. Soap-less polymerization was preferred to emulsion polymerization for the better defined surface properties of the resulting particles.

The polystyrene particles were synthesized by soap-less emulsion polymerization in presence of acrylic acid as co-monomer:

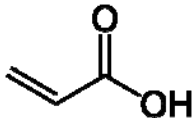

Acrylic acid

They are electrostatically and sterically stabilized. The electrostatic stabilization is due to the repulsive interaction between the negative charges on the surface of the particles.

They come from the anionic radical initiator ammonium persulfate and from the acrylic acid. Since acrylic acid is a weak acid, its negative charge is pH dependant.

The use of acrylic acid provides also steric stabilization [49, 50]. Emulsion co-polymerization of styrene with small amounts of acrylic acid results in poly (styrene-co-acrylic acid) polymer chains, partially situated inside the particles and partially at the water-particle interface. The acrylic acid-enriched chains, more hydrophilic, are situated preferentially at the water-particle interface; this creates a hairy layer that surrounds the particles. When the particles come closer together, the concentration of "hairy polymer" increases in the overlap region. This results in an increase of osmotic pressure that pushes more solvent from the surrounding medium, with a consequent force to separate the particles (Figure 2.3).

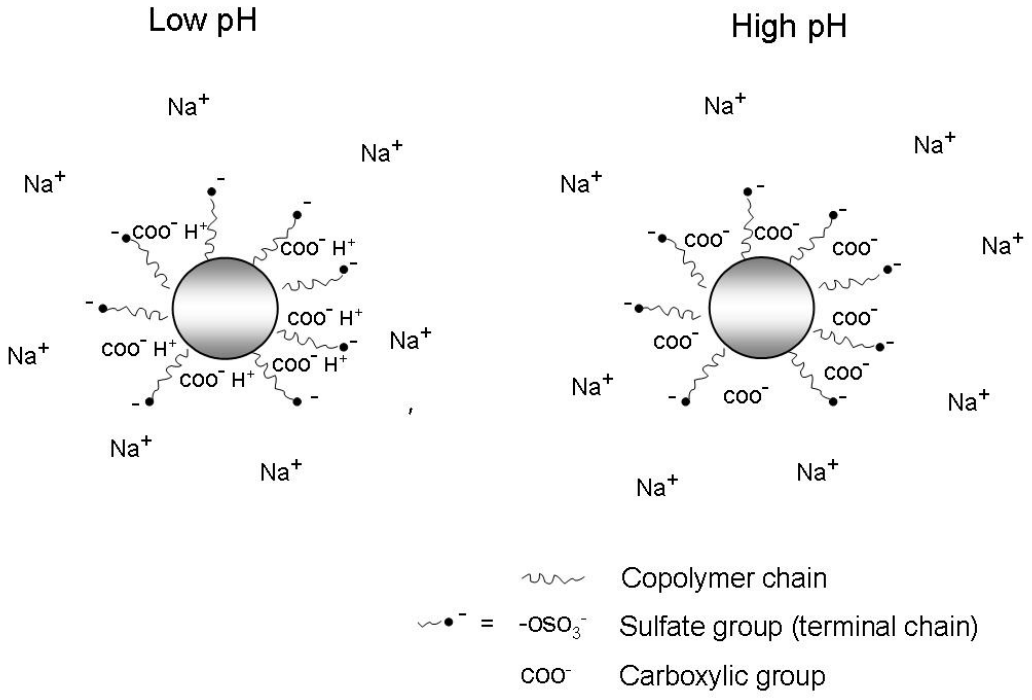

Figure 2.3. Schematic representation of the particles surface at low pH (carboxylic groups are protonated, only sulphate groups are charged) and high pH (all groups are charged). The sketch is partially reproduced from ref.[50].

The amount of the co-monomer acrylic acid added to the reaction mixture was typically 0.5-4% w/w with respect to styrene (next paragraph and experimental part in Chapter 8 for details).

Dependent on the reaction parameters, particles with a diameter between 200 and 700 nm were obtained. As an example, Figure 2.4 shows the SEM images of polystyrene particles of different size obtained at different reaction conditions (Table 2.1).

The particles from reaction (a) and (b) are 280 and 520 nanometers in diameter, respectively. They are prepared in the same way except for the amount of styrene in the reaction mixture.

Particles size increases with the amount of styrene. Particles from reaction (c) are the largest. They are synthesized by using more styrene and more sodium chloride with respect to reaction (a) and (b). Increase of ionic strength by salt addition destabilizes the polymer nuclei because of screening effects. This causes a prolongation of the period during which they are unstable and grow by collision; hence, fewer particles are formed and their size increase because of the increase of the amount of styrene per particle.

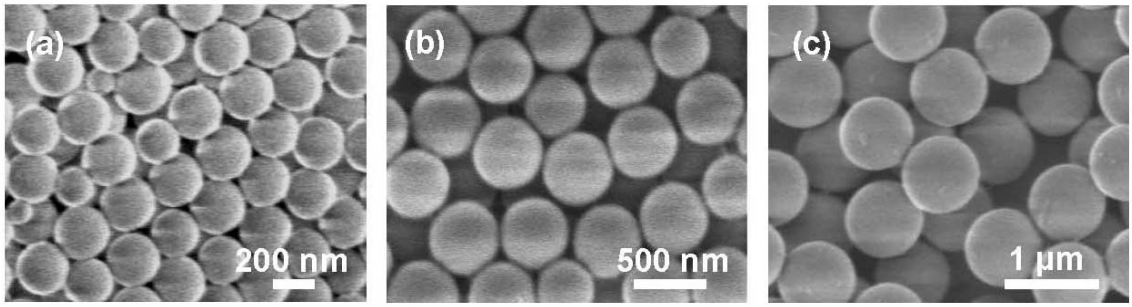

Figure 2.4. SEM images of polystyrene particles of different sizes obtained with the reaction parameters listed in table 2.1.Particle size: 280 nm (a), 520 nm (b), and 740 nm (c).

Also initiator concentration and temperature can contribute to tune particle size. Increasing the initiator concentration[51] leads to a reduction of the particles size because the larger number of stabilizing groups coming from the initiator (i.e. sulphate groups) favourites the formation of a greater number of nuclei. Increase in temperature results in a decreased particle size. At higher temperature[47] the reaction is faster. As a consequence, a larger number of surface active oligomers are formed at the beginning of the reaction. These latter, in turn, are able to stabilize a larger number of nuclei.

The yield of the reaction was in the range of 60-70%. Generally, in reactions with high styrene content (~10 % w/w with the respect to water) or high sodium chloride content (~10^{-2} M), a coagulum was found (the coagulum is the formation of polystyrene in bulk and not in the form of particles).

In some cases, (e.g. particles fluorescently labeled by “swelling method“, discussed in par. 7.1.2) polystyrene particles were co-polymerized with a small amount of divinylbenzene (~1% w/w with the respect to styrene). Divinylbenzene, with its two double bonds available for the polymerization, acts as crosslinking agent between polystyrene chains. Crosslinked particles are less soluble, harder to swell and have a higher Tg than uncrosslinked ones, and they may be desirable when these physical properties are needed (par. 7.1.2).

As mentioned in the introductive chapter, for the design of superhydrophobic surfaces by raspberry particles, micrometer-sized roughness is desirable. This latter is more likely obtained by using micrometer-sized particles.

For this reason, particles from the first step were grown up to 1 μm by seeded emulsion polymerization.

Since emulsion polymerization is limited to nano-sized particles, seeded polymerization[52, 53] is a well established method to increase the size up to 1 micrometer or more.

Table 2.1. Parameters of the synthesis of the polystyrene particles illustrated in Figure 2.4

			Amount in grams			
Reaction	Diameter (nm)[1]	Initiator	Styrene	Acrylic acid	Sodium Chloride	Distilled water
(a)	280* ± 20	0.11	9.1	0.15	0.12	300
(b)	520* ± 30	0.11	15.4	0.15	0.12	300
(c)	740* ± 30	0.11	25	0.15	0.2	300

1. Particles size measured from SEM images taking the average over 100 particles.
2. Initiator: Ammonium persulfate; Reaction temperature: 75 ˚C.

It consists in performing emulsion polymerization in presence of pre-formed particles. They are swollen with styrene and when the polymerization starts, they are the main locus of polymerization, becoming bigger in dependence of the amount of styrene.

As an example, Figure 2.5 shows Scanning Electron Microscope (SEM) images of the typical products after the first (a) and the second step (b), respectively (experimental parameters listed in Table 2.2).

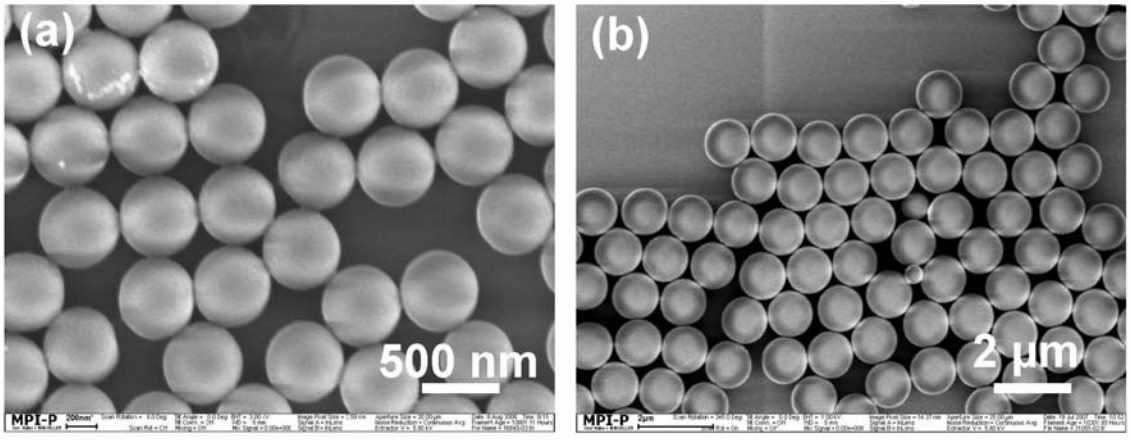

Figure 2.5. SEM images of polystyrene particles obtained by soap-less emulsion polymerization. Nanometer sized particles from 1 step reaction (a), and micrometer sized particles after seeded polymerization reaction (b).

A typical procedure consists in synthesizing particles of about 600 nm in the first step (Figure 2.5a, experimental conditions in Table 2.2a) and taking part of the reaction mixture for the growing step. The second step is performed in a similar fashion as the first one (Figure 2.5b, Table 2.2b); the amount of styrene calculated on the base of geometrical parameters (i.e. the

amount needed to grow the particles from 600 nm in diameter to 1 μm, roughly). One disadvantage of this method is that secondary nucleation can occur. In such a case, the particles obtained by this reaction have a bi-modal size distribution. In general, the smaller ones can be removed by subsequent centrifugation steps if the size difference is large enough. Figure 2.5 (b) shows the particles after cleaning and removal of the small particles (a residual small particle is still visible).

Table 2.2. Parameters of the synthesis of the polystyrene particles illustrated in Figure 2.5.

		Amount in grams					
Reaction	Diameter (nm)	Initiator	Styrene	Acrylic acid	NaCl	Distilled water	Seeds
(a)	600	0.11	25	0.15	0.2	300	-
(b)	1200	0.4	7.2	0.04	0.12	300	38 ml reaction mixture (a)

Initiator: Ammonium persulfate; reaction temperature: 75˚C

2.2.2 Growth of polystyrene particles during emulsion polymerization

Polystyrene colloids suitable for silica coating should have a smooth surface. Unfortunately, regularly we obtained “donut-like” polystyrene particles. To get more information on the growth process, we followed the reaction with time focusing on the morphological evolution of the particles. Scanning electron microscopy is the most convenient experimental technique for that purpose, since it can provide information about particle size and morphology at the same time and for a large number of particles. Every 15 minutes a small aliquot was taken from the reaction mixture. The aliquots were diluted and imaged without purification (Figure 2.6).

During the first hour no particles could be identified within the background of unreacted polystyrene. After 1.75 hours almost monodisperse particles embedded in the polymer melt were visible, Figure 2.6(a). With increasing reaction time the particles grew further, but still remained soft and contained significant amount of unreacted styrene. During evacuation the styrene evaporates, leading to particle collapse which resulted in their donut-like shape, Figure 2.6(b). After another 2.5 hours not only the size of the particles, but also their hardness increased. The particles appeared much more spherical (Figure 2.6(c)) although still evaporation of styrene caused formation of small dimples in the particle surface. Only after another couple of hours the particles appear smooth in SEM, Figure 2.6(d). From the SEM images the diameter of the polystyrene was measured. Figure 2.7 illustrates the

increase of particle diameter with time. Within the first 5 hours it grows linearly with time.

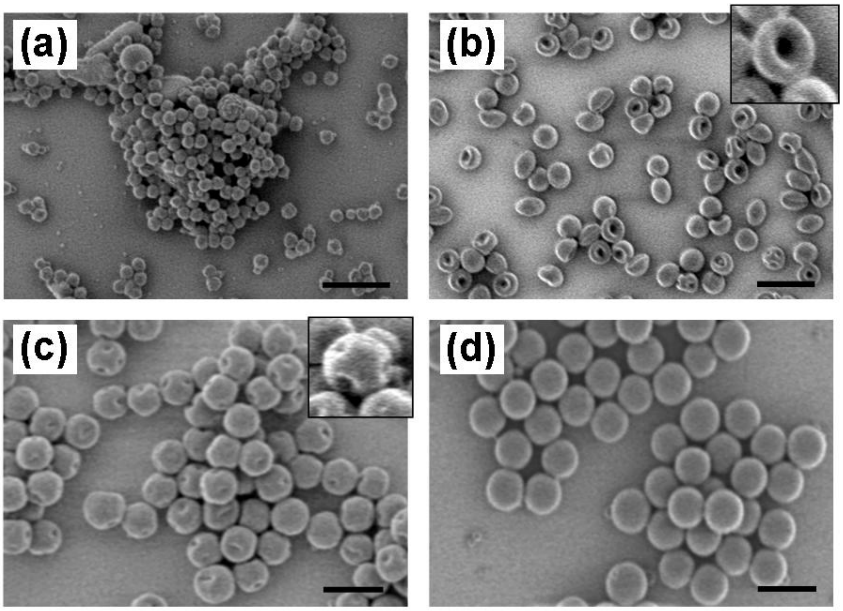

Figure 2.6. SEM images of polystyrene particles obtained by soap-free emulsion polymerization, taken after 1.75 hours (a), 4.5 hours (b), 7 hours (c), and after 24 hours (d). Scale bar: 1 µm; insets: Images at higher magnification.

Thereafter, the growth rate slowed down, until after about 8 hours hardly any increase of the diameter could be detected. However, still the particle surface changed according to scanning electron microscopy images.

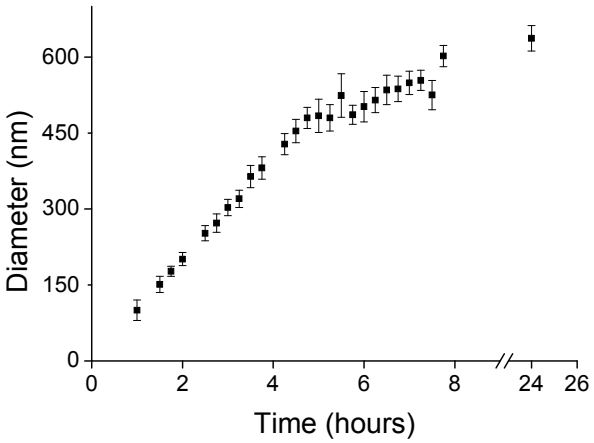

Figure 2.7. Growth of polystyrene particles during emulsion polymerization. Experimental conditions: Ammonium persulfate: 0.11g; Acrylic acid: 0.15g; Sodium chloride: 0.2g; Milli-Q water: 300 ml; Styrene: 25g; Divinylbenzene: 0.25g.

2.2.3 Characterization of the surface charge of the polystyrene particles

Most of the polystyrene particles synthesized for this thesis work were prepared by soap-less emulsion polymerization in presence of acrylic acid as co-monomer and ammonium persulfate as initiator. Hence, on the particle surface there are sulphate groups (fully dissociated) and carboxylic groups (pH dependant dissociation). In order to characterize the effective surface charge, the amount of sulphate and carboxylic groups on the particles was determined by polyelectrolyte titration. This technique has been previously reported as suitable method to characterize particle surface charge [54, 55] and it takes advantage of the interaction between the charges on the surface of the particles and the opposite charges of a low molecular weight polyelectrolyte. In this case, the particle charge is negative and the titration was done with the cationic polyelectrolyte polydiallyldimethyl ammonium chloride (PDAD-MAC), fully dissociated in water.

For the present study, three batches of polystyrene particles were synthesized at the same experimental conditions except for the amount of acrylic acid. The experimental conditions are listed in Table 2.3.

The amount of acrylic acid added to the reaction mixture was 0.7, 1.5, and 3.7 % w/w with respect to styrene. For each of these batches, two suspensions of particles were prepared; at pH 2 and at pH 10.

At pH 2 all the carboxylic groups are protonated and the charge detected by titration can only be assigned to the sulphate groups coming from the initiator.

At pH 10 all the groups are deprotonated and the charge detected by titration is the sum of the number of sulphate and carboxylic groups.

The number of carboxylic groups can be calculated from the difference between the charges at pH 2 and pH 10.

The experiment was performed by titrating an aqueous colloidal suspensions of known solid content with a standard solution of polyelectrolyte in water (10^{-3} M). The potential was monitored in dependence of the volume of polyelectrolyte until the potential became zero (particles are neutral).

It is possible to calculate the amount of surface groups per nm^2 by the following equation:

$$[groups/nm^2] = \frac{V \times M \times N_A \times D_n \times \rho \times 10^{-21}}{6 \times SC}$$

where V is the volume of used polyelectrolyte in L, M is the molar concentration of charges on the polyelectrolyte in mol/L, NA is Avogadro's constant ($6.022 \cdot 10^{23}$ mol^{-1}), SC is the solid content of the particle suspension in grams, ρ is the density of polystyrene in g/cm^3 and D_n is

the diameter of the particles in nanometres. The number of charged groups per nm^2 expressed in this formula is the ratio between the total amount of charged groups on the surface and the total surface of the sample in study. The total number of groups can be calculated from the volume of polyelectrolyte standard solution necessary to neutralize the particle charge; the total surface of the particles is calculated from the size of the particles and the concentration of the suspension. The results obtained for samples prepared at different concentrations of acrylic acid in the reaction mixture are shown in Table 2.3.

Table 2.3. Experimental condition and results of the three reactions performed to characterize the surface charge on the polystyrene particles.

			Charged groups/nm^2		
Sample[1]	Radius[2] (nm)	PDI[2]	pH 2 only $-O-SO_3^-$ groups[3]	pH 10 $-O-SO_3^-$ + COO^- groups[3]	Carboxylic groups
0.7 % w/w Acrylic acid	297	0.014	0.46	1.03	0.57
1.5 % w/w Acrylic acid	302	0.002	0.36	1.02	0.66
3.7 % w/w Acrylic acid	280	0.05	0.40	1.48	1.08

1. All the other experimental conditions are the same for the three reactions: Styrene: 15 ml; Ammonium persulfate: 0.11 g; NaCl: 0.2 g; milli-Q water: 300 ml
2. Particle radius measured by DLS; PDI = polydispersity index
3. From the average on at least three titrations.

Within experimental accuracy, the size of the particles does not depend on the amount of acrylic acid. This is consistent with the results published by Holzapfel et al[54] who found a constant size until 10 % of acrylic acid concentration in the reaction mixture.

Table 2.3 shows that the charge at pH 2 is almost identical for the three samples. This supports that charges come exclusively from the sulphate groups of the initiator, considering that the reactions are all performed with the same amount of ammonium persulfate. The charge at pH 10 represents the sum of sulphate and carboxylic groups. So, the number of carboxylic groups is given by the difference between the charge at pH 10 and pH 2, last column of Table 2.3. The amount of carboxylic groups on the particle surface increases with increasing amount of carboxylic groups. For example, increasing the amount of acrylic acid in the reaction mixture by a factor of five (from 0.7 to 3.7 %w/w) induces a doubling of its surface concentration.

2.3 Dispersion polymerization

2.3.1 Reaction mechanism

Dispersion polymerization[56] is a suitable method to get monodisperse particles in the micrometer size in one-step reaction. For this reason, it represents a convenient alternative to seed-emulsion polymerization and it was employed for the synthesis of the 2 μm polystyrene cores discussed in chapter 3.

Differently from emulsion polymerization, in dispersion polymerization the monomer is soluble in the reaction mixture but the corresponding polymer is not soluble in it. The whole initial reaction mixture is a one-phase system. In case of styrene, for example, it consists of a homogeneous mixture of solvent (generally ethanol), styrene, radical initiator and polymer stabilizer (e.g. polyvinylpyrrolidone, poly(acrylic acid) etc.).

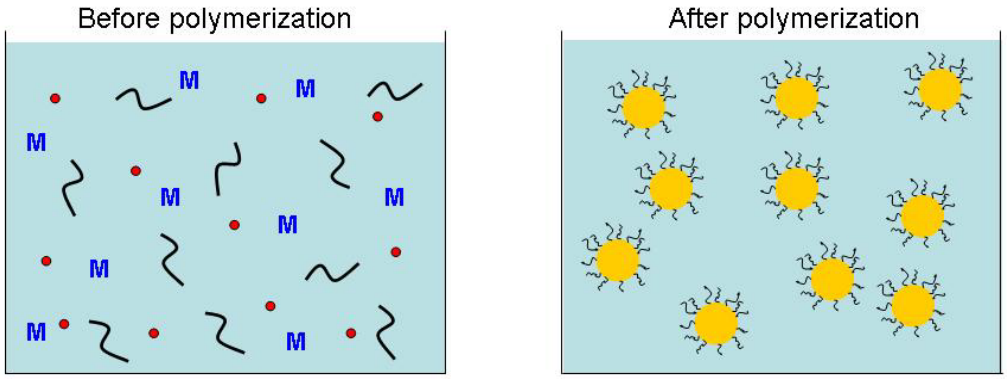

Figure 2.8. Illustration of the initial and final states of dispersion polymerization. In the initial state the mixture is homogeneous; in the end polystyrene particles dispersed in the medium are obtained. Particles are stabilized by the polymer adsorbed on its surface (M = monomer, red dots = initiator, black rods = polymer stabilizer, yellow circles = polymer particles).

When the radical initiator is activated by heating, it attacks the styrene molecules dissolved in the medium and an oligomer starts to grow. When its size reaches a critical value, it is no longer soluble in the reaction mixture and it collapses to form a polymer nucleus. These nuclei collide and merge until they become stable. Stability is conferred by the polymer stabilizer adsorbed on particle surface. From now on, the number of particles is constant and they simply grow until all the monomer is consumed.

A representation of the initial and final states of dispersion polymerization is shown in Figure 2.8.

In the end, polymer particles stabilized by the polymer adsorbed on its surface are obtained. Generally, dispersion polymerization can produce nicely monodisperse particles in the 1-15

μm range. Reaction parameters[57, 58], such as concentration of reagents and type and molecular weight of the polymer stabilizer have a great influence in the size and monodispersity of the resulting particles.

For example, an increase of initiator concentration results in larger particles[57]. More initiator implies more free polymeric radicals in solution with consequent decrease of their molecular weight. Lower molecular weight polymer chains are more soluble in the media; hence the number of nuclei is decreased, which led to a lower number of particles but with larger size.

The type, amount and molecular weight of the polymeric stabilizer have also an influence on the resulting particle size. In this study, polyvinylpyrrolidone and poly(acrylic acid) were tested. Polyvinylpyrrolidone is a non-charged polymer and it can provide only steric stabilization, whereas poly(acrylic acid) is partially dissociated in water and, beside of steric stabilization, can also provide electrostatic stabilization. Furthermore, larger amounts and higher molecular weight of polymeric stabilizer lead to smaller and generally more monodisperse particles. Obviously, this is due to the resulting increase in stabilization at the particle/medium interface during the nucleation.

Table 2.4. Composition of the reaction mixtures of the polystyrene particles obtained by dispersion polymerization.

		Polymer stabilizer					
Sample	AIBN	PVP Mw = 55 kg/mol	PAA Mw = 100 kg/mol	PAA Mw = 450 kg/mol	Water	Ethanol	Size (μm)
(a)	0.160	0.5	---	---	---	39.5	4, polydisperse
(b)	0.200	0.5	---	---	---	39.5	6, polydisperse
(c)	0.100	---	0.400	---	1.5	35	~ 2, polydisperse
(d)	0.100	---	---	0.250	2.5	35	2, monodisperse

- Reactions carried out at 70˚C
- Amounts in grams
- Amount of styrene: 4,5 g
- AIBN = azobisisobutyronitrile (radical initiator)
- PVP = polyvynilpyrrolidone
- PAA = poly(acrylic acid)

Addition of small amount of water to the reaction medium (generally ethanol) reduces the particle size[59]. Since water is a poorer solvent for polystyrene than ethanol, the critical chain length for the precipitation of the oligomers decreases with increasing water content. Hence, the number of nuclei increases and the particle diameter decreases.

2.3.2 Results

Dispersion polymerizations were performed in order to get monodisperse polystyrene particles of about 2 μm in diameter. They were subsequently used as sacrificial templates in the synthesis of hollow silica particles. For this reason, the reaction parameters were not varied one by one (Table 2.4, detailed experimental conditions in par. 8.2.3). Size and polydispersity were determined by SEM (Figure 2.9).

Reaction (a) and (b) were carried at the same condition except for the concentration of the initiator. This resulted in a larger size for the sample prepared with more initiator, as already

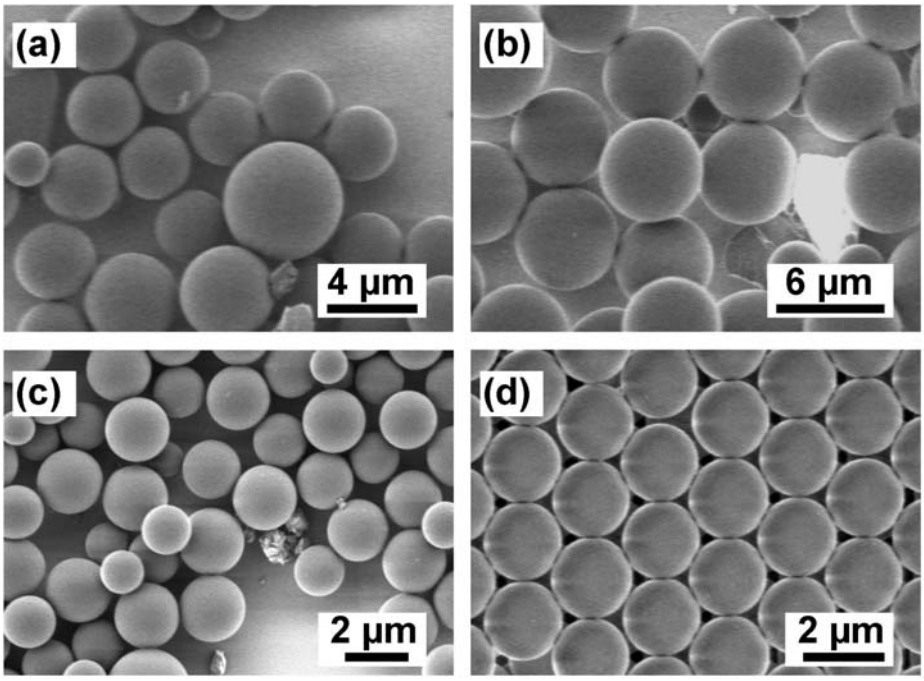

Figure 2.9. Scanning Electron Microscopy of 2 μm polystyrene particles synthesized in dispersion polymerization with poly(acrylic acid) as stabilizer.

discussed. Both reactions yielded particles with a broad size distribution; probably the low molecular weight of PVP was not sufficient to provide an effective steric stabilization.

In reactions (c) and (d) two different amounts and molecular weights of PAA were used as stabilizers. Evidently, lower amount of stabilizer but with higher molecular weight improves monodispersity. Particles from reaction (d), in fact, resulted to be highly monodisperse and were chosen for the silica coating as described in chapter 3.

3 Synthesis and characterization of hollow silica shells

The following chapter discusses the synthesis of core-shell particles made of a polystyrene core and a smooth silica shell. Hollow silica shells can be obtained from these particles by removal of the polystyrene core.
Characterization of these hollow spheres is performed by Atomic Force Microscope (AFM) and Nuclear Magnetic Resonance (NMR).
Motivations behind this work can be found in chapter 1.

3.1 Synthesis of core-shell polystyrene-silica particles: reaction scheme

The synthesis of the core-shell particles was performed according to the scheme in Figure 3.1. Negatively charged polystyrene particles were coated with poly(allylamine hydrochloride) (PAH) to reverse their charge. This procedure was performed in water. After that, the particles were transferred in ethanol/poly(vinylpyrrolidone)(PVP) solution and kept under stirring to coat them with PVP.
By addition of the reagents for the synthesis of silica following the Stöber method (tetraethoxysilane and ammonia in water), a smooth silica shell on polystyrene surface is obtained.

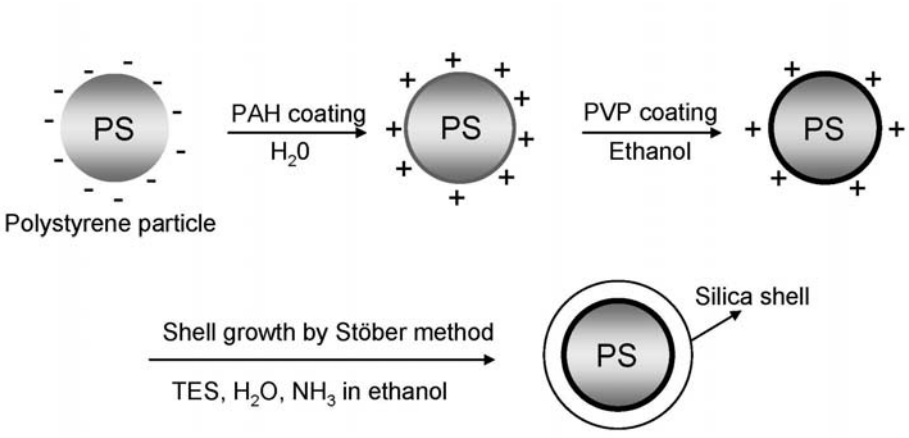

Figure 3.1. Scheme of the preparation of core-shell polystyrene-silica particles.

Stöber method itself is a well know procedure to get monodisperse silica particles. Before going in to details of the preparation of core-shell particles, a paragraph is dedicated to this approach.

3.1.1 Synthesis of silica particles by Stöber method

Stöber et al developed in 1968[60] a method to synthesize monodisperse colloidal silica in the size range between 50 nm and 2 µm. The reaction consisted in the hydrolysis and condensation of tetraalkoxysilanes performed in alcohols and catalysed by ammonia. It is largely used to obtain well defined model systems for fundamental research purposes.
In this work, tetraethoxysilane (TES) as silica precursor and ethanol as solvent were used.
The following scheme (reproduced from van Blaaderen et al.[61]) summarizes the possible reactions:

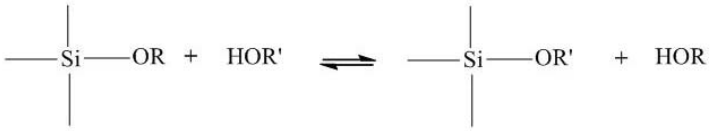

(1)

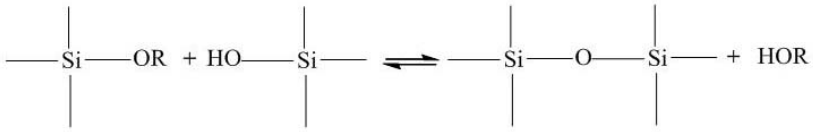

(2)

R and R' can be hydrogen atom or an ethyl group. The bonds of the silicon atoms which are not explicitly sketched can be an ethoxy group, a silanol group or a siloxane bond.
The nomenclature currently in use to define silicon atoms involved in different bonds is the following: Q^4 (quaternary) is a silicon atom involved in 4 siloxane bonds, Q^3 (ternary) is a silicon atom involved in 3 siloxane bonds, etc.
The reaction 1 is an ester exchange (both direct and inverse reaction) in case R and R' are ethyl groups; if R' is a hydrogen atom, the direct reaction is hydrolysis and the inverse reaction is esterification. Reaction 1 is a base catalyzed reaction passing through a bimolecular nucleophilic attack on the silicon atom (SN_2), producing a negatively charged pentacoordinate transition state.
The nucleophile that attacks the silicon atom is OH^-, hence the rate of the hydrolysis is enhanced by increasing the concentration of water and/or NH_3.
The reaction 2 is a condensation reaction, producing water or ethanol and leading to the formation of siloxane bond.
As in the hydrolysis reaction, condensation occurs via base catalysed nucleophilic attack resulting in a pentacoordinate transition state whose rate depends on the concentration of

NH_3 and water. In this case, the nucleophile is a deprotonated silanol group. Anyway, this step is much faster than the hydrolysis reaction (rate determining step).

One big advantage of Stöber synthesis is the possibility to functionalize the particles. In fact, the synthesis can be performed also in presence of organo-alkoxysilanes, producing particles with different surface properties and physical parameters like density and refractive index. Van Blaaderen and Vrij in 1993[61] described the synthesis of organo-silica particles prepared from a mixture of TES and 3-aminopropyltriethoxysilane (APS) by Stöber method. They showed that particle density was lower (1.51 g/cm^3) than the one of pure silica (1.98 g/cm). The refractive index, instead, was found to be slightly higher, with a difference of about 0.02.

Furthermore, alkoxysilane coupling gives the possibility to label[62, 63] silica particles with Rhodamine isothiocianate and investigate local arrangements and dynamics of particles by confocal laser scanning microscopy (CSLM). Labeled silica particles have been largely used for CSLM studies[62, 64, 65].

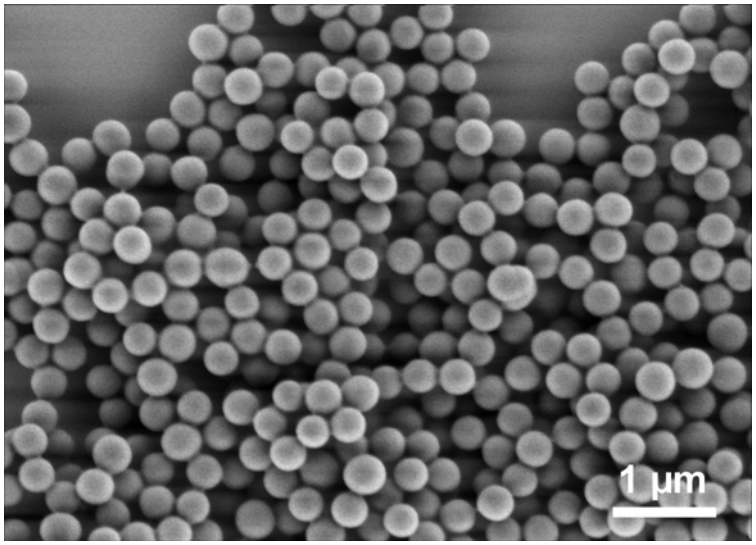

Figure 3.2. SEM image of organo-silica particles with a diameter of 300 nm obtained by Stöber method.

The procedure to get dyed colloids will be discussed in chapter 7.

Here, the particles obtained by Stöber method in presence of APS are shown in Figure 3.2. Monodisperse and smooth silica particles (diameter = 300 nm) are obtained mixing TES and APS (31 % with respect to the volume of TES) in ethanol and using water/ammonia as catalysts at the temperature of 60° (the procedure is described in the experimental part, par. 8.2.6).

3.1.2 Synthesis of core-shell polystyrene-silica particles and hollow silica spheres: results and discussion

As discussed in chapter 2, most of the polystyrene particles used for subsequent silica coating were synthesized by soap-free emulsion polymerization. They are negatively charged and show a negative Z-potential of about -55 ± 5 mV in water. The first part of the synthesis is the coating (in water) of these particles with poly(allylamine hydrochloride) (PAH), a positively charged polyelectrolyte:

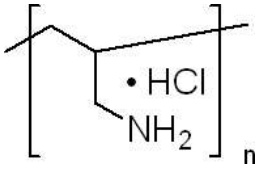

poly(allylamine hydrochloride)
(PAH)

This step resulted to be necessary in order to get smooth and closed silica shell. When the PAH coating is not performed, the same reaction leads to rough and incomplete silica shells (chapter 4).

The second step involves the coating (in ethanol) of the particles with polyvinylpyrrolidone (PVP), a non-charged and amphiphilic polymer:

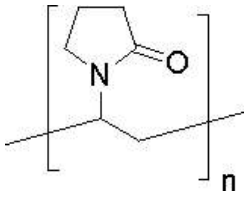

Polyvinylpyrrolidone (PVP)

The last step, after the surface preparation, is the addition of TES and ammonia.

PVP coating is reported in literature[66] as suitable way to favorite growing of silica shells by Stöber method on different kinds of colloidal particles, included negatively charged polystyrene particles. In course of these studies, it was found that smooth silica shells were also obtained without performing the PVP coating and using polystyrene particles with or without functionalization with acrylic acid. Figure 3.3 shows the simplified procedure to obtain smooth silica shell without performing the PVP coating. The crucial step for the synthesis of

smooth silica shells resulted to be the PAH coating. Without performing it, rough shells are obtained.

The morphology of the silica shells depends on the details of the nucleation of silica on polystyrene. In presence of PAH coating, the number of nucleation centers is higher and more homogeneously distributed, to such an extent that from a given point of the reaction the silica nuclei start to merge while growing. This hypothesis is supported by the AFM images at high resolution showing that the shell surface is formed by the "fusion" of many small particles (Figure 3.8b).

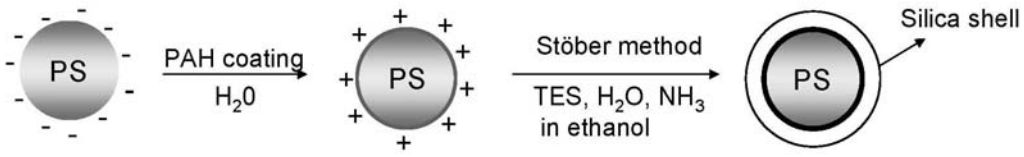

Figure 3.3. Simplified scheme of the preparation of core-shell polystyrene-silica particles without performing the PVP coating.

Evidently, the nucleation centers are fewer when the reaction is performed without PAH and this leads to a rough surface. The synthesis of rough silica shells is discussed in chapter 4.

The reason of the increased nucleation by means of PAH is still unclear. The electrostatic interactions may play a role[67-69], since silica and PAH carry charges of opposite sign in water (silica is negatively charged and PAH is positively charged). However, the reaction is carried out in ethanol in presence of little amount of water (~5-7% v/v) and the degree of dissociation (both of silica and PAH) is reduced with respect to pure water.

For the determination of the mechanical properties, silica hollow particles of tunable size and shell thickness were prepared.

The size of the particles was adjusted by using polystyrene templates of different diameter (800 nm and 2 μm) and the shell thickness was tuned by the amount of TES added to the reaction mixture.

- Synthesis of 800 nm core-shell particles

Polystyrene particles with a diameter of about 800 nm were prepared by soap-less emulsion polymerization in one step. The reaction conditions are listed in Table 3.1 (procedure in chapter 8).

Table 3.1. Ingredients for the synthesis of 800 nm polystyrene particles by soap-less emulsion polymerization.

	Amount in gr.
styrene	25
divinylbenzene	0.25
acrylic acid	0.15
ammonium persulfate	0.11
milli-Q water	300

After cleaning the particles by subsequent centrifugation steps with water and ethanol, these particles were redispersed in water and directly used for the reaction of silica coating.

- Synthesis of 2 µm core-shell particles

Polystyrene particles of about 2 µm were prepared by dispersion polymerization using poly(acrylic acid) as stabilizer during the reaction. In this case, the particles resulted not to be suitable for direct silica coating. Indeed, by performing the reaction of silica coating on such particles, an incomplete shell was obtained (Figure 3.4a). This fact is attributed to the difference in surface charge of these particles with the respect to the ones obtained in emulsion polymerization.

In dispersion polymerization, the surface charge comes from the poly(acrylic acid) (PAA) adsorbed on particles surface during the synthesis. This charge is subject to decrease after the several washing steps performed to clean the particles. Since the adsorption of PAH depends on the charge density on the surface of the particles, probably it was too low to provide a satisfying coating.

For this reason, the surface of these particles was functionalized with poly(acrylic acid-co-styrene) according to a procedure reported by Tuncel et al[70]. This further step consists in the swelling of the particles with a small amount of styrene, acrylic acid and initiator to such dispersion for one day at room temperature. By heating this mixture at 75 °C, styrene and acrylic acid co-polymerize giving rise to chemically bonded carboxylic groups on the particle surface. After this step the reaction of silica coating produced a smooth shell (Figure 3.4b).

In Table 3.2 details of the first and second step of the synthesis of the particles by dispersion polymerization are given.

In Figure 3.4 it is possible to compare the different results obtained from particles without and with surface modification.

The silica shells were prepared with identical reaction conditions. The only difference is the surface functionalization of the two polystyrene samples.

Without any surface modification (Figure 3.4a), silica shells are not completely closed and rough.

After surface modification (Figure 3.4b), shells are smooth and compact.

Table 3.2. Details of the synthesis of 2 µm polystyrene particles by dispersion polymerization and subsequent functionalization.

	Amount (g)	
	1st step	2nd step
Styrene	9.1	1.27
polystyrene latex	-	6.4
Acrilic acid	-	1.05
poly(acrylic acid) (Mw= 450 kg/mol)	0.5	-
azobisisobutyronitrile	0.200	0.06
milli-Q water	5	50
Ethanol	67	39.5

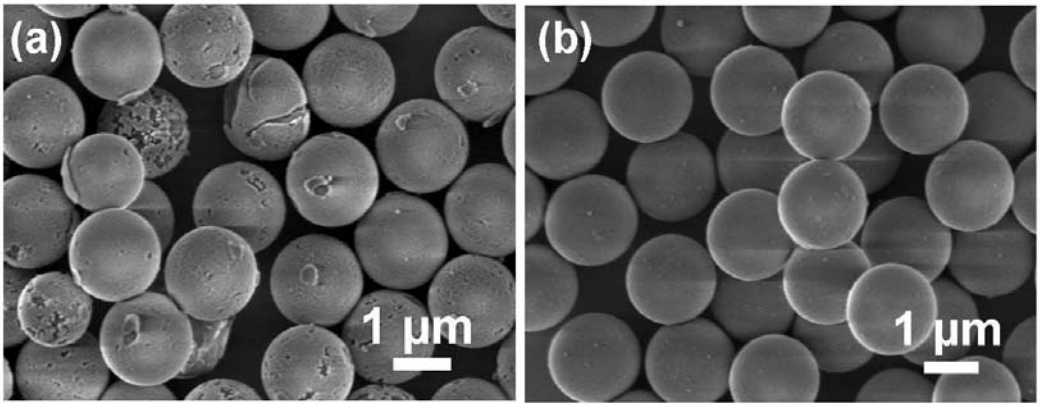

Figure 3.4. SEM images of silica shells on polystyrene particles prepared in dispersion polymerization without (a) and with (b) surface modification. Rough and incomplete shells (a) and close silica shells of 40 nm (b).

- Silica hollow shells

Once the polystyrene cores (either from emulsion and dispersion polymerization) were proven to be suitable to get smooth silica shells, systematic reactions were carried out in order to tune the shell thickness.

Shell thicknesses could be easily regulated by the amount of tetraethoxysilane TES.

Table 3.4 shows the amount of TES added to the reaction mixture and the corresponding shell thickness obtained for both polystyrene batches.

All the other experimental details are specified in the experimental part. The particle diameter was determined by SEM images averaging on about 100 particles. The shell of the 800 nm particles was directly measured from the TEM images at high magnification, as shown in Figure 3.5.

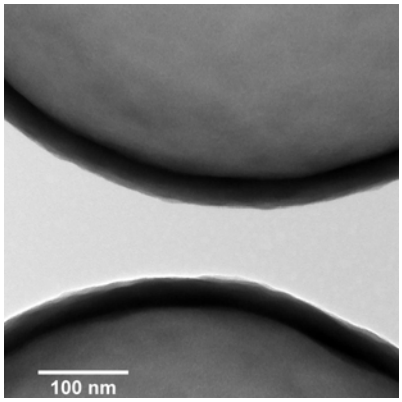

Figure 3.5. TEM image at high magnification used to determine the shell thickness. It corresponds to the batch of hollow particles with a diameter of 790 nm and shell thickness of 37 ± 4 nm.

The shell thickness of the 2 μm particles was indirectly obtained from SEM images by taking the difference between the diameter before and after coating.

Table 3.4. Amount of TES and corresponding shell thicknesses for the silica coating of polystyrene samples obtained by emulsion and dispersion polymerization.

Polystyrene sample from polymerization in:	Diameter (nm)[1]	TES (ml)	Shell thickness (nm)
Emulsion (PSE)	790 ± 70	0.10	15[2]
Emulsion (PSE)	790 ± 70	0.20	23[2]
Emulsion (PSE)	790 ± 70	0.30	37[2]
Dispersion (PSD)	1870 ± 60	0.12	30[3]
Dispersion (PSD)	1870 ± 60	0.24	50[3]
Dispersion (PSD)	1870 ± 60	0.30	70[3]

1. From SEM, average on ~ 100 particles.
2. From TEM
3. From SEM

The core-shell particles were heated in a furnace from room temperature to 500˚C (heating rate ~15˚ C/hour) and kept at this temperature for 3.5 hours. The polystyrene cores burned away and left empty shells. As an example, Figure 3.6 shows TEM and SEM images of the

particles before and after thermal treatment. The images of the core-shell particles before heating are taken with SEM. They show that the surface of the silica shells is smooth.

The hollow particles obtained after burning the polystyrene were imaged by TEM (Figure 3.6, right side) because it allows verifying that they are completely empty and estimate directly the thickness of the shell. In fact, when the particles are not empty, but still filled with polystyrene, they are less permeable to the electron beam and their image appears to be black (inset in Figure 3.6a).

The thinnest silica shell obtained was 15 nm and the hollow particles resulted to be floppy; in fact, some of the empty particles collapse likely because of the vacuum performed in the TEM chamber (Figure 3.6b, right side). Nevertheless, also in this case it was possible to find close and intact shells suitable for mechanical characterization.

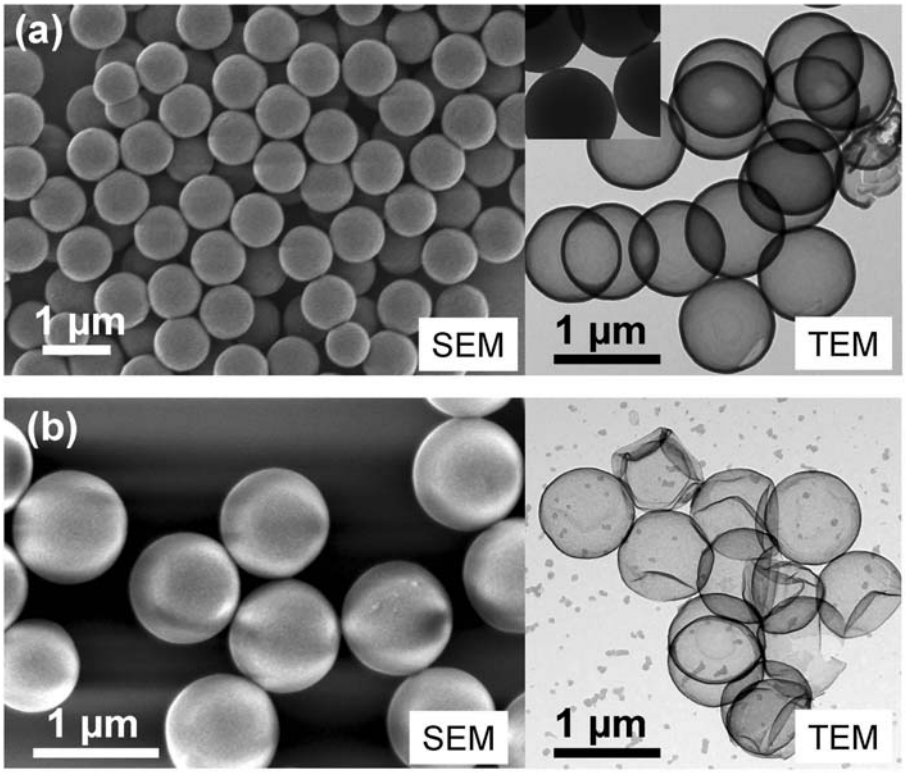

Figure 3.6. Images of the particles before (SEM) and after (TEM) burning away the polystyrene core. 800 nm particles with 35 nm silica shell (a) and 800 nm particles with 15 nm silica shell (b). Inset: TEM image of the filled particles before burning.

Hollow shells can also be obtained by dispersing the core-shell particles in a solvent for polystyrene (THF, toluene). The polystyrene in the core passes through the pore of the silica shell and solves in the dispersant. This method did not work for silica shells thicker than 30 nm when the polystyrene cores were prepared by emulsion polymerization and about 50 nm

in case of polystyrene cores prepared by dispersion polymerization. This different behavior could be explained assuming that the silica shells grown on polystyrene cores prepared by emulsion polymerization have smaller pores with the respect to silica shells grown on polystyrene particles prepared by dispersion polymerization. In both cases, the permeability of the shells decreases with the shell thickness.

Attempts to measure the pore size were done by High Resolution TEM (HRTEM). By HRTEM, it was not possible to distinguish the pores from the structure of the copper grid on which the particles were dried.

The shape persistence of the core-shell particles[71] was tested in collaboration with Dr. Tim Still and Prof. Georg Fytas by Brillouin Light Scattering recording their vibrational eigenmodes as a function of temperature. A thin silica shell (40 nm) on 400 nm polystyrene core protects the spherical shape of the polystyrene core at temperatures above the Tg of the polymer. After the thermal treatment the shell is still intact and no polystyrene leakage was detected.

3.2 Mechanical properties of hollow silica spheres

The mechanical properties of the hollow silica spheres with different size and different shell thickness, prepared as described in the previous paragraph, were characterized by AFM. In this section, experiments and results are described. The AFM and NMR measurements were not performed by the author of this thesis; they were done in close cooperation with Dr. Li-Juan Zhang and Dr. Robert Graf, respectively.

3.2.1 Preparation of samples for AFM measurements

The elastic moduli of the hollow silica spheres were determined by applying a point load on a single hollow sphere using a sharp AFM tip with a radius of 20 nm. To prevent the spheres from shifting or rolling on the substrate during measurements, they were partially embedded in a thin PS film (initial polystyrene solution: 5.0 mg/mL, M_w = 130 000 g/mol dissolved in toluene) obtained by spin coating ((Delta 80 μB, Süss MicroTec Laboratory Equipment GMBH, Germany, 1000 rpm for 60 s, Figure 3.7). After that, hollow silica spheres dispersed in ethanol were deposited onto the glassy PS film by spin coating of the dispersion (2000 rpm for 60 s). The substrates were placed in an oven and kept at 150 °C for about 1 h. The melting of the film causes capillary forces that suck the spheres into the film and lead to a strong fixation onto the substrate. After cooling down to room temperature, the thickness of the PS films was measured using a surface profiler (KLA Tencor, LOT-Oriel GmbH & Co. KG, Germany) and was found to range between 55 and 75 nm depending on position.

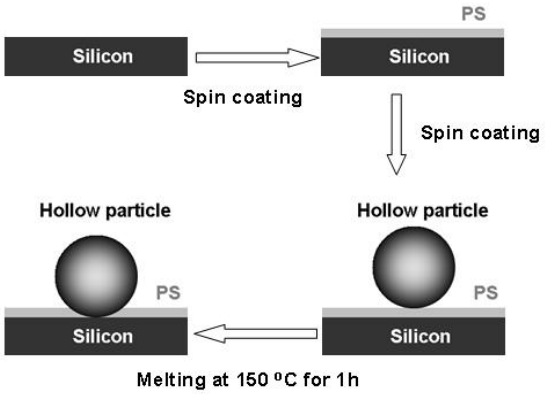

Figure 3.7. Schematic representation of the procedure used to immobilize the spheres on the substrate

3.2.2 AFM imaging

Before investigating the elastic response of the hollow silica spheres, particles were systematically imaged. In AFM images, the hollow spheres always appeared slightly larger and less spherical (Figure 3.8a) than in TEM, (Figure 3.6a, right side).

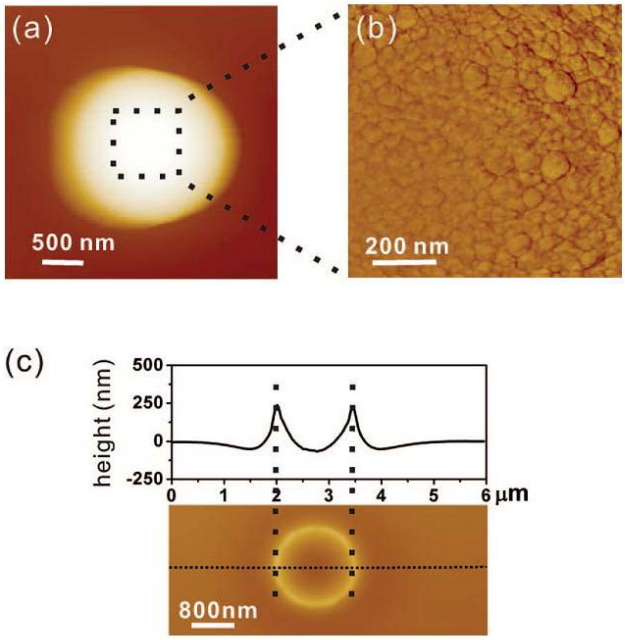

Figure 3.8. AFM height image of a hollow silica sphere with a diameter of 1.9 µm and a shell thickness of 50 nm (a) and a zoom in on the top of the sphere (b). The shell has a roughness of about 2.5 ± 0.5 nm. (c) Section analysis and an image of the groove formed after the sphere was removed. The depth of the groove h_{groove} is about 67 nm, which is close to the thickness of the PS film, $h_{PS} \approx 69$ nm, determined using a surface profiler.

This is a typical artifact from the convolution between the tip shape and the actual shape of the sphere. Zooming in on the top of the sphere allowed us to determine the surface roughness of the spheres (Figure 3.8b). Surface roughness was determined from height images by flattening the sphere top area (400 x 400 nm^2) and calculating the root-mean-square (rms) roughness. The shells grown on PS spheres synthesized by dispersion polymerization had a roughness of about 2.5 ± 0.5 nm, whereas the shells grown on PS synthesized by soap-free-emulsion polymerization had a surface roughness of only 1.6 ± 0.2 nm. In both cases, the shell seemed to consist of small silica particles (20-70 nm in diameter) merged together.

For the analysis of the force measurements, it is important to know whether the measured deformation originates only from deformation of the shells and not from deformation of the spin-coated PS film. If the immobilized spheres are separated from the silicon substrate by a thick PS layer, deformation of the softer PS film upon applying a point load to the top of the sphere might contribute substantially to the measured deformation. To check the thickness of the PS layer remaining underneath the spheres, we sheared off several spheres using a line scan of the AFM tip and imaged the resulting surface dimple. Figure 3.8c shows a height image (bottom) and cross section (top) along the dotted line. The bridge-like height profile shows the thickness variation of the PS film with respect to the thickness of the undistorted PS film (height ≡ 0). When approaching the groove from either side, the relative height levels first decrease by a few nanometers, then increase strongly, pass a maximum, and meet at negative values. The height of the PS ring depends on the wetting behavior of the silica-coated spheres toward PS. The difference between the thickness of the PS film as determined by the surface profiler h_{PS} and the groove depth h_{groove} yields the height of the residual PS layer Δh_{PS}. According to this analysis, only a few nanometers of the PS film (Δ_hPS ≈ 2-5 nm) remain between the sphere and the substrate.

3.2.3 Force versus deformation

Force versus distance curves on hollow silica spheres are obtained by applying a point load on their top with the AFM tip (Figure 3.9, details in the experimental part in par. 8.1.3).

At large distances, the force is zero, as the tip does not touch the sphere. When tip and sphere start to come into contact, the sphere starts to deform. A transition region of about 1 nm width where the relation between force and deformation was nonlinear was observed. After this regime, further approach led to a strong linear increase of the force. We used a fit of this linear part for evaluating the elastic properties and determining the distance for zero deformation. To obtain a force-deformation curve, for each force-distance curve we

determined the deformation at maximum applied force F_{max}. F_{max} is given by the intersection of the linear extrapolation of the force versus distance curve with the force axis (A in Figure 3.9). The corresponding deformation was determined from the intersection of the linear fit with the linear extrapolation of the zero deformation line (B in Figure 3.9). From each such force distance curve, one obtains a single data point (B, A) for the corresponding force versus deformation dependence. About 30 force curves were recorded for each maximum applied force.

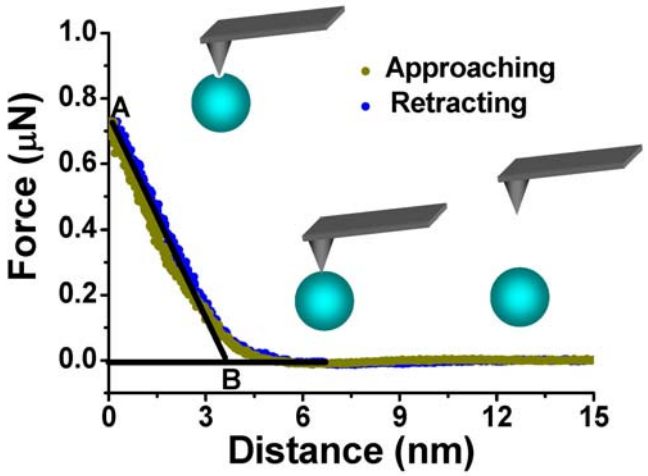

Figure 3.9. A typical force curve of a hollow silica sphere with a shell of 50 nm and a diameter of 1.9 μm, sample PSD (defined in Table 3.4). The open spheres denote the approach, and the filled spheres denote the retract part of the curve. Hardly any hysteresis is visible, i.e., the deformation is elastic.

From taking force curves at different defined maximum forces, we obtained the dependence of the deformation on the applied force shown in Figure 3.10. The plot shows a linear increase of force F_{max} with deformation for deformations of up to 30 nm. The clustering of the data points in Figure 3.10 gives the experimental error for each fixed load. It may be due to slight lateral variations of the shell thickness, as the position may change by a few nanometers while recording the force curves.

For deformations smaller than the shell thickness (Figure 3.9), the approaching and retracting curves are almost congruent and linear, indicating a fully reversible/elastic behavior. For larger deformations, the linear dependence of the deformation on the applied load breaks down indicating plastic deformation (inset in Figure 3.10).

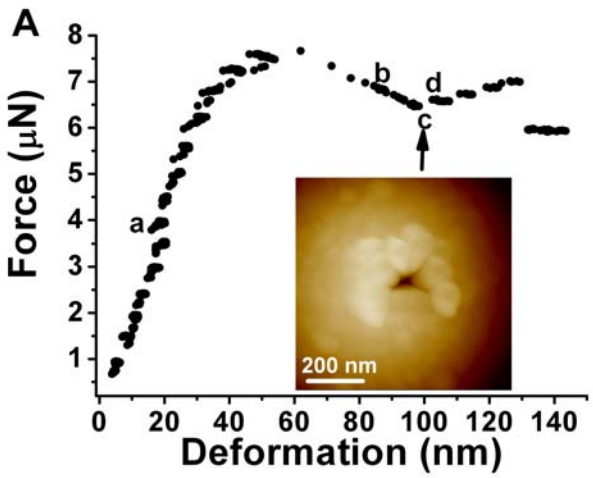

Figure 3.10. Deformation of a single hollow silica sphere under increasing cantilever deflection (Sample PSD: 1.9 μm sized silica capsule with a shell thickness of 70 nm). The force versus deformation curves are obtained from the approaching force versus distance curve in Figure 3.9. In the first part of the curve, the deformation of the shell increases linearly with the maximum loading force. Inset: AFM image taken after the approach curve showed a jump in. The dark spot in the middle of the sphere represents a hole in the shell.

3.2.4 Elastic response

At small deformations, i.e., as long as the reversible deformation increases linearly with the loading force, the Young's modulus *E* is given by the thin shell model[39]. The ratio between shell thickness and radius is smaller than ~1/10.

$$E = \frac{\sqrt{3(1-\nu^2)}}{4}\frac{FR}{dh_S^{\,2}} \qquad (2)$$

where *d* is the measured deformation divided by 2 (the thin shell theory only considers the deformation of one hemisphere. In our case, both, the upper and the lower hemisphere deform, i.e. the measured deformation need to be divided by 2), h_s is the shell thickness, *R* is the radius of sphere, *F* is the loading force, and *v* is the Poisson ratio. Assuming the Poisson ratio to be *v* = 0.17,2 eq. 2 reads

$$E = 0.43\frac{FR}{dh_S^{\,2}} \qquad (3)$$

Under these assumptions, the Young's modulus of the hollow spheres was found to be about 35 ± 6 GPa (Figure 3.11), irrespective of shell thickness and particle size. However, the measured value for the elastic modulus is only half of that for fused silica, E = 76 GPa[43].

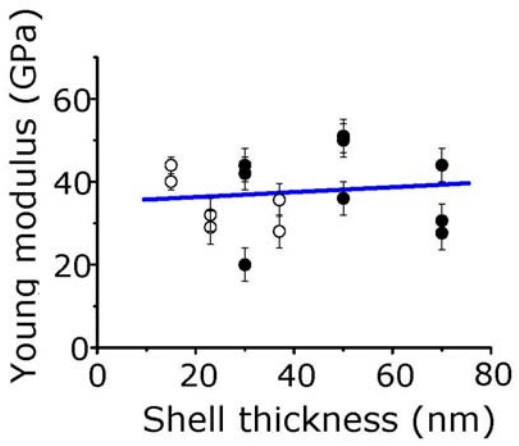

Figure 3.11. The Young's modulus E hardly depends on shell thickness h_s. Solid line: linear fit through the data points. Hollow circles: sample PSE; filled circles: sample PSD.

3.2.5 Force versus deformation curves at different annealing temperatures

The Young's modulus of single silica capsules by AFM force measurements resulted to be 35 ± 6 GPa for the sizes and thickness investigated[41]. This value is much smaller than that of fused silica[43], that is 72-76 GPa.

Is this difference due to the preparation procedure? It is known from elemental analysis that silica particles prepared by the Stöber method[60] still contain ethoxy and silanol groups and have a lower density than amorphous silica[72-74]. Does removal of the silanol groups increase the Young's modulus?

In order to clarify that, the dependence of the mechanical properties of silica capsules on annealing temperatures and the changes of its chemical structures and surface roughness after annealing was investigated. The deformations of silica microcapsules (diameter: 1.81 ± 0.04 μm; shell thickness: 52 ± 3 nm) were measured by AFM at room temperature and after annealing different temperatures. To investigate whether capsule stiffness and Young's modulus depend on temperature force curves on 1.81 ± 0.04 μm sized silica capsules annealed at different temperatures were taken.

3.2.6 Temperature dependence of the Young modulus

To calculate the Young's modulus the diameters and thicknesses of the capsules were first measured by SEM and TEM (Table 3.5). In SEM diameters were obtained by analyzing about 40-180 capsules and calculating the arithmetic mean. TEM data were collected by measuring the diameters or thicknesses of about 5-15 capsules at high magnification. Diameter measurements performed by TEM tended to give slightly larger values than SEM data. This may be caused by smaller statistical samples. Therefore, we used the SEM values for further data evaluation. In previous measurements the shell thickness was determined from the difference between particle diameters before and after growing the silica shell. This was not possible here, as annealing caused the diameters of silica microcapsules and their shell thickness to decrease continuously. Therefore, shell thickness was determined by TEM only (see darker area of the inserted image in Figure 3.12). After tempering at 1100 °C the capsule diameter decreased by almost 20%.

Table 3.5. SEM and TEM data of diameters and thicknesses of silica capsules before and after annealing at different temperatures. The numbers in brackets denote the number of capsules evaluated.

Temperature (^{o}C)	Diameter (μm) SEM	Diameter (μm) TEM	Thickness(nm) TEM
25	1.81 ± 0.04 (150)	1.83 ± 0.04	52 ± 3
300	1.75 ± 0.04 (180)	1.80 ± 0.04	43 ± 3
500	1.65 ± 0.04 (130)	1.72 ± 0.04	43 ± 6
850	1.63 ± 0.04 (140)	1.72 ± 0.03	43± 5
1000	1.62 ± 0.05 (40)	1.66 ± 0.04	39 ± 4
1100	1.52 ± 0.04 (140)	1.59 ± 0.04	42 ± 7

The Young modulus was calculated from the shell theory as described in the previous paragraph. For annealing temperatures below 850 ^{o}C, the Young's modulus slowly increases from ~ 15 to 40 GPa. Annealing at temperatures above 1000 ^{o}C causes a strong increase of the Young's modulus which becomes close to the value of fused silica, 72-76 GPa[43]. In this study, the calculated values slightly exceeded those of fused silica.

Adhesion or embedding of the particle to the substrate could make the contact on this side larger than pointlike. This would cause a slightly lower deformation there than at the top, and thus lead to a small overestimation of E. It also cannot be excluded that the applied load compresses the PS film between the capsule and the silica substrate, although its thickness has been determined to be below 5 nm (Figure 3.8c)). Both effects are expected to be marginal but easily may cause an overestimation of the Young's modulus by 10 %.

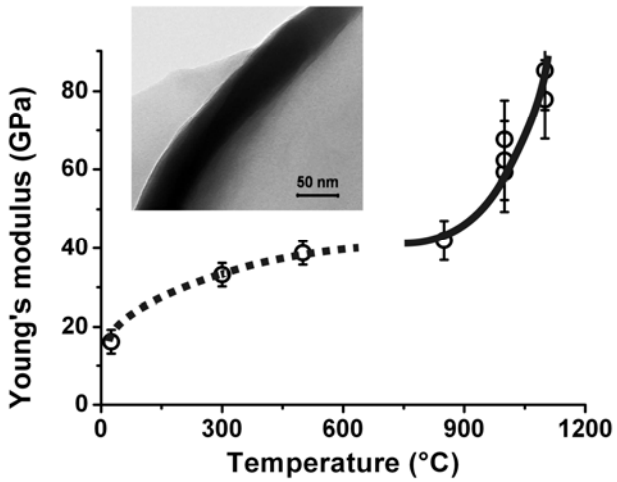

Figure 3.12. The Young's modulus increases with annealing temperature and approaches the value of fused silica after tempering at 1100 °C. The dashed line denotes the value for fused silica whereas the dotted and solid lines are guides to the eye. Insert: TEM image of a shell at high magnification. The dark area representing the shell shows uniform thickness.

3.2.7 Temperature dependence of the chemical structure studied by NMR

^{29}Si solid state NMR is a well established method to study the chemical environment of the silicon atoms in silica[61, 72, 75]; this technique permits to distinguish between Q^2, Q^3 and Q^4 silicon atoms (not sketched bonds are siloxane bonds; R = ethyl group or hydrogen):

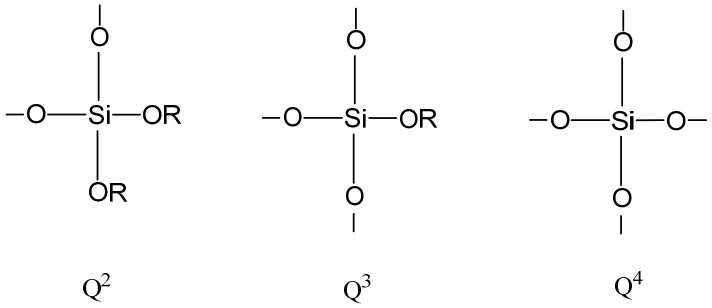

Q^2 Q^3 Q^4

From the relative amount of these different silicon atoms it is possible to quantify the level of condensation.

In order to relate the changes in the mechanical properties to changes in the chemical structure during the annealing process, ^{29}Si solid state NMR measurements have been performed at different stages of the annealing treatment.

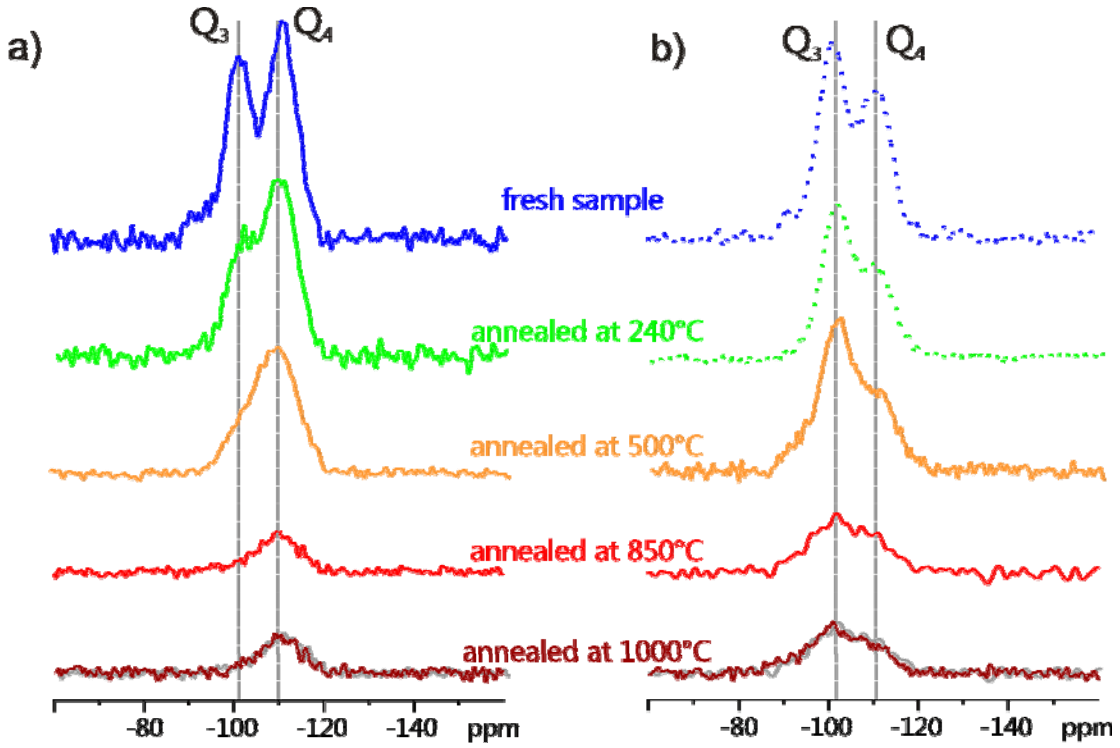

Figure 3.13. ^{29}Si magic-angle spinning nuclear magnetic resonance spectra recorded at 5 kHz MAS spinning frequency and ambient temperature. a) Direct excitation ^{29}Si MAS NMR spectra obtained with 15 s relaxation delay between subsequent transients for the three lower temperatures and 90 s for the two highest temperatures and a low tip angle. b) ^{29}Si cross-polarization magic-angle spinning NMR spectra recorded with 3 ms CP contact time and polyvinylpyrrolidone coating of the silica capsules after annealing.

^{29}Si MAS spectra obtained from direct excitation applying ^{1}H hetero-nuclear dipolar decoupling and relaxation delays of 20 s and 90 s (samples annealed at T > 800 °C) are shown in Figure 3.13a. The spectrum of the freshly prepared sample shows two broad signals at 101 ppm and 110 ppm of similar intensity, which can be assigned to Q^3 and Q^4 sites, respectively. The relative amount of 45% Q^3 and 55% Q^4 sites was estimated by deconvolution of the two signals. A low amount of Q^2 site could also be present in the sample, as indicated by the weak shoulder towards lower ppm values. The substantial line width of the NMR signals is indicative of the amorphous nature of silica. Upon annealing, the amount of Q^3 sites is strongly reduced and after annealing at 500 °C only a minor contribution of Q^3 sites to the spectrum is observed, resulting in an asymmetric line shape of the Q^4 site signal. The observed reduction of Q^3 sites proves that the formation of a denser silica network containing more Q^4 sites starts already at relatively low temperatures.

The sample annealed at 850°C showed a marked increase in T_1 relaxation time, compared to samples annealed at lower temperatures, so that the relaxation delay had to be increased to 90 s in order to obtain a spectrum. A weak reduction of Q^3 sites leads to a more symmetric line shape of the Q^4 site signal compared to that of the sample annealed at 500 °C. The sample annealed at 1000 °C did not exhibit any changes in the ^{29}Si MAS NMR spectrum within experimental accuracy. In order to allow for easier comparison, the ^{29}Si MAS NMR and ^{29}Si CP-MAS NMR results of the sample annealed at 850 °C have been overlaid in grey color to the NMR results of the sample annealed at 1000 °C. Thus, no structural changes in the silica network upon annealing at temperatures above 850 °C are observed.

A second solid state NMR approach via ^{1}H-^{29}Si CP-MAS after coating the annealed silica spheres with PVP is given in Figure 3.13b. In contrast to the direct excitation method it is difficult to quantify CP-MAS measurements. The CP-MAS method relies on polarization transfer from protons located at the surface of the particle to the silica sites in the material and the transfer efficiency strongly depends on the distance between the two spins involved. Therefore the signals of Q^3 sites, which in a perfect silica network are located at the surface only, are strongly over-represented. However, comparing ^{1}H-^{29}Si CP-MAS spectra recorded under the same conditions can provide additional information on possible changes in the network structure at the surface of the silica particles. The ^{1}H-^{29}Si CP-MAS spectra shown in Figure 3.13b are recorded with a CP contact time of 5 ms and a repetition time of 3 s between subsequent scans, taking advantage of the short T_1 relaxation time of the protons in the surface coating. For the samples without annealing or annealing at temperatures below 300 °C, the CP-MAS spectra are taken without PVP coating using the PS precursor particle as proton source. They are therefore displayed with dotted lines and should not be compared with the results from high temperature annealing with PVP coated particles. These two CP-MAS spectra indicate a minor reduction of Q^4 sites upon low temperature annealing, unlike the results from direct excitation. This difference, however, comes from PS leakage upon annealing. The PS, leaked out from the cores upon heating, wetted the outer surface of the silica shells leading to an overestimation of Q^3 sites. The fact that CP-MAS experiment monitors predominantly the particle surface, where the Q^3 sites are more abundant than in the bulk is clearly reflected in the experimental results given Figure 3.13b. Q^3 sites are observed in the CP-MAS measurements, even for the samples annealed at highest temperatures, where the single pulse excitation NMR spectra suggest a very dense silica network build from Q^4 sites only. Moreover, the ^{29}Si CP-MAS measurements confirm the conclusion from the direct excitation results, that the curing of the silica network is almost completed at an annealing temperature of T ~ 800 °C and that annealing at higher temperatures does not change the ratio of Q^3 and Q^4 sites in the silica network. Thus the substantial increase in stiffness obtained for samples annealed at T = 1000 °C and at

1100 °C cannot be attributed to a significant condensation of the capsules' silica network. Moreover, it should be pointed out, that the ^{29}Si MAS NMR measurements do not provide any evidence for an onset of crystallization in the silica network, which would lead to much narrower NMR signals.

3.2.8 Temperature dependence of the surface topography

Therefore the surface topography of single capsules before and after annealing by AFM was investigated. The surface of native capsules appears rough and is composed of small silica particles chemically bonded together (Figure 3.14a). Annealing the capsules at 1100 °C (close to their melting point of ~ 1150 °C) causes the surface to smoothen (Figure 3.14b). Even after sintering the capsules remain intact, although both their diameter and shell thickness decrease by approximately 20 %. According to SEM images, the capsules retain their spherical shape without any defects (Figure 3.14c). Smoothening also manifests itself in a decrease in RMS roughness from 1.9 for temperatures below 850 °C nm to 1.0 nm after annealing the capsules for 3.5 hours at 1100 °C, determined on an area of 400 × 400 nm^2.

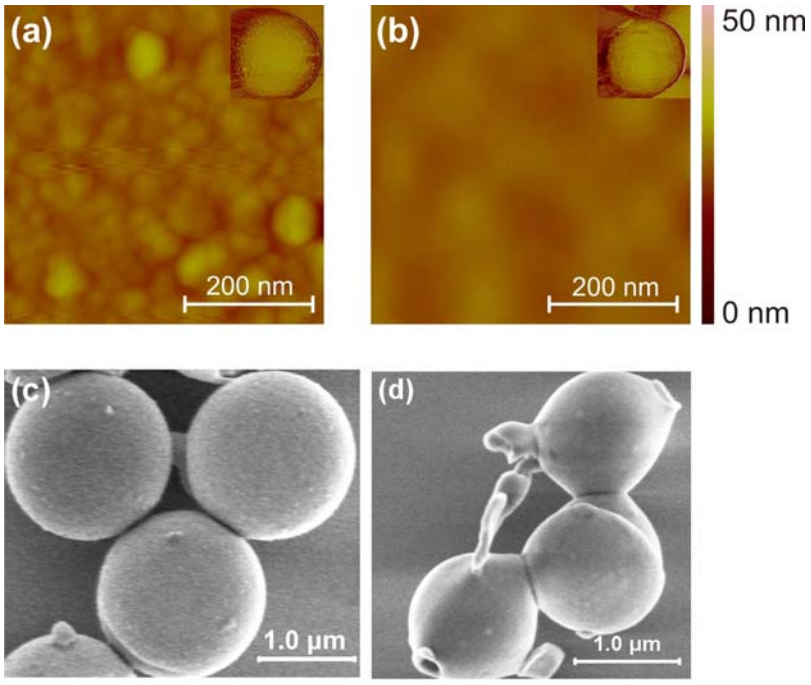

Figure 3.14. AFM height images of the surface of silica microcapsules before (a) and after (b) annealing at 1100 °C for 3 hours. AFM phase images of the whole capsules are given in the insets. SEM images of silica microcapsules annealed at 1100 °C for 3 hours (c) and 1150 °C for 3.5 hours (d). The surfaces of silica capsules smoothen upon heating to 1100 °C. The silica capsules stay spherical at 1100 °C, but change their morphology and begin to coalesce when annealed at 1150 °C.

When heated to 1150 °C the capsules start melting and their shells deform (Figure 3.14d). The decrease of the RMS roughness goes in line with a decrease of the pore size. After annealing at 850 °C and redispersing in ethanol about one third of the particles were floating, i.e. its pore size decreased below approx 6 A^2. This finding is supported by temperature dependent porosity measurements on porous silica films, showing a strong decrease of the porosity after annealing the films at temperatures above 850°C[76]. It is also completely in line with temperature annealing experiments performed on photonic crystals made from Stöber silica spheres where significant compaction on larger than nm length scales was also observed only at temperatures above 950 °C[77].

3.2.9 Conclusions

The Young's modulus of silica microcapsules as determined by AFM force-distance spectroscopy depends on surface and internal roughness and the number of silanol groups, which both depend on the annealing temperature. Measurements performed after annealing at temperatures between 20 ^oC and 1100 ^oC revealed that condensation and density increase upon heat treatment is a two-step process. Heating up to 850 ^oC strongly decreases the number of silanol groups significantly, but leaves the grainy surface structure unmodified. The change of the local chemical bond structure causes only a moderate increase of the Young's modulus with annealing temperature. At even higher temperatures, a strong increase of the Young's modulus accompanied by a smoothening of the capsule's surface and increase in density was observed. The resulting reduction of the effective capsule surface was demonstrated by AFM imaging, where a decrease in roughness was detected. The nano-sized silica particles of which the shells are composed of fuse together at temperatures > 1000 °C. Remarkably, the capsules retain their perfect spherical shape, although the diameter and shell thickness decrease by 20 %. Thus, high temperature annealing provides a method to obtain silica capsules with a completely closed shell with a thickness as thin as a few tens of nm and stiffness comparable to that of fused silica. Furthermore, characterizing the dependence of the Young's modulus on temperature and on changes in bond structure and surface morphology offers the possibility to use this dependence for tuning the mechanical properties of silica capsules.

4 Synthesis of core-shell particles with raspberry-like morphology

The present chapter describes the synthesis of hybrid raspberry-like particles that are used for the preparation of superhydrophobic surfaces[38]. They consist of a polystyrene core and a completely closed and rough silica shell. The synthesis of the polystyrene cores and the synthesis of core-shell particles with smooth silica shells are discussed in chapter 2 and 3, respectively.

Hence, this chapter is focused on the procedure to induce nanometer-sized roughness by growing small silica particles on polystyrene surface.

4.1 Synthesis of hybrid raspberry-like particles: reaction scheme

The preparation starts with the synthesis of micron-sized polystyrene particles by soap-free emulsion polymerization.

The next step is the coating of the particles with poly(vinylpyrrolidone) (PVP). By addition of the reagents for the synthesis of silica by Stöber method (tetraethoxysilane and water), small silica particles are grown on polystyrene surface. The particles obtained at this stage are called 'composite particles'.

The composite particles are coated with poly(allylamine hydrochloride) (PAH) in water and after that they are coated with PVP in ethanol. Stöber synthesis is performed again, and a smooth silica shell is formed throughout the 'composite particle' surface.

As a result, polystyrene particles completely encapsulated in a silica rough shell are obtained. They are called raspberry-like particles (shortcut "raspberry particles").

A general scheme of the reaction strategy is given in Figure 4.1.

4.1.1 1st Step: synthesis of "composite particles"

The synthesis of raspberry particles starts with the coating of the negatively charged polystyrene particles with polyvinylpyrrolidone (PVP)[78, 79]. Later on it turned out that this step is superfluous (par. 4.1.1.4), but since most reactions were performed including PVP coating, this step is considered in the general discussion.

Silica nanoparticles are grown on the PVP coated surface following the Stöber method, that is formation of silica by hydrolysis and condensation of tetraethoxysilane (TES) catalyzed by ammonia. We refer to these particles as "composite particles".

The preparation of composite particles is a crucial step in the whole preparation, because it permits the introduction of the desired nano-sized roughness. To investigate the possibility to tune the roughness by varying the reaction parameters, several systematic experiments were performed and they are discussed in the following paragraphs.

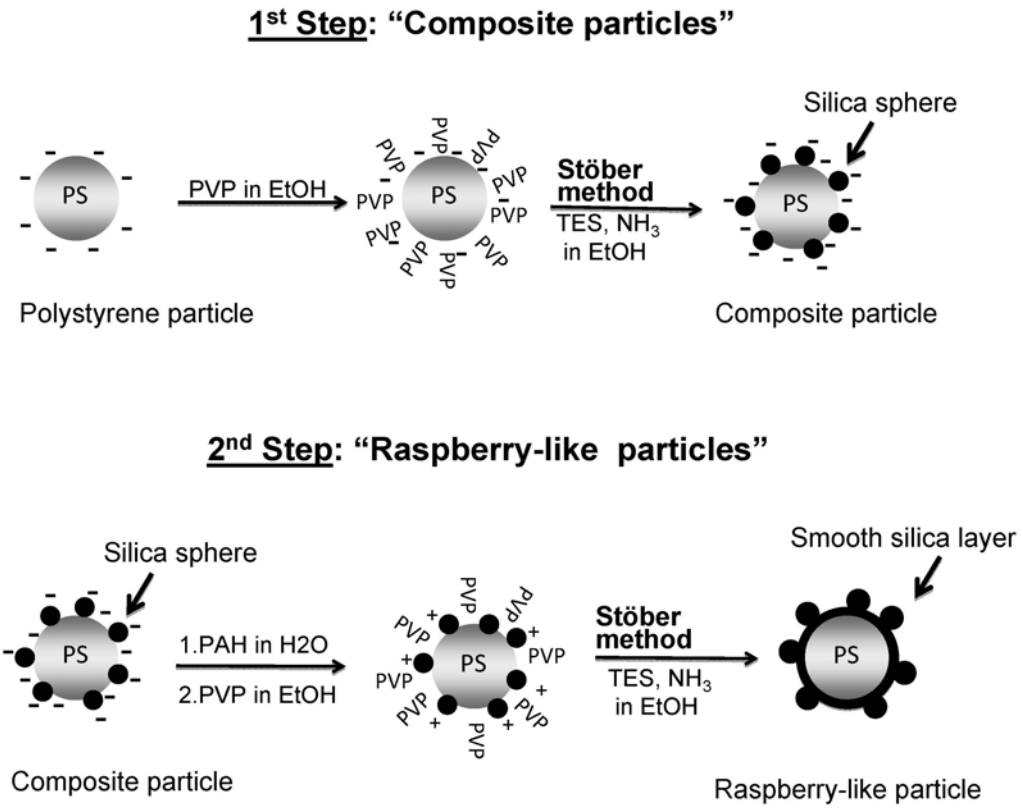

Figure 4.1. Schematic illustration of the synthesis of raspberry-like particles. First step: synthesis of composite particles. They consist of nano-sized silica particles adsorbed on the surface of micron-sized polystyrene particles. Second step: synthesis of raspberry-like particles. They consist of a polystyrene core completely encapsulated in a rough silica shell.

For this study, several batches of polystyrene particles were synthesized (reaction conditions in Table 4.1, experimental procedures in par. 8.2.2). These particles were used as templates for the synthesis of composite particles (reaction conditions in Table 4.2, experimental procedures in par. 8.2.5). The general experimental procedures are described in detail in chapter 8. The results of the different reactions are discussed in the next paragraphs, focusing on the meaning of acrylic acid, TES as well as PVP.

Table 4.1. Primary PS particles are obtained by soap-free emulsion polymerization. The amount of acrylic acid is given with respect to the amount of styrene in the reaction mixture. Batch E2E1 refers to seeded soap-free emulsion polymerization. 38 ml of the reaction mixture E2 was transferred in a clean 500 ml flask and 300 ml of milli-Q water were added. Particle radius is measured by SEM images averaging over more than 100 particles.

Batch	ammonium persulfate (g)	NaCl (g)	acrylic acid % wt/wt	styrene (g)	radius (nm)
E1	0.11	-	1	15.4	225 ± 8
E2	0.11	0.2	0.6	25	334 ± 40
E3	0.11	0.2	0.8	13.6	282 ± 16
E4	0.11	0.2	1.6	13.6	290 ± 13
E5	0.11	0.05	1.7	11.8	223 ± 9
E6	0.11	0.05	-	11.8	215 ± 9
E2E1	0.4	-	0.6	7.2	540 ± 30

Table 4.2. Reaction conditions for the synthesis of composite particles according to the Stöber mechanism.

Batch	PS particles (g)	PVP/ethanol (g/ml)	ammonia 25 % (ml)	TEOS/ethanol (ml/ml)
S1	1.54	1.63/80	6.6	2/18 (in 4 steps in 5 h)
S2	0.05	0.013/5.8	0.44	0.16/0
S3	0.153	0.163/8	0.66	0.5/1.5
S4	0.153	No PVP/8	0.66	0.5/1.5
S5	0.156	0.04/8	1.32	0.5/0
S6	0.153	0.163/8	1.32	0.5/1.5

4.1.1.1 Size of PS templates

Synthesis of composite particles can be performed on PS particles of a wide range of sizes. Their overall diameter can be tuned by the size of the PS template. As an example, in Figure 4.2 the composite particles are shown obtained by using 400 and 1000 nm polystyrene particles as template. Both small (Figure 4.2a) and large (Figure 4.2b) polystyrene templates are decorated by a large number of irregularly distributed silica spheres with an almost uniform size of 100 ± 20 nm. According to the image taken at higher magnification (Figure 4.2c) the silica colloids are not spherical but slightly elliptical. This hints that after nucleation or early attachment the growth of silica takes place predominantly on pre-existing silica

instead of the PS surface. The size of the silica granules does not depend on the size of the PS template.

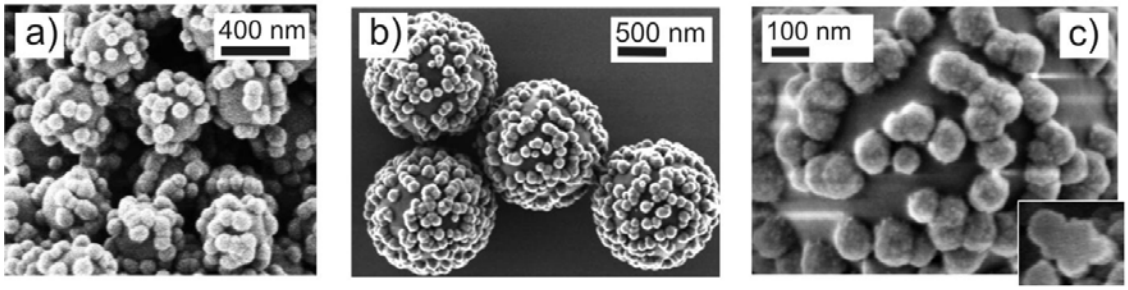

Figure 4.2. SEM images of composite particles using PS templates of different diameter: a) 400 nm sized PS particles (Table 4.1, E1). b) The 1000 nm sized PS (Table 4.1, E2E1). c) High magnification image of the surface of a particle shown in b). The Stöber reactions were performed according to procedure S5 (Table 4.2) and S1 (Table 4.2). Inset: Small silica particles detached from polystyrene surface.

4.1.1.2 Growth of silica colloids

To investigate the growth process in more detail we imaged aliquots of the reaction mixture without further purification after increasing reaction times. The size of the colloids increased in course of the reaction (Figure 4.3).

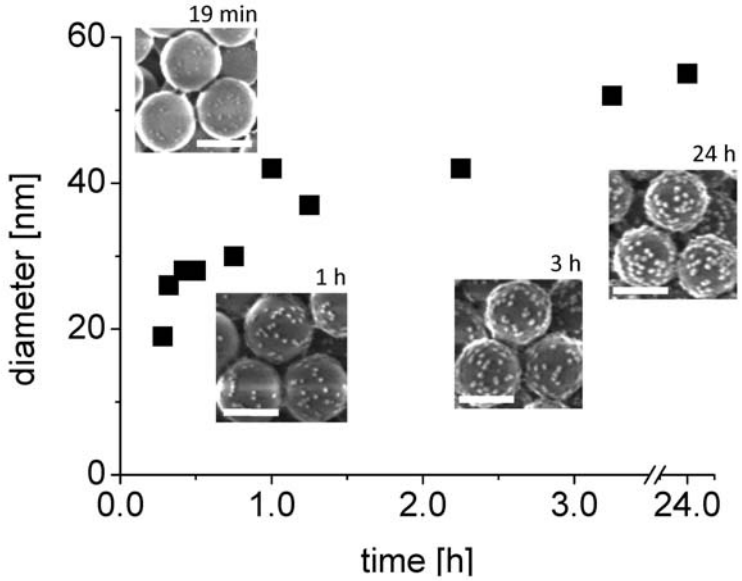

Figure 4.3. Dependence of the size of the silica colloids on reaction time. The PS particles were synthesized according to procedure E4 and the Stöber synthesis according to S2. Scale bar: 0.5µm

Already after 20 min, 30 nm sized silica colloids appeared on the surface of the PS particles. After this initial fast growth, the silica grain size steadily increased until it approached 55 ± 5 nm after 3 h. Thereafter, the size remained almost constant. The growth process is limited by lack of reaction material. From the images in Figure 4.3 it cannot be decided whether silica particles nucleate on the template surface or new particles nucleated in the bulk continuously attach to it.

4.1.1.3 Acrylic acid (AA) dependence

The number of the silica colloids attached to the surface of the PS particles depends on the amount of acrylic acid included in the template synthesis (Figure 4.4). SEM images revealed that silica particles were attached to the surface of PS particles at all AA concentrations tested. However, at low AA concentrations the colloids detach during centrifugation and only a small number of silica colloids stick to the PS surface (Figure 4.4a). Only at AA concentrations larger ≈ 1 % wt/wt the silica spheres are sufficiently strongly bonded to the surface that they remain attached even after several centrifugation steps (Figure 4.4b). However, still a large number of silica particles were found in solution, having almost the same size as those at the surface. This suggests that either nucleation only happens in the solution and the small particles afterwards bind to the large particles or that nucleation happens both at the surface of the large particles and in solution at the same time (Figure 4.4b, inset). Therefore, AA is responsible for binding silica particles to the PS surface.

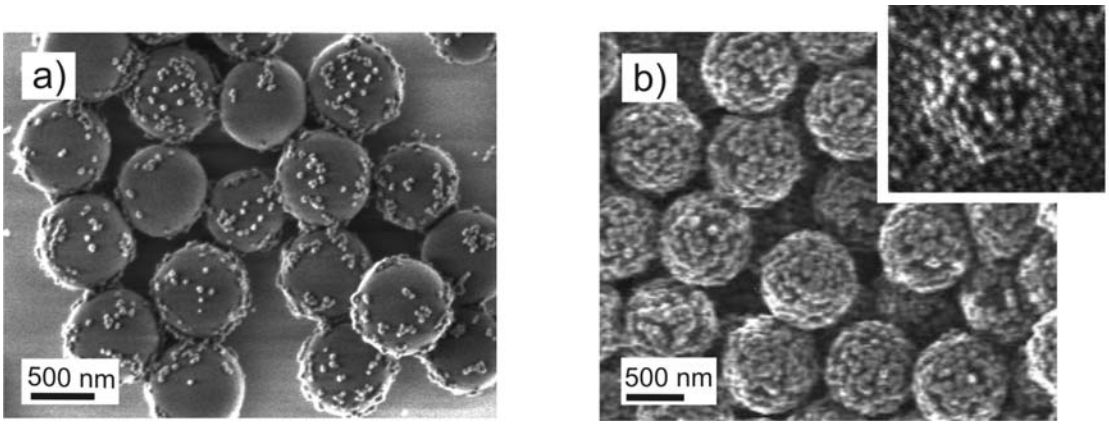

Figure 4.4 SEM images of composite particles. The PS templates contain different amounts of acrylic acid. a) Table1, batch E3; b) Table 1, batch E4. The Stöber synthesis was performed according to procedure S2 (Table 2). Nucleation of silica particles occurs thoughout the reaction mixture, indicated by abundant silica particles not attached to the PS surface in an unwashed sample (inset).

To further confirm this statement, polystyrene particles without acrylic acid were synthesized (batch E6) and used in the synthesis of the composite particles (batch S6). The particles obtained (Figure 4.5) are no composite particles because hardly any silica particles stuck to polystyrene surface. Silica grew mostly in solution. Only few particles grew on the polystyrene surface but they detached from it upon centrifugation.

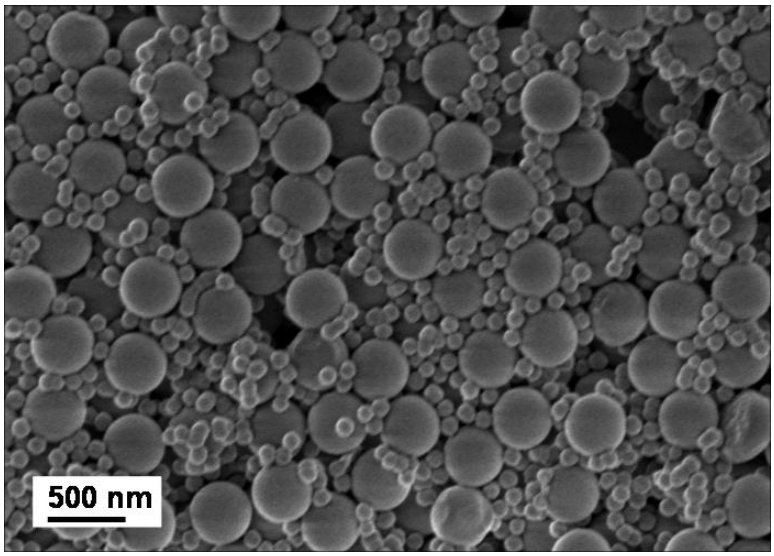

Figure 4.5. Synthesis of composite particles (batch S6, Table 4.2) performed with polystyrene particles synthesized without acrylic acid in the reaction mixture (batch E6, Table 4.1).

4.1.1.4 PVP dependence

Why silica attaches to the PS surface is still unclear. Silica may bind directly to the PS surface due to hydrogen bond interaction between AA and silica. On the one hand higher AA concentrations may secure a better PVP coating due to formation of hydrogen bonds between AA and PVP and therefore better binding of silica. The compatibility between PS and silica can be increased by coating PS with PVP[41, 66, 78, 79]. To gain more insight on the influence of PVP on nucleation or attachment of silica on PS, composite particles with (Figure 4.6 a) and without PVP (Figure 4.6b) were synthesized. TEOS and ammonia were added to the reaction mixture without removing excess PVP. Whereas the diameter of silica colloids was 50 ± 20 nm with PVP coating, under otherwise identical conditions it increased up to 120 ± 30 nm if uncoated PS particles were used. To investigate whether silica particles detached or nucleate in solution, a drop of the reaction mixture (not washed) was put on top of a SEM substrate and let it dry. SEM images of uncleaned suspensions revealed that in

case of PVP coating the number of silica colloids in solution is much higher than without PVP coating (Figure 6b, inset). Due to the huge number of silica particles, the SEM images appear smeared and therefore are not shown. The increase of the number of particles for smaller sizes is consistent with conservation of total volume of silica, which is determined by the amount of TEOS. This strong increased number of silica particles is explained by the fact that the sample were not cleaned after PVP coating; hence, dissolved PVP induces disseminated silica nucleation in the solution. Conversely, without PVP coating nucleation in the bulk fluid is strongly reduced and the colloids grow to a larger size. These (Figure 4.6) and further experiments varying the ammonia content show that the number of silica colloids bonded to the PS surface does not depend on previous PVP coating, i.e. PVP does not influence attachment of silica particles. Therefore AA is responsible for attachment of silica. This can be due to formation of hydrogen bonds between carboxylic groups (AA) and hydroxyl groups (silica) under assumption that silica hardly dissociates in ethanol (Figure 4.6c, bottom).

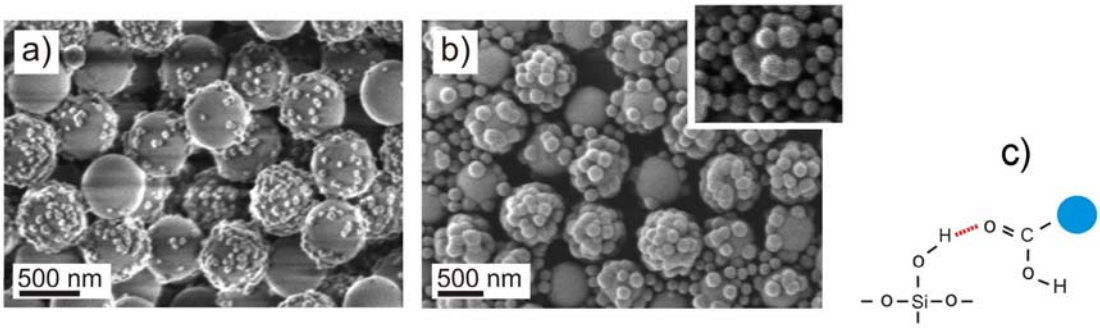

Figure 4.6. Composite particles synthesized using PS templates coated with (a: S3) or without (b: S4) PVP. The diameter of the silica colloids is 50 ± 20 nm (a) and 120 ± 30 nm (b), respectively. Inset: Silica particles also nucleate in solution, however, their size does not depend on whether they grow in solution or on the surface. Polystyrene Batch E5, Tab. 1. (c) Sketch: formation of hydrogen bonds between silica and the carboxylic groups of the PS particle.

4.1.2 2nd Step: synthesis of hybrid raspberry-like particles

The “composite particles” already present the dual scale roughness required for the fabrication of superhydrophobic surfaces. Nevertheless, the concept of inducing polymer bridges via polystyrene leakage (chapter 6) is only feasible if the particles are coated by complete silica shells. To encapsulate the composite particles, a smooth shell is grown on them according to the synthesis discussed in chapter 3. The composite particles are immersed in a water solution of poly(allylamine hydrochloride) (PAH). Subsequently, they are

coated with PVP and Stöber synthesis is performed again (second step in Figure 4.1, recipe in chapter 8, par. 8.2.5).

The resulting “hybrid raspberry-like particles” have a polystyrene core and a completely closed rough silica shell with unchanged nanoscale roughness with respect to the composite particles (Figure 4.7a). The thickness of the shell can be tuned via the amount of TES (chapter 3). To ensure that the silica coverage is complete, a small amount of sample was heated to 500 ˚C for 4 hours in order to remove the polystyrene core. SEM images (Figure 4.7b) after thermal treatment show that the particles are still intact and their shape is unchanged. The shell thickness can be estimated from the few broken ones to be a few tens of nm (Figure 4.7c).

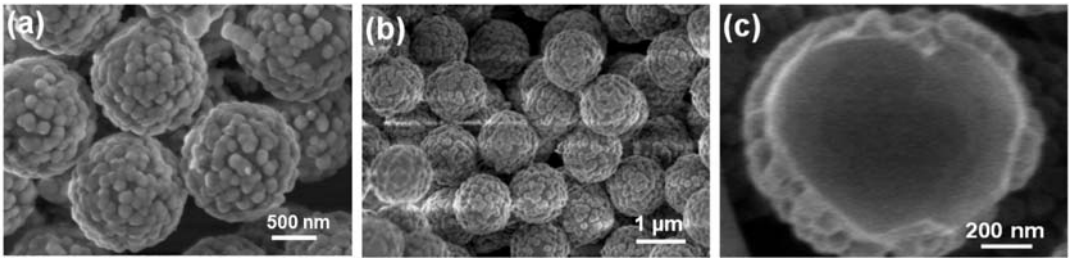

Figure 4.7. SEM images of raspberry particles. Particles before thermal treatment (a), hollow particles after thermal treatment at 500 ˚C (b), and a broken empty shell(c).

5 Superhydrophobic monolayer with raspberry-like particles

The present chapter and the next one will describe the preparation and characterization of superhydrophobic surfaces made of the raspberry particles synthesized as described in Chapter 4.

In particular, this chapter describes and compares the preparation of a superhydrophobic monolayer using two different techniques: Langmuir-Blodgett deposition and layer-by-layer (LbL) assembly.

The monolayers obtained by the Langmuir-Blodgett technique were closely packed, forming an ordered arrangement with the particles positioned at short mutual distances.

On the contrary, the samples prepared by the layer-by-layer assembly showed a disordered arrangement of the particles with a much larger mutual distance.

The hydrophobicity of the surfaces prepared in the two different ways was compared; only the sample arranged by the layer-by-layer technique was superhydrophobic.

Nevertheless, these kinds of coating showed a high fragility. The preliminary attempts that were subsequently made to improve the mechanical resistance of the samples are discussed.

5.1 Monolayer formation using the Langmuir-Blodgett technique

The Langmuir-Blodgett technique is a well established method that allows an ordered monolayer (or crystals) of molecules or colloids to be formed on a solid substrate. In the case of colloids, the colloidal particles are mixed with a volatile solvent, which acts as a spreading solvent. The colloid-solvent mixture is then spread drop-wise to an air-water interface between two Teflon barriers. After the solvent evaporates, the particles remain at the interface, where their separation distance is large due to the large area per particle and their inter-electrostatic repulsion (if they are charged). The distance between the particles can be controlled by compressing the two Teflon barriers, which cause the interfacial area per particle to be reduced. The beginning of a compression causes the particles to become closer, but to still show a disordered state. Further compression results in a transition from this disordered state to an ordered distribution of particles; this process can be compared to a liquid-solid transition. Additional compression causes a compact monolayer. A substrate may be coated with the particles in this ordered state by using the Langmuir-Blodgett technique. Briefly, a substrate that was inserted in the water phase before spreading the colloids is vertically lifted slowly through the colloidal monolayer, after the monolayer was brought to the desired state.

A key factor in transferring a close-packed monolayer on the substrate consists in establishing the level of compression corresponding to a compact monolayer. In order to do that, the surface pressure is monitored with respect to the compressed area, while the temperature of the water is kept constant. The presence of particles at an air-water interface reduces the surface tension of the air-water interface. The compression of the particles results in a greater number of particles per surface area, causing a lower interfacial tension. The instrument used for the Langmuir-Blodgett deposition is called “Langmuir trough” and its schematic illustration is given in Figure 5.1.

It consists of a Teflon trough filled with water to the upper level. The particles dispersed in a solvent other than water (generally lighter and more hydrophobic) are spread on the water surface by gently depositing them with a syringe at several positions on the area available.

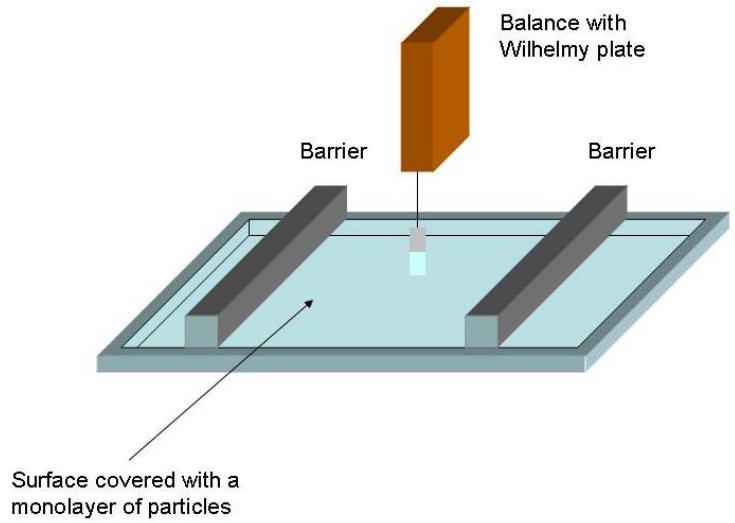

Figure 5.1. Schematic illustration of a Langmuir trough with a Wilhelmy plate electrobalance measuring the surface pressure, and barriers for reducing the available surface area (Sketch partially reproduced from ref. [80]).

After the solvent evaporated, only the particles remain at the water-air interface, forming a disordered monolayer at high reciprocal distances.

The barriers are then moved towards the center, causing a reduction in the interfacial area. At the same time, the change in the surface tension is monitored according to the following relationship:

$$\Pi = \gamma_0 - \gamma \qquad (1)$$

Where γ_0 is the surface pressure of pure water, and γ is the surface pressure in presence of particles. By means of this Π-area curve, it is possible to detect the surface tension corresponding to a closed packed monolayer (a practical example is shown hereinafter). The vertical lifting must start at this value of surface tension/degree of compression.

In the experiments performed, the solid substrate was a microscope glass slide (1 x 2 cm) and 1 μm raspberry particles were used (more practical details in paragraph 8.2.10).

Several tests were performed, in order to find the right conditions to get a compact monolayer.

Figure 5.2 shows the surface pressure as defined in eq. (1) versus surface area. The experiment was performed by spreading 700 μl of particles dispersed in ethanol (c = 40 g/L). After evaporation of ethanol, the compression was started and the surface pressure changes were registered.

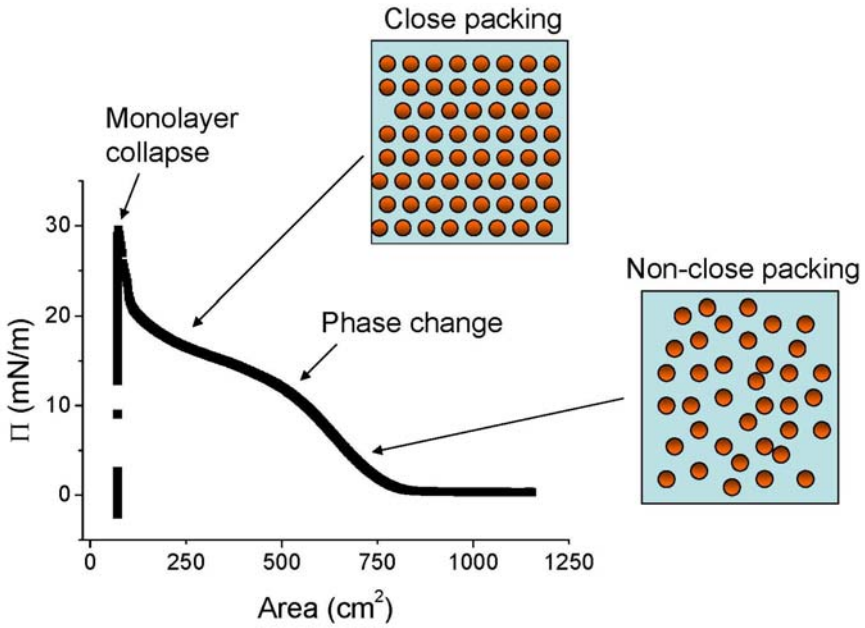

Figure 5.2. Changes in surface pressure plotted versus compressed area of raspberry particles suspended at water/air interface and sketches of the particle distribution corresponding to different regions of the graph (speed of compression: 5 cm^2/min).

In the very beginning of the compression, no change in the surface pressure was detected because the area available per particle was too large. The influence of the particles on the surface pressure is negligible. When the surface area reached approx. 800 cm^2, the surface pressure increased (corresponding to a reduction of the interfacial tension of the interface, eq.1) until the slope of the curve changes. This region corresponds to particles arranged closer to each other, but still not closely packed (ordered and disordered regions coexist).

After the change in slope[81], the next region (500-200 cm^2) corresponds to particles arranged in an ordered packing (comparable to a solid phase). Further compression of the area causes multilayer formation or sinking of the particles. So, in the case under study, the suitable surface pressure for transfer was around 20 mN/m.

Several samples were prepared by starting the vertical lifting at a pressure from 16 mN/m to 20 mN/m. Observation of the sample under a microscope showed an ordered arrangement of the particles. However, the packing was not perfectly closely-packed. The same experiments were then performed by spreading a slightly larger amount of particles (800 µl from a 40 g/L dispersion) at a surface pressure from 16 mN/m to 20 mN/m. These parameters were seen to be the most suitable to give a good coating.

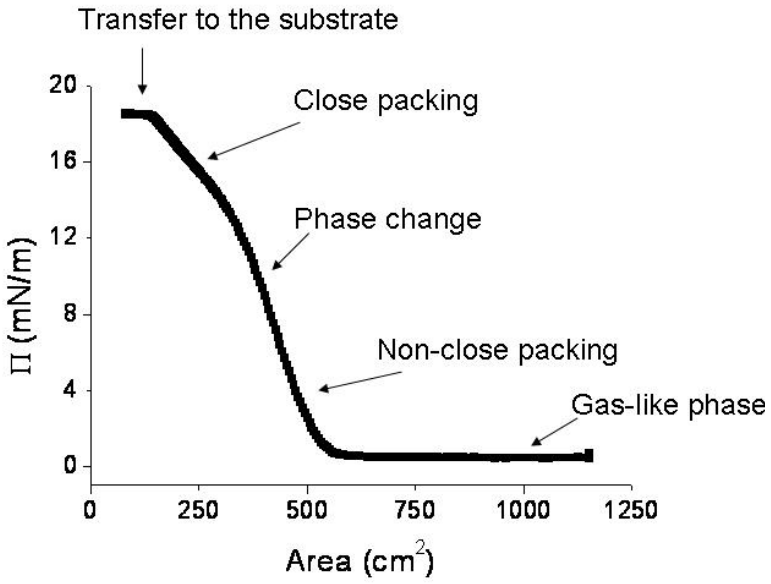

Figure 5.3. Changes in surface pressure plotted versus compressed area of raspberry particles suspended at water/air. The constant slope of the curve for small value of the area correspond to the transfer of the particles on the glass substrate.

As an example, Figure 5.3 shows the isotherm for the monolayer transfer, which was performed at a surface pressure of 18 mN/m.

The region between 200 and 100 cm^2, where Π is constant, corresponds to the transfer of the particles on the substrate. The constancy of the surface pressure indicates that the system was stable during the transfer.

The ordered structure of the monolayer could be easily verified inspecting the whole surface by optical microscopy (Leica CTR 6000). An example is shown in Figure 5.4, which shows a microscope image of one monolayer at a magnification of 50 times. Each bright spot

corresponds to a raspberry particle with a diameter of ~1 μm. Large ordered domains are visible and an inspection of the whole area of the sample shows the same feature.

SEM images were taken at different position of the same sample, at different magnifications, and for samples prepared at different surface tensions. Their feature is well represented by the images shown in Figure 5.5, where ordered domains of particles are visible as well as some defects. The defects were mostly due to groups of particles at higher relative distances or single particles deposited on the top of the ordered monolayer.

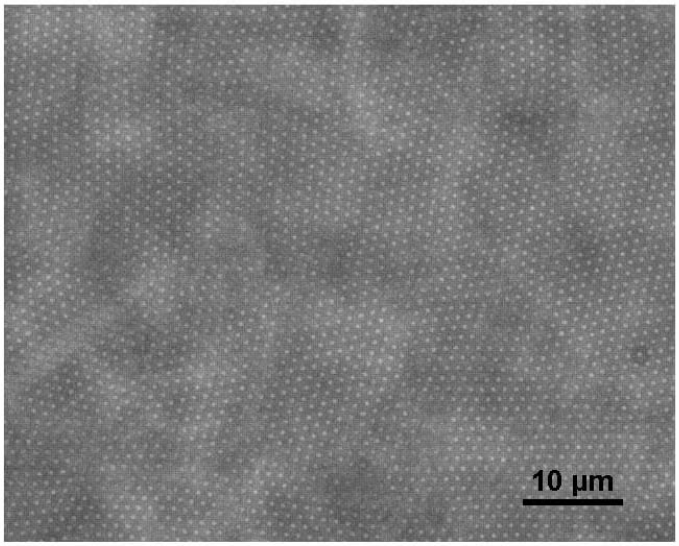

Figure 5.4. Optical microscope image of a monolayer of raspberry particles (diameter ~ 1 μm). Image taken with a 50x objective.

As already highlighted, no substantial difference in the morphology of the films prepared at 16, 19 and 20 mN/m could be quantified.

After hydrophobization by chemical vapor deposition (CVD) of trichloro(1*H*,1*H*,2*H*,2*H*-perfluorooctyl)silane (details on this procedure in chapter 8, par. 8.2.12), the surfaces were characterized by contact angle and tilting angle measurements. Contact angle experiments showed values of about 145 ± 5˚. However, no roll-off of the water drop could be observed, even for tilting angles as high as 90˚(Figure 5.6). Upon tilting the plane by 90˚, the drop is strongly deformed by gravity (Figure 5.6b) but it does not roll off (the hysteresis is high).

These results are consistent with the ones reported by Lee[36] et al. They also prepared compact and ordered monolayer of raspberry particles made of pure silica and found a high contact angle hysteresis.

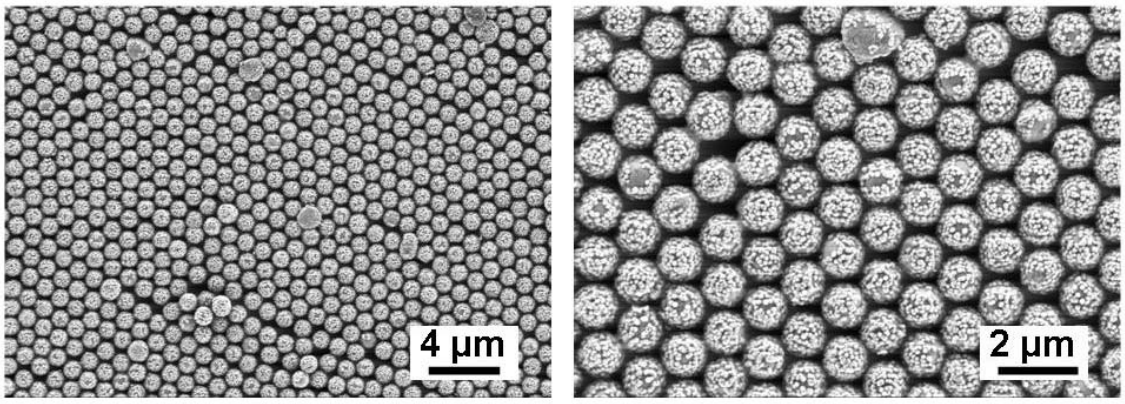

Figure 5.5. SEM at different magnification of a monolayer of raspberry particles prepared by Langmuir-Blodgett technique.

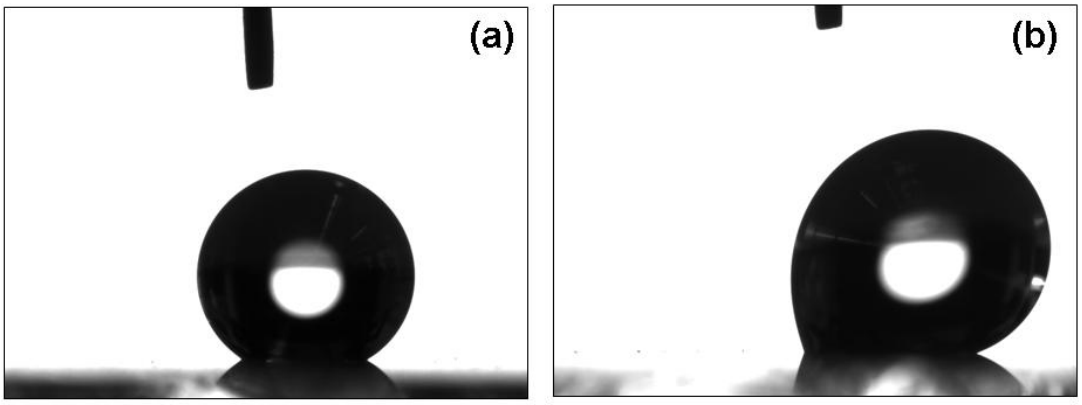

Figure 5.6. Images of a 3 µl water drop on a monolayer of particles prepared by Langmuir-Blodgett technique (a). 5 µl water drop on the same surface upon tilting the plane by 90˚.

5.2 Monolayer by layer-by-layer technique

Layer-by-layer technique offers the possibility to deposit particles on a glass substrate by means of the electrostatic attraction between opposite charges. Silica surface in water is negatively charged and the same stands for the glass substrate used as support. By reversing the charge of the glass slide by a positively charged polyelectrolyte it is possible to adsorb the raspberry particles on the slide by dip-coating.

In practice, a clean microscope glass slide (1 x 2 cm) was dipped into a water solution of poly(allylamine hydrochloride), in order to reverse its charge from negative to positive. After rinsing two times with fresh water, the slide was then immersed for 5 minutes in a dispersion

of raspberry particles in water (negatively charged). The schematic illustration of the procedure is shown in Figure 5.7 (chapter 8, par. 8.2.9 for details).

After drying, the sample surface was hydrophobized by chemical vapor deposition (CVD) of trichloro(1*H*,1*H*,2*H*,2*H*-perfluorooctyl)silane, a semi-fluorinated silane.

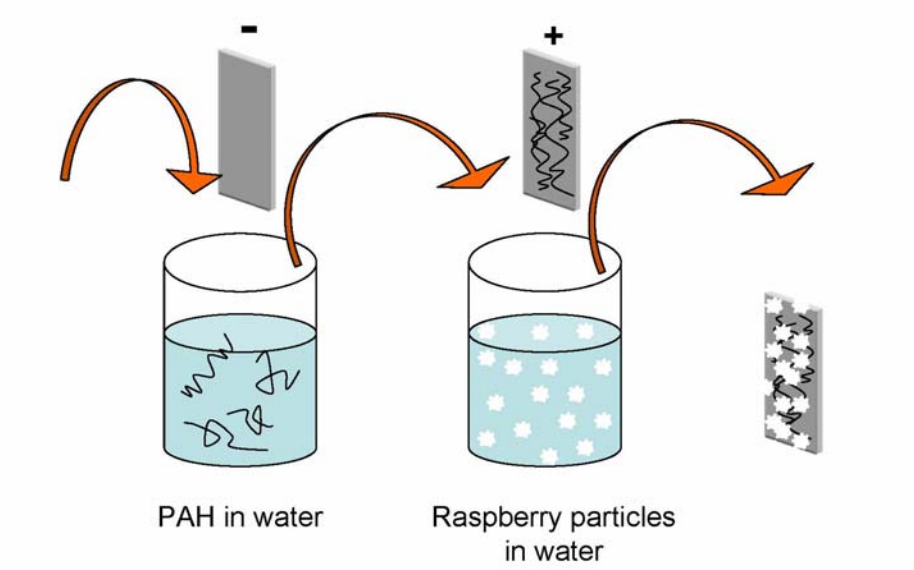

Figure 5.7. Sketch of the preparation of superhydrophobic monolayer with raspberry-like particles. The slide is dipped in a PAH solution and then in a particle dispersion. After each immersion there is always an intensive rinsing step with fresh water.

The samples prepared in this way were superhydrophobic, with a contact angle ≥ 160° and a tilting angle of a few degrees (< 10°).

The description of the contact angle and tilting angle measurements are given in chapter 8 (par. 8.1.6 and 8.1.7).

Figure 5.8 shows the Scanning Electron Microscopy image of a surface obtained using this procedure (a) and a water drop deposited on this surface (b).

The particles form a homogeneous “2D network” that only partially covers the glass surface. As SEM can image only a relatively small area of the sample, parallel inspections throughout the whole surface were regularly done by optical microscopy in order to verify the homogeneity of the surface over a large scale. The samples show the same 2D structure everywhere, such as the one shown in figure 5.8(a).

Several attempts were made to get a multilayer of particles by simply repeating the above procedure several times on the same substrate. Unfortunately, it was not possible to go beyond the first layer, apart for a few particles found attached on the ones in the first layer. This is likely due to the large size of the particles (1 ~ μm). It is possible that the electrostatic

attraction is not strong enough to keep them on top of one another, especially considering the fact that the highly rough surface limits the possibility of contact.

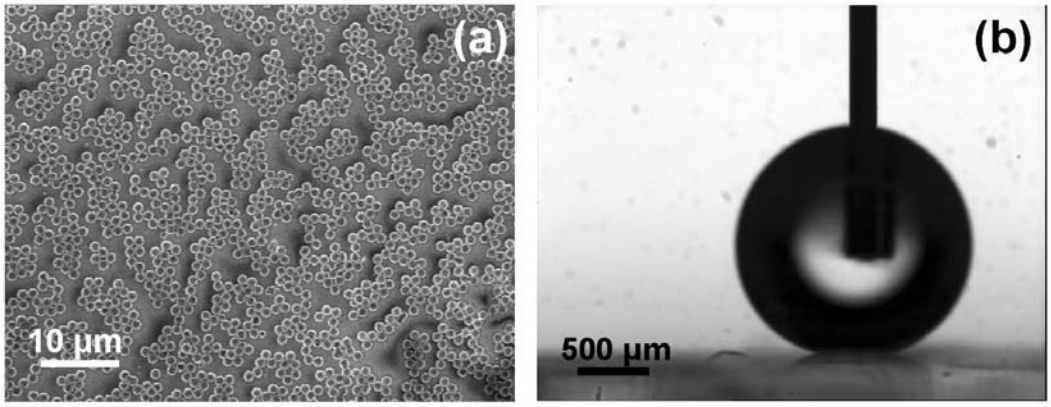

Figure 5.8. SEM image of the film prepared with 1 layer of raspberry particles (a), and image of a water drop deposited on the surface (b).

Despite the very good superhydrophobicity and the high reproducibility of the procedure, these surfaces suffer from a bad mechanical resistance.

The structure is kept together by electrostatic attraction only at the point of contact between the glass and the particles. It therefore breaks under even a very small stress.

Upon contact with a water drop, the detachment of particles from the surface can be visualized. After removing the drop, locally the sample looses its superhydrophobic behavior.

In the following paragraph, the first attempts to improve the mechanical properties are discussed.

The main idea behind them is to combine the mechanical properties of silica and polystyrene, in order to design a more resistant surface.

5.2.1 Surfaces with improved mechanical properties

The procedure described in the previous paragraph can be in principle also applied to other kinds of particles, as long as they are negatively charged.

Polystyrene particles, synthesized as described in Chapter 2, are also negatively charged. They can interact with positively charged surfaces as well. Hence, they were used to form a "hybrid" multilayer by alternating a layer of polystyrene particles with a layer of raspberry-like particles.

The preparation consists of dipping the glass slide in PAH, in order to make the outer surface positively charged. The slide was then dipped in a dispersion of polystyrene particles, again

in PAH solution to reverse the charge, and then in a dispersion of raspberry-like particles. Two consecutive rinsing steps with milli-Q water followed each dipping step. Figure 5.9 schematically shows the preparation.

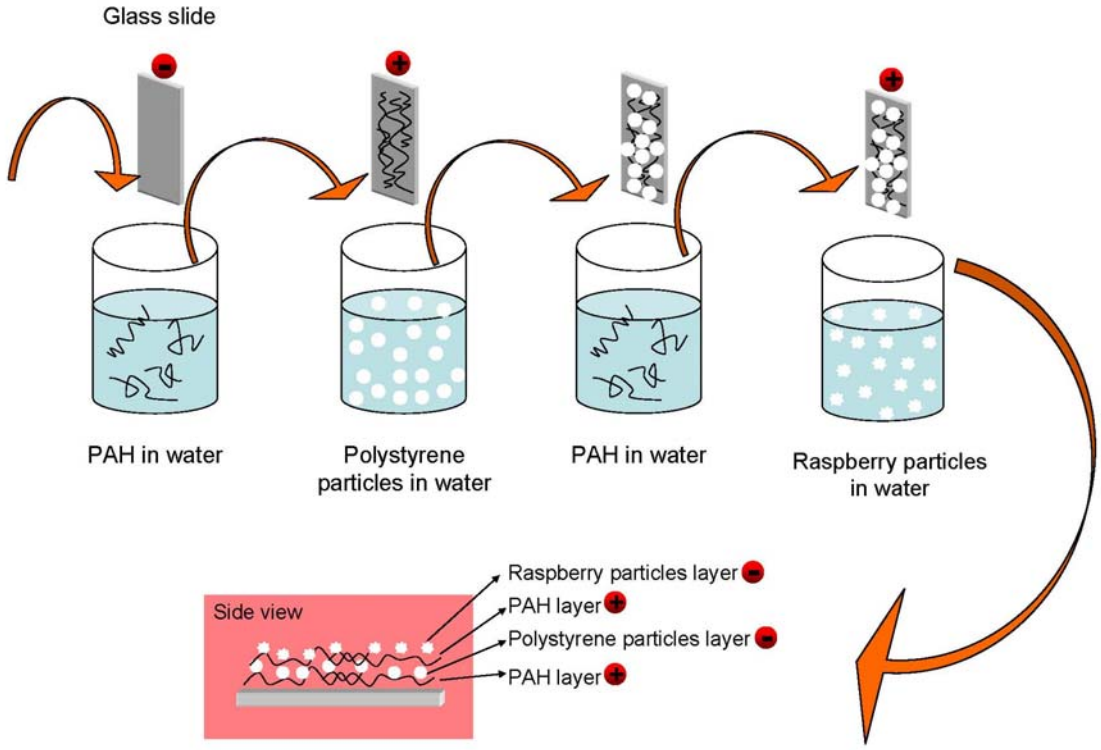

Figure 5.9. Sketch of the preparation of the "hybrid" multilayer. The slide is dipped in a PAH solution and then in a polystyrene and raspberry particles dispersions, successively. There were always two intensive rinsing steps with fresh water after each of these immersions.

The procedure illustrated in Figure 5.9 is repeated 2 times. The "hybrid" multilayer that was obtained was heated at 170 ˚C for 1 hour. This temperature is well above the glass transition temperature (Tg) of polystyrene, causing the polystyrene particles to soften and to spread on the glass surface. This results in a polymer film beneath the raspberry particles.

The morphology of the surface is shown in Figure 5.10a and b at different magnifications. As in the case of the bare monolayer, it can be seen that the surface coverage is also incomplete in this case. At higher magnifications (Figure 5.10b), the "molten" polystyrene between the glass slide and the raspberry particles is well visible. The sample was then hydrophobized with the semi-fluorinated silane as before and the hydrophobicity investigated. The inset in Figure 5.10a shows the optical microscope image of a water drop deposited on the surface. The contact angle was 160 ± 5˚ and the tilting angle a few degrees (< 10˚).

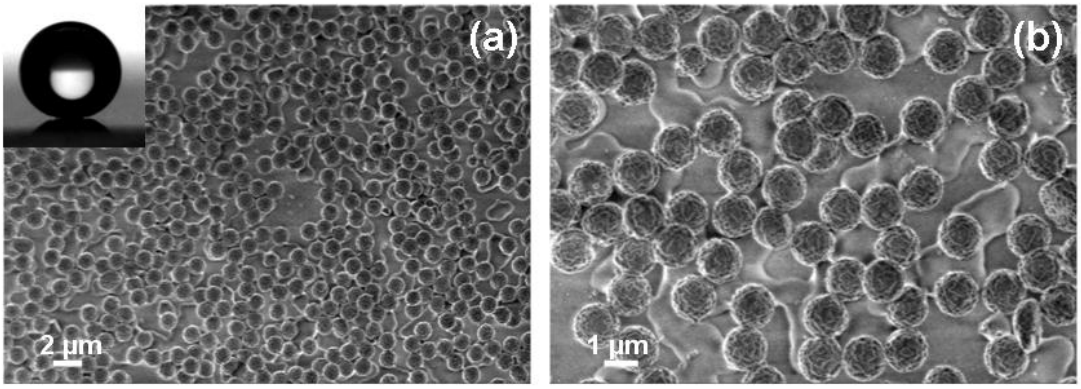

Figure 5.10. SEM images of the film prepared by repeating two times the sequence illustrated in Figure 5.9, after softening the polystyrene particles by thermal treatment. Lower magnification (a) and higher magnification (b) Inset: water drop deposited on the surface.

The mechanical resistance of the samples prepared in this way resulted to be much higher than the samples prepared only with the raspberry particles. The sample did not show any damage, even though its superhydrophobicity was tested by deposition of a large number of water drops.

Furthermore, after one year since the samples were prepared, the samples still show the same superhydrophobic behavior.

Unfortunately, the reproducibility of the fabrication route was not high. Among several samples, only 20-30 % of them were superhydrophobic. The others showed contact angles in the range of 140-150˚ and did not display a roll-off of the water drop upon tilting of the surface.

This is likely due to the influence of the polystyrene. Although it is hydrophobic, its affinity for water is higher than that of fluorinated silica. Hence, its contribution to the overall hydrophobicity is negative. More quantitatively, the contact angle of water on a smooth polystyrene surface is about 90˚, while that on a fluorinated material is about 120˚.

Hence, molten PS partially covers the more hydrophobic fluorinated-silica surface, inducing pinning sites and leveling out the (intended) surface roughness conferred by the particles.

6 Superhydrophobic surfaces by multilayer assembly of raspberry-like particles

The work presented in this chapter is aimed to the development of thick and stable superhydrophobic surfaces[38]. The preparation of thick surfaces by multilayer assembly is described. The improvement of the mechanical stability of these surfaces by the formation of polystyrene bridges is also discussed.

6.1 Polystyrene leakage

As already discussed in chapter 1, mechanical stability of superhydrophobic surfaces is still an issue. Raspberry particles, although proven as suitable to induce superhydrophobicity, have been so far assembled only in the form of thin and fragile layers.

In this work, the possibility to connect the particles by polystyrene bridges is shown. The idea is to induce leakage of polystyrene from the core by exposing the surfaces to the vapours of a good solvent (e.g. Tetrahydrofuran, THF).

First, the feasibility of polystyrene leakage is proven.

A dilute dispersion of raspberry particles was dried on two carbon grids. One of them was imaged by TEM without any treatment (Figure 6.1a) and the second grid was put in a close chamber under THF vapour at room temperature. After few hours this latter sample was imaged by TEM as well (Figure 6.1b).

The particles appear black as they are impermeable to the electron beam. After exposing the sample to THF vapour polymer bridges are formed between the particles visualized by dark areas between them (Figure 6.1b).

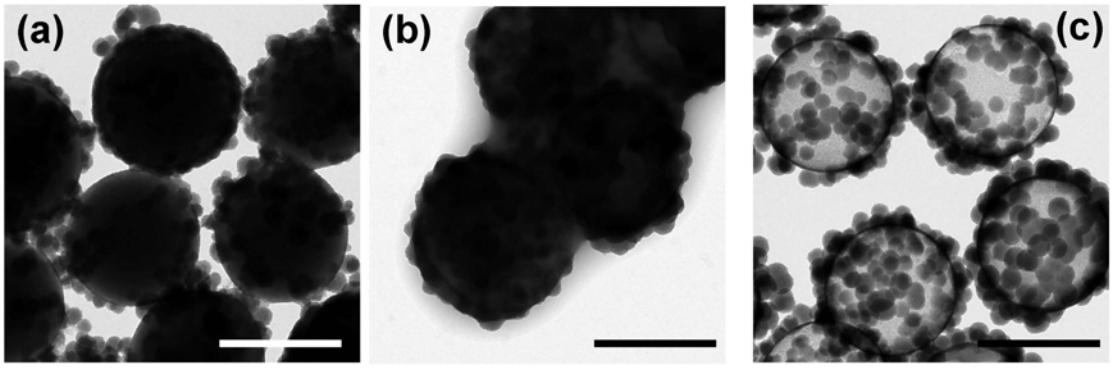

Figure 6.1. TEM images of the raspberry particles before THF exposure (a), particles after THF exposure (b) and after immersion in liquid toluene (c). Polymer bridges between the particles, due to polystyrene leakage, are visible (b). The shell thickness is ~20 nm. Bar: 1 μm .

Aliquots of particles were dispersed in liquid THF and then washed in fresh THF by several centrifugation steps. After dispersion in liquid THF the difference in contrast in comparison to the original particles indicates that the polystyrene has been removed and hollow shells are obtained (Figure 6.1c). The dark spots denote the nanometer-sized silica spheres.
The shell thickness was estimated by TEM images of the empty particles or by SEM from some broken shells occasionally found. In the case of the particles subsequently used for multi-layers preparation, the shell thickness was about 20 nm (measured by TEM images as shown in par. 3.1.2, Figure 3.5).

6.2 Preparation and characterization of multi-layers

The raspberry particles are hydrophilic and can be dispersed in water. Multi-layers of raspberry particles were prepared by evaporation of water, a facile and low-cost method. A dispersion of raspberry particles in an aqueous solution (details in chapter 8, par. 8.2.11) was filled in a sample holder with a glass floor and removable Teflon walls and the water let to evaporate. Particles sediment within ~ 2 hours*. Subsequently the particle multilayer was exposed to THF vapor. The procedure is illustrated in Figure 6.2.

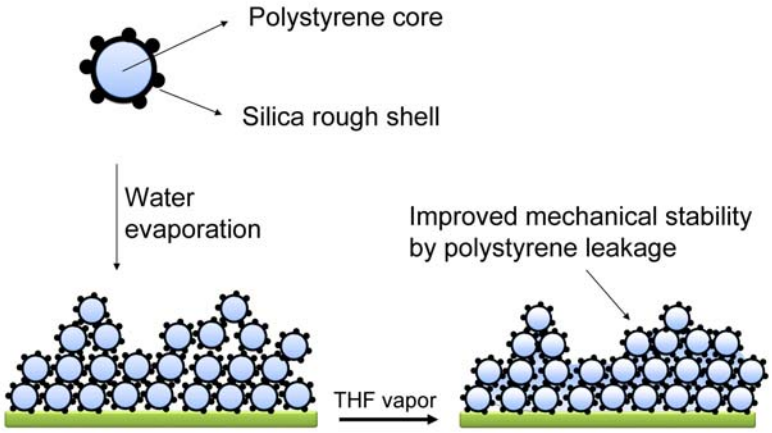

Figure 6.2. Schematic illustration of the preparation of a multilayer with improved mechanical stability by polystyrene leakage.

*The sedimentation time can be roughly estimated as t = h/v, where h is the height of the dispersion in the holder and v is the sedimentation velocity. Sedimentation velocity at equilibrium is given by the balance of gravity force (Fg, pushing the particles towards the bottom of the sample) and viscous force (Fv, that opposes to sedimentation) if the interaction between particles are neglected.
The gravity force is Fg = mg, where m is the mass of the particle and g is the gravity constant.
The viscous force is Fv = 6ΠηRv, where η is the viscosity of the medium, R and v are the radius and the velocity of the particles, respectively. Since at equilibrium, Fg = Fv, and considering that m = 4/3 $\Pi R^3 \rho$ where ρ is the density of the particles, the following relationship to calculate the sedimentation time can be obtained: $t = h/v = 9h\eta/2R^2g\rho$.

A SEM image of a film prepared by evaporating water at 50°C is shown in Figure 6.3. At lower magnification the surface topography which consists of micro- and nano-asperities can be seen. At higher resolution (inset) the polymer bridges between neighboring raspberry particles are visible. Whereas in samples prepared without THF exposure particles detached during deposition and in contact with moving water drops, the polymer bridges prevent detachment upon water contact or mechanical stress.

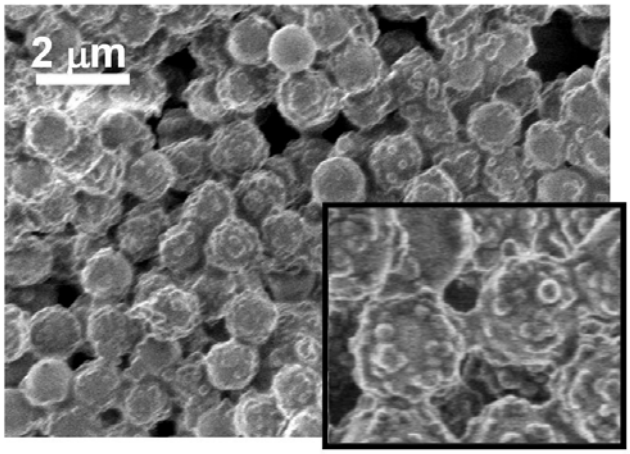

Figure 6.3. Scanning electron microscopy (SEM) images of films prepared by water evaporation at 50˚C, after THF exposure and silanization, subsequently.

After silanization most of these films showed tilting angles of a few degrees. However, in samples with high polystyrene leakage the tilting angle was 20° or higher (the tilting angle value is proportional to the contact angle hysteresis).

6.2.1 Plasma cleaning

During THF exposure polystyrene (PS) leaking out of the particles forms bridges between particles, i.e. PS fills some of the voids in the network and masks some asperities on the silica shells. If the amount of leaked-out PS is large, this affects the dual scale roughness and reduces the number of hydroxyl sites on the silica shells available for silane binding. The effect of polystyrene was tested by comparing the value of the water contact angle before and after removal of the polystyrene by plasma cleaning. Reactive species, i.e. ions and free radicals formed in the plasma induce surface crosslinking and degradation of PS. After 5 minutes of plasma treatment organic contaminants physically bonded to the surface are removed. Prolonging the treatment ensures that PS is indeed etched away. In silanized samples with identical initial contact angles (Table 6.1), 45 min of plasma cleaning

significantly improve water contact angles as compared to plasma cleaning for 5 min. After longer plasma cleaning times part of the PS is removed from in between the silica colloids and between the raspberry particles (Figure 6.4b). This increases the total surface area and thus the number of silane binding sites. Furthermore, after 45 minutes of plasma cleaning the mechanical stability was increased due to partial crosslinking of residual PS.

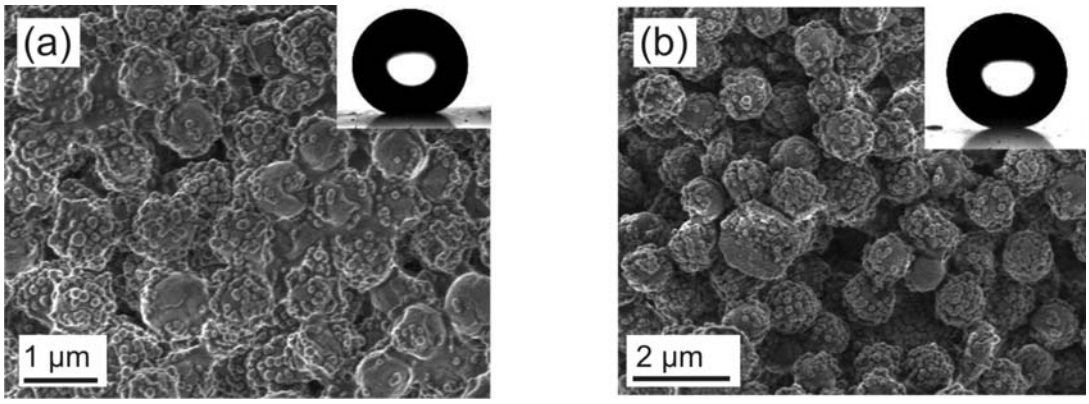

Figure 6.4. SEM images of films prepared from raspberry particles that were treated by Argon plasma for 5 minutes (a) or 45 minutes (b) respectively. Before measuring the contact angle the films were silanized. Inset: Image of a water drop deposited on the film.

Table 6.1. Water contact angles with their standard deviation. Contact angles were measured at positions corresponding to 3, 6, 9, and 12 of a clock and at the centre of samples.

Time of plasma cleaning	Contact angles before plasma cleaning	Contact angles after plasma cleaning
5 min.	150 ± 3˚	153 ± 2˚
45 min	151 ± 3˚	160 ± 4˚

6.2.2 Drying procedure

The roughness of the films, given by the arrangement of raspberry particles during drying, is influenced by the temperature at which the water is evaporated. Evaporation induced convection interacts with sedimentation of particles, causing that they sediment inhomogeneously. A three-dimensional view of the surface topography was obtained with a confocal profilometer (Nanofocus, par. 8.1.10 in chapter 8 for details). The surface consists of irregularly distributed “hills and valleys” (Figure 6.5). For analyzing the surface topography, 3D profiles were taken in different parts of the samples over areas of 800 x 800 μm^2. To quantify the roughness, this area was further divided in small squares of 50 x 50 μm^2. For

each of these squares the average height and its standard deviation were determined. Each value of standard deviation is associated to one of these squares and here will be referred to as “roughness”. This procedure is performed in order to minimize the effect due to a millimetre scale roughness eventually present.

Multilayers at different evaporation temperatures were prepared and their surface roughness and hydrophobicity were determined and compared (Table 6.2 and Figure 6.6).

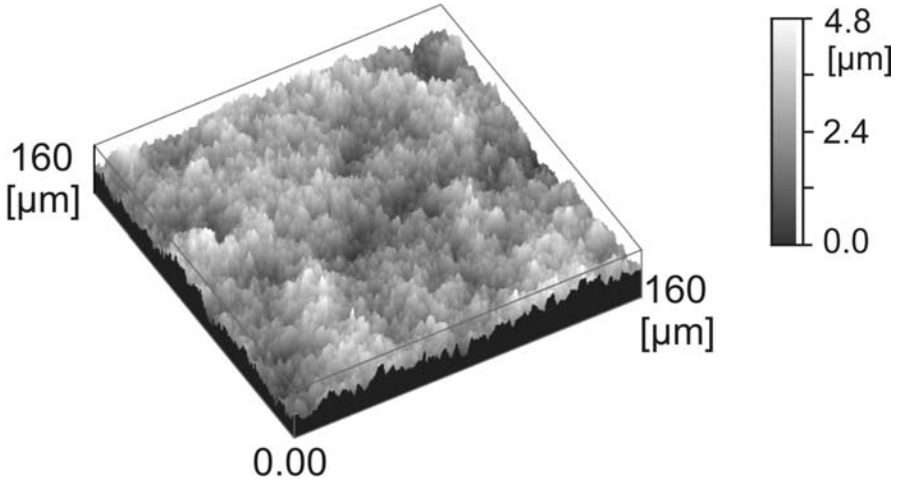

Figure 6.5. 3D profile over an area of 160 × 160 µm^2 of a raspberry film dried at 50°C. Height is indicated by grayscale intensity.

Table 6.2. Dependence of the tilting angle and roughness on the evaporation temperature. The films were prepared by water evaporation, THF exposure and subsequent silanization. The contact angles were measured after annealing the silanized samples at 70° for 2 hours to ensure complete evaporation of remaining solvent.

temperature (°C)	evaporation time (h)	tilting angle	roughness	
20	20	6°	0.52 ± 0.03	
50	5	10°	0.56 ± 0.05	
70	2	9°	0.62 ± 0.06	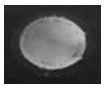
90	0.5	15°	0.73 ± 0.1	

Evaporation time decreases and roughness increases with drying temperature. The rising roughness is due to an increased influence of advection of particles by the solvent while sedimenting. At room temperature sedimentation time (~2 h) is short compared to water evaporation time (~20 h). This reverses at high evaporation temperatures (Table 6.2). After drying the sample at 90° even by eye the surface appears inhomogeneous (Table 6.2). Measuring the roughness at different positions on the same sample or on different samples led to almost identical results, Figure 6.6b.

As long as sedimentation is determined by gravity instead of evaporation, evaporation temperature hardly influences the tilting angle. However, in case of high evaporation temperature (90 °C) the tilting angle shows a strong dependency on position, varying between 4° and 40°.

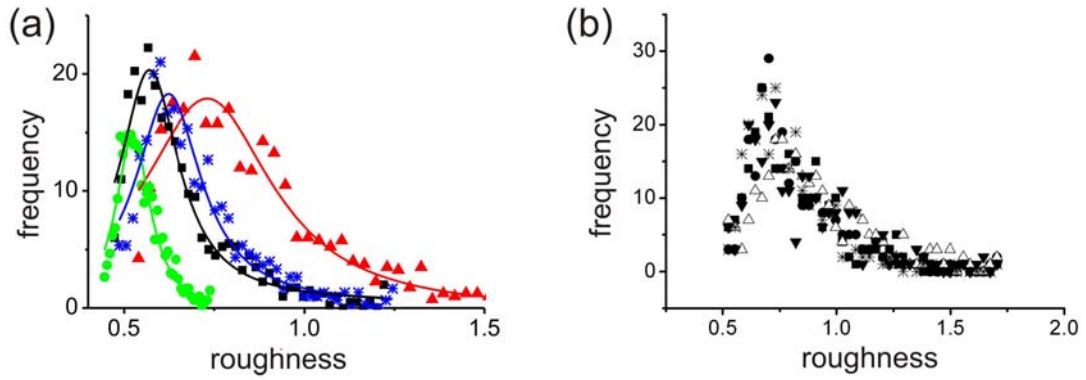

Figure 6.6. a) Dependence of the surface roughness on the drying temperature. Typically, the roughness was measured at positions corresponding to 3, 6, 9, and 12 of a clock and at the centre of samples. To minimize large scale inhomogenities or sample tilt the imaged areas of 800 × 800 μm^2 were divided in 256 small squares of 50 × 50 μm^2 each and the roughness was determined for each of these squares. The solid lines serve as guides to the eye. Evaporation temperature: circles: 20 °C, squares: 50 °C, stars: 70 °C, triangles: 90 °C. b) Reproducibility of roughness measurements of a film dried at 70°C. The different symbols denote different samples and positions.

7 Fluorescently labeled core-shell particles

This chapter is dedicated to the procedures adopted to obtain fluorescently labeled core-shell particles. Both polystyrene cores and silica shells are suitable to be labeled with a fluorescent dye by means of easy procedures. Therefore, it was possible to obtain core-shell particles with fluorescent cores and/or fluorescent shells. This work is part of a broader project (still in progress) in collaboration with Marcel Roth aimed to study interactions and arrangement of particles by Confocal Laser Scanning Microscopy (CLSM)[82].

CLSM is historically known for its large use in biology and biochemistry. More recently, its use has been extended to the study of concentrated colloidal dispersions[83, 84].

The advantage of studying colloidal dispersion by confocal microscopy is due to the possibility to get complementary information with respect to other techniques like light scattering. Light scattering (LS) of dilute colloidal dispersions can provide information about average shape, size and polydispersity. From LS of concentrated colloidal dispersion, it is possible to gain insight into the cristallinity of the sample as well as average particle-particle distance. CSLM gives the possibility to detect the particle coordinates and to do a 3D reconstruction of their distribution in concentrated dispersions. While LS techniques give "averaged" information about the arrangement of the particles, CSLM permits local observations and to get quantitative information on particle arrangement in disordered systems. One of the ideas behind this project is to investigate the interaction between colloidal silica particles during sedimentation, mechanical stress and evaporation. In order to be imaged by confocal microscopy with a reasonable resolution, silica particles need to be in the micrometer range. Unfortunately, due to silica's high density (~2g/L), size-range sedimentation can be fast compared to imaging and gravity strongly influences the arrangement of the particles. To overcome this inconvenience, core-shell particles with a lighter polystyrene core and a smooth silica shell can be used.

Furthermore, the synthesis of raspberry particles with a fluorescent core or fluorescent shell will allow analyzing the roughness of the superhydrophobic surfaces at a higher resolution compared to the confocal profilometer so far used (chapter 6). All the experiments described in the following paragraphs were done with these aims in mind; the work is not yet completed and it represents the basis for future work.

7.1 Core-shell particles with fluorescent polystyrene cores

In order to obtain labeled polystyrene particles, two strategies were tested. The first attempts were done by introducing the fluorescent dye in the reaction mixture, as reported by Winnik

et al[85]. The second approach was the “swelling method” reported by Schaertl and Sillescu[86] which consists in the introduction of the dye in pre-formed slightly crosslinked particles by swelling them in an organic solvent in presence of the dye. The next two paragraphs are dedicated to the description of these two possibilities and the corresponding results are compared.

7.1.1 Dispersion polymerization of styrene in presence of the dye

Polystyrene particles can be simultaneously synthesized and labeled by dispersion polymerization of styrene in presence of a suitable dye. This approach can be employed only if the dye is soluble in the reaction mixture. In general, dispersion polymerization is sensitive to the addition of reagents other than styrene to the reaction mixture. For instance, several authors communicate that the addition of a co-monomer like divinylbenzene or a dye molecule results in polydisperse, non-spherical particles. It has been reported that this problem can be overcome by adding the “problematic” reagent 1 hour after the reaction has started, when the nucleation step is finished or in an advanced state[85, 87]. This procedure is referred in literature as “two-stage dispersion polymerization”. This approach was followed to incorporate a fluorescent dye.
For this work, the dye used was Nile Red:

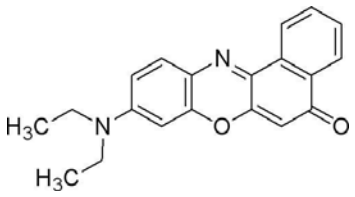

It is insoluble in water but soluble in ethanol and organic solvents like toluene, xylene etc. Nile Red is a fluorescent molecule[88, 89] whose excitation/emission spectrum varies in dependence of the surrounding environment (e.g. in water it is quenched while in ethanol and xylene the excitation/emission maxima are 559/629 and 523/563, respectively). Dispersion polymerization was performed using polyvinylpyrrolidone with a molecular weight of 55000 g/mol. In the first stage of the polymerization, only styrene and the stabilizers were added in order to have an “undisturbed” nucleation.
Nile red was added 1 hour after the polymerization had started (procedure in chapter 8, par. 8.2.7). Differently from the result expected, this reaction produced particles with smooth surface but broad size distribution. The size range varied from about 2 μm up to ~6 μm (Figure 7.1).

A monodisperse 2 μm-sized distribution coexists with polydisperse particles in the 4-6 μm size range. In principle it would be possible to separate them by filtration, but this procedure often involves massive lost of material.

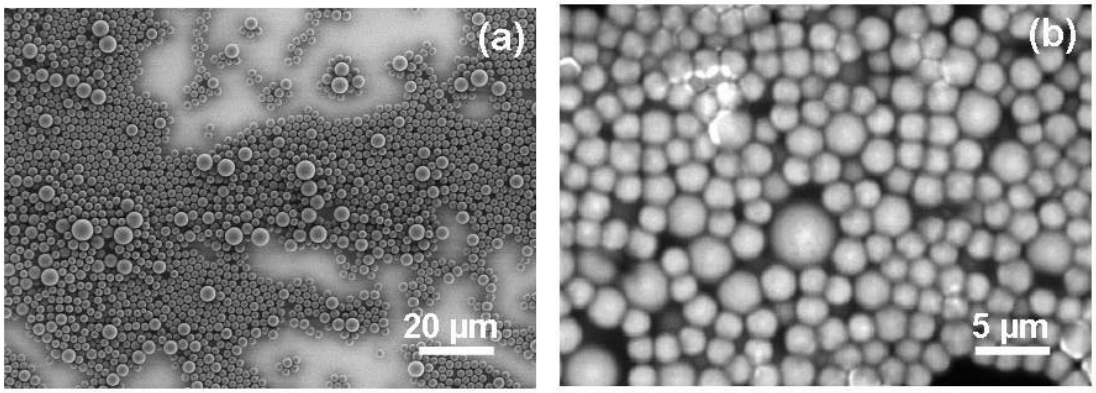

Figure 7.1. Images at different magnification of Nile Red dyed polystyrene particles obtained by "two-stage dispersion polymerization"; SEM image (a) and CLSM (b).

The fluorescence of the particles was tested by CSLM of a dispersion of particles in water (c = 0.1 g/L) sedimented on a microscope holder (Figure 7.1a).
The brightness of the particles was high; indicating that sufficient dye was incorporated within the particles.
Further work aimed to improve the reaction conditions in order to have more monodisperse particles was not performed. For example, the use of stabilizer with higher molecular weight could produce more monodisperse particles. Fortunately, the second approach ("swelling method") gave rise to satisfying results and it was chosen as favorite route to get fluorescently labeled polystyrene particles.

7.1.2 Introduction of the dye by "swelling method"

Nile Red was incorporated inside the polystyrene particles according to the procedure described by Schaertl and Sillescu[86], here referred as "swelling method". It consists in the preparation of a double-phase system formed by particles dispersed in water and Nile Red dissolved in xylene. Dye and xylene molecules diffuse through to the water medium into the polystyrene particles. At the end of this process, the particles are dyed but also strongly swollen with xylene. It is important to remove all the xylene before cleaning the particles by centrifugation; otherwise the particles easily form big and irreversible aggregates.
Polystyrene particles, 1 μm in diameter, were synthesized by two-step emulsion polymerization. They were slightly crosslinked by co-polymerization with 1% w/w of

divinylbenzene with respect to styrene (chapter 2, par. 2.2.1). The crosslinking reduced the swelling degree and as a consequence the particles are more stable. A typical procedure was the following: 10 ml of polystyrene particles dispersed in water (concentration: 8% w/w) was taken. On the dispersion 1 ml a solution of Nile Red in xylene was gently put (concentration: 1.4 mg/ml). This double phase system was slightly stirred for 2 hours until the particles turned red. The organic phase was removed by a separating funnel. After that, the residual of xylene present in the water dispersion (both in water and inside the particles) was removed by applying vacuum at room temperature for several hours until no smell of xylene was detectable. In order to further clean the sample, it was washed in ethanol and water and stored in water. If the particles were stored in ethanol instead of water they slowly release Nile Red (soluble in ethanol). However, this process takes several days because of the slow diffusion of the dye inside the polystyrene matrix. Nevertheless, the aqueous dispersion resulted to be completely stable towards the release of dye because it is insoluble in water.
The fluorescence of the particles so obtained was also tested by CLSM (Figure 7.2).

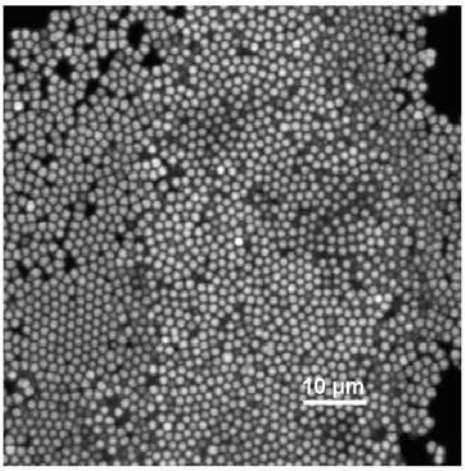

Figure 7.2. CLSM images of fluorescent polystyrene particles prepared by “swelling method”.

7.1.3 Synthesis of silica shells on fluorescent polystyrene particles

Fluorescent polystyrene particles were coated with silica according to the reaction described in chapter 3. The coating of particles obtained by dispersion polymerization resulted in a rough and incomplete silica shell (Figure 7.3a) while the particles synthesized by emulsion polymerization and dyed by “swelling method” gave rise to a smooth and close shell (Figure 7.3b). The reason behind these discordant results can be attributed to the different surface chemistry of the particles (chapter 3). Because of the smoothness of the silica coating and

the monodispersity of the polystyrene cores, the swelling method was chosen as preferred route for the synthesis of fluorescently labeled silica shells.

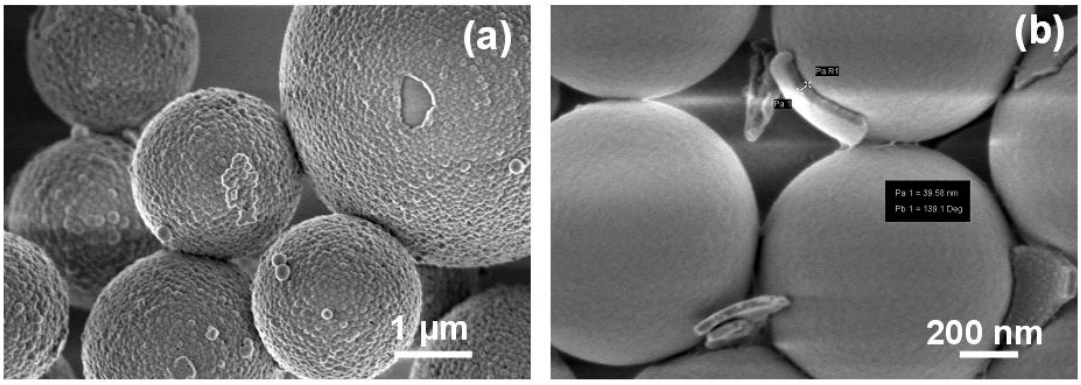

Figure 7.3. SEM images polystyrene particles coated with silica. The fluorescent polystyrene cores were dyed with Nile Red by: “two-stage dispersion polymerization (a) and “swelling method (b).

7.2 Core-shell particles with fluorescent silica shells

It has been largely reported that silica synthesized by the Stöber method can be easily labeled by covalently binding a fluorescent dye during the reaction mixture.

Both fluorescein and rhodhamine functionalized with an isothiocyanate group are reported to be suitable to covalently bind silica[62, 63]. The reaction consists in two subsequent steps. The first step is the formation of a chemical bond between the isothiocyanate groups of rhodamine (or fluorescein) and the ammine groups of (3-amino-propyl)triethoxysilane:

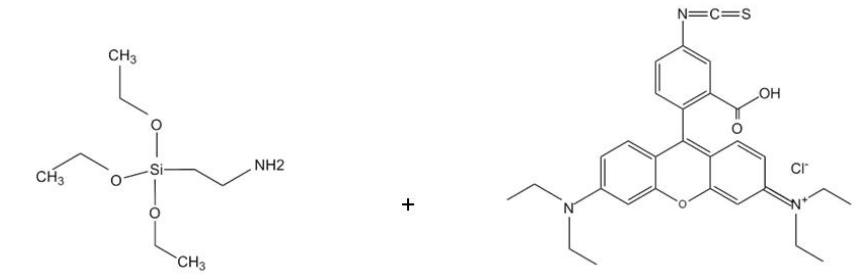

(3-amino-propyl)triethoxysilane (APS) Rhodamine isothiocyanate (Rh)

APS is a silane coupling agent commonly used to functionalize silica; after its reaction with rhodamine, it still has three alkoxy-groups able to condense by Stöber synthesis. Hence, the second step is its addition to the Stöber reaction mixture to produce fluorescently labeled silica particles:

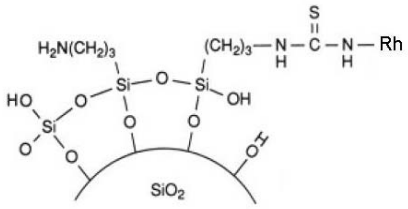

By means of this reaction, synthesis of fluorescent silica particles has been reported. In this study, the same reaction has been combined with the synthesis of silica shell on polystyrene particles. Polystyrene particles with a fluorescent silica shell were obtained (synthesis in the experimental part, par. 8.2.8).

As an example, in Figure 7.4 SEM and CLSM images of such particles are shown. The silica shells resulted to be as smooth as the ones obtained without incorporation of the dye. The confocal images reveal a bright signal only on the contour of the spheres, according to the fact that only the shells are labeled.

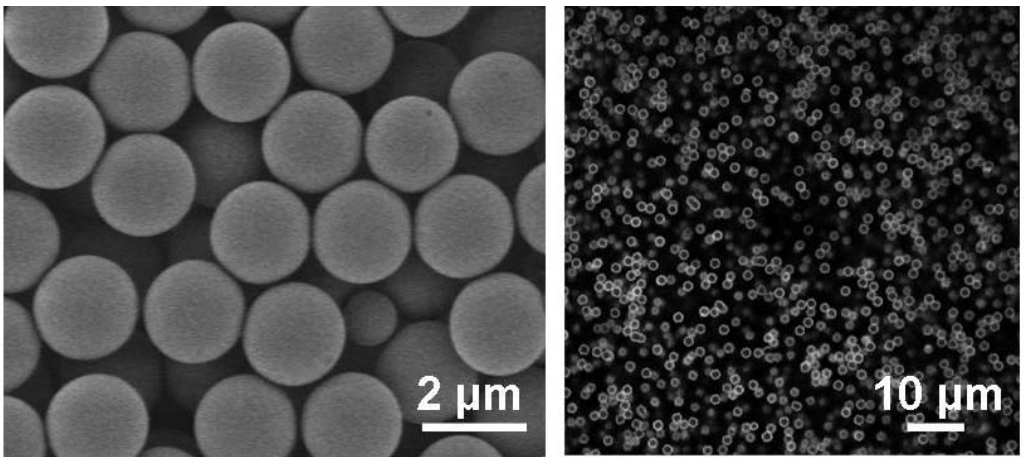

Figure 7.4. SEM (a) and CLSM image (b) of core-shell polystyrene-silica particles with a polystyrene core of 2 µm in diameter and 80 nm fluorescently labeled silica shells. The particles are dispersed in a refractive index matching liquid (η = 1.5780 from Cargille labs).

8 Characterization methods and experimental procedures

The present chapter describes the characterization techniques employed in this thesis work and the implemented experimental procedures.
The experimental procedures are given in detail in order to complete the discussion of the previous chapters and provide the possibility to exactly reproduce the work.

8.1 Characterization methods

8.1.1 Scanning Electron Microscopy (SEM)

Scanning Electron Microscopy (SEM) allows obtaining high resolution images exploiting the interaction between the sample and an incident electron beam. This latter is produced at the top of the microscope by an electron gun while the whole chamber is held in vacuum. The beam is focused toward the sample by passing through appropriate electromagnetic fields and lenses. Once the beam hits the sample, electrons are ejected from the sample.
Detectors collect backscattered electrons and secondary electrons and convert them into a signal. In turn, this signal is converted in an image.
In this work, SEM “LEO 1530 Gemini” (Oberkochen, Germany) was used. It is able to obtain high resolution (6-8 nm) at low operating voltage (0.7-3 kV). It was largely used to characterize colloids in terms of sphere size and surface roughness. Samples were prepared by evaporation of a small drop of a dilute dispersion of spheres in water or ethanol on a silicon substrate (~ 5 x 5 mm).
The SEM images were taken by Gabriele Schäfer and Maren Müller.

8.1.2 Transmission Electron Microscopy (TEM)

Transmission Electron Microscopy, like SEM, obtains images by means of the interaction between the sample and an electron beam. In this case, however, the surface where the sample is deposited is permeable to the electron beam. In TEM, a beam of electrons is focused on the sample. The electrons interact with the sample and only those that can go through it are able to hit the detector on the other side. At this point, the electrons are converted to light and an image is formed. The dark areas of the image correspond to areas on the specimen where fewer electrons were able to pass through (either absorbed or scattered upon impact); the lighter areas are where more electrons did pass through. The

instrument used in this work was a TEM “Tecnai F20” (FEI; 200 kV) and was employed to verify that hollow particles were empty and estimate the shell thickness (chapter 3).
The samples were prepared by evaporation of a small drop of a dilute dispersion of spheres in water or ethanol on a copper grid.The TEM images were taken by Kathrin Kirchhoff.

8.1.3 AFM Imaging and Force Measurement

Tapping-mode AFM imaging and force measurements were performed with a MultiMode Nanoscope IIIa SPM from Digital Instruments (Veeco Metrology Group, Plainview, NY) at 25 ± 2° C using silicon AFM probes (OMCL-AC 160TS, Olympus, Japan) with a resonance frequency of about 300 kHz and a tip radius of less than 20 nm. The spring constants of the cantilevers were determined by the thermal noise method, as described in ref[90]. They were found to be 42 ± 12 N/m. For each experiment, a fresh silicon substrate and one of the samples were mounted on the same AFM specimen holder. Before starting the force measurements, the immobilized silica spheres were imaged in tapping mode, and a well-shaped sphere was chosen. By repeatedly zooming in, the top of the target sphere was carefully located. For the ensuing force measurements, the substrate was periodically moved up and down at a constant scan rate (1.0 Hz) while the cantilever deflection was measured. The result is a graph of the cantilever deflection signal in volts versus the height position of the scanner. For each of these measurements on the spheres, about 60 reference curves were recorded on the bare silicon substrate to obtain the deflection sensitivity, i.e., the conversion factor between the measured deflection signal in volts and the actual cantilever deflection in nanometers. Recording the deflection sensitivity before and after each experiment allowed us to exclude that changes in the deflection sensitivity occurred during measurements. Force versus distance curves were calculated from the deflection versus piezo position curves by multiplying the cantilever deflection with the spring constant to obtain the force and subtracting the cantilever deflection from the height position to obtain the distance. Zero distance was derived from the linear contact part of force curves as described previously[91]. Within a series of force measurements, the maximum cantilever deflection was increased step by step, corresponding to increasingly higher force loads on the spheres. For each particle and each fixed load, typically 30 force curves were recorded.

8.1.4 Polyelectrolyte titration

The amount of charged groups on the surface of polystyrene particles (chapter 2) was determined by polyelectrolyte titration using a particle charge detector (PCD 02, Mütek

GmbH, Germany) in combination with an automatic titrator (702 SM Titrino, Metrohm AG, Switzerland). Carboxyl and sulfate groups were titrated with 10^{-3}M polyelectrolyte standards, the cationic polyelectrolyte polydiallyldimethyl ammonium chloride (PDADMAC) to determine the point of zero charge. Each measurement consisted in the titration of 10 mL of cleaned latex samples in water with a solid content of 3 g/L prepared at pH 2 and pH 10. Each result is the average of three measurements. In practice, the titration was performed by adding the PDADMAC solution drop by drop to the particles dispersion under continuous mixing. At the same time, the potential in monitored. This latter is negative in the beginning and decreases upon addition of the positive polyelectrolyte until it reaches zero value (particles are uncharged). The titration is stopped automatically at the point of zero charge and from the volume of the polyelectrolyte used and the known solid content of the particle dispersion it is possible to determine the surface charge as described in chapter 2.

8.1.5 Zeta-potential measurements

Zeta-potential measurements provide information about the sign of the surface charges and the stability of the dispersion.

The charge on a colloidal particle affects the distribution of ions in its surrounding by attracting ions of opposite charge with respect to the charge of the particle. This concentration of ions at the surface of the particles is called “electrical double layer”.

Within the electrical double layer two regions can be distinguished: an inner region (Stern layer), where the ions are strongly bonded to surface and an outer layer where they are only weakly attracted. In practice, when the particle moves, the ions in the inner region move together with the particle while the ions in the outer region do not come along.

The boundary between this two regions is called “slipping plane” and the potential at the boundary is known as “Zeta-potential”.

When an electric field is applied, charged particles dispersed in a solvent move towards the electrode of opposite charge. The viscous force opposes this movement. At the equilibrium, the particles move with constant velocity (electrophoretic mobility). This velocity is calculated and put in relation to the Zeta-potential by the Henry equation:

$$U_E = \frac{2\varepsilon z f(ka)}{3\eta}$$

where z is the Zeta-potential, U_E is the electrophoretic mobility, ε is the dielectric constant of the medium, η is the viscosity of the medium and f(ka) is Henry’s function. This latter is

generally approximated to 1.5 in the Smoluchowski approximation and to 1 in the Huckel approximation.
The Zeta-potential gives an indication of the stability of a colloidal dispersion. Generally, a colloidal dispersion is considered stable if the Z-potential is higher than +30 mV for positively charged particles and smaller that -30 mV for negatively charged particles.
In this study, the Zeta-potential of the polystyrene particles was measured by a Delsa counter using a dispersion of particles in water at a concentration of 0.01 g/L.

8.1.6 Contact angle measurements

Contact angle measurements were performed with a contact angle meter DSA 10 (Krüss GmbH, Germany).
2-3 µl water drops were gently deposited on the surface by a syringe equipped with a Teflon coated needle with external diameter of 0.31 mm and internal diameter of 0.13 mm. After removal of the needle from the drop, an image was taken. For good superhydrophobic surfaces, previous attempts to measure the contact angle with bigger metallic needles failed because of the impossibility to remove the needle from the drop. Due to the low adhesion towards the surface, water drops tend to stick to the needle unless the size is so big to cause the drop to fall down. Unfortunately, in this case gravity is no longer negligible.
The contact angle of the imaged drops was then manually measured with the program Image-Pro Plus (MediaCybernetics) after adjustment of the contrast.
For each sample the average contact angle between 4-5 drops in different positions of the sample was taken.

8.1.7 Tilting angle measurements

The angle of inclination at which a drop rolls off from a surface is commonly called tilting angle. It is related to the contact angle hysteresis. The lower the tilting angle, the lower the hysteresis and the more superhydrophobic the surface is. Although this is an indirect method, it was chosen because it was regarded as more reliable than direct measurements of hysteresis.
In principle, hysteresis can be directly measured by recording a movie while adding/withdrawing water to a drop with a needle inside (chapter 1). When the surface is superhydrophobic, it is hard to settle the needle in the centre of the drop; due to the low adhesion to the surface, it tends to stick to the side of the needle and this affect the measured contact angle. It was always higher at the side closer to the needle. Performing

tilting angle measurements allows overcoming this inconvenience and reduces the manipulations that could affect the result.

Tilting angle measurements were performed with a contact angle meter Dataphysics OCA35 (Data Physics Instruments GmbH, Germany). The tilting angle was measured for each sample at 5 different positions after depositing a 5 µl water drop on the surface, removing the needle and tilting the stage at a speed of 1.3°/s. Simultaneously the shape of the drop was recorded. Increasing the speed by one order of magnitude or the drop volume by a factor of two did not change the tilting angle within experimental accuracy.

8.1.8 Solid state NMR.

All solid state NMR measurement of this study were performed on a Bruker Avance II console operating at a ^{1}H Larmor frequency of 300.23 MHz using commercial 7 mm double resonance MAS equipment spinning at 5 kHz MAS frequency. 50 kHz radio frequency (RF) nutation was adjusted on both, the ^{1}H and the ^{29}Si channel and 50 kHz hetero-nuclear dipolar decoupling was applied during acquisition using the SPINAL64 scheme. Direct excitation spectra have been recorded with a tip angle of 25° corresponding to a pulse length of 1.4 µs and a relaxation delay of 20 s, if not stated differently. All cross-polarization magic angle spinning (CP-MAS) spectra were recorded with a CP contact time of 5 ms at 5 kHz MAS spinning frequency and a repetition time of 3 s. In order to ensure sufficient protons close to the silica surface for the polarization transfer, silica surfaces were coated with polyvinylpyrrolidone (PVP, Fluka, K90, $M_w \approx 360\,000$ g/mol) after high temperature annealing, such as 800°C, 1000°C.

In ^{29}Si MAS NMR spectra different chemical sites Q^n in the silica network, where n gives the number of silicon atoms attached to the four oxygen atoms at the corners of a SiO_4 tetrahedron, can easily be distinguished. Q^2 sites, corresponding to a SiO_4 unit in a chain, are observed in the range from -85 – -90 ppm, whereas Q^3 sites, SiO_4 branching points in a chain, are assigned to chemical shifts around -100 ppm. Completely condensed Q^4 sites with four attached Si sites show the lowest chemical shift values and are observed in the range of -110 ppm. The quantitative distribution of the Q^n sites in a silica network can be determined by direct excitation of the fully relaxed ^{29}Si spins under MAS conditions. In many cases, however, it is difficult and very time-consuming to record these spectra, because the T_1 relaxation times of silica networks are often in the range of several minutes and may differ depending on the Q site.

8.1.9 Confocal Laser Scanning Microscopy

Confocal Laser Scanning Microscopy gives the possibility to take 2D and 3D images of concentrated colloidal dispersions[83] with 2D resolution of about 200 x 200 nm and axial resolution in the order of 600 nm. The reason behind the improved quality of the images with the respect to traditional optical microscopy is the combination of the basic principles: point-by-point acquisition of the image and removal of the out of focus light. A schematic illustration of a confocal microscope is given in Figure 8.1.

A laser light (blue line) is addressed toward two rotating mirror by means of a dichroic mirror. The function of the rotating mirror is to scan the sample in xy plane and in the z plane.

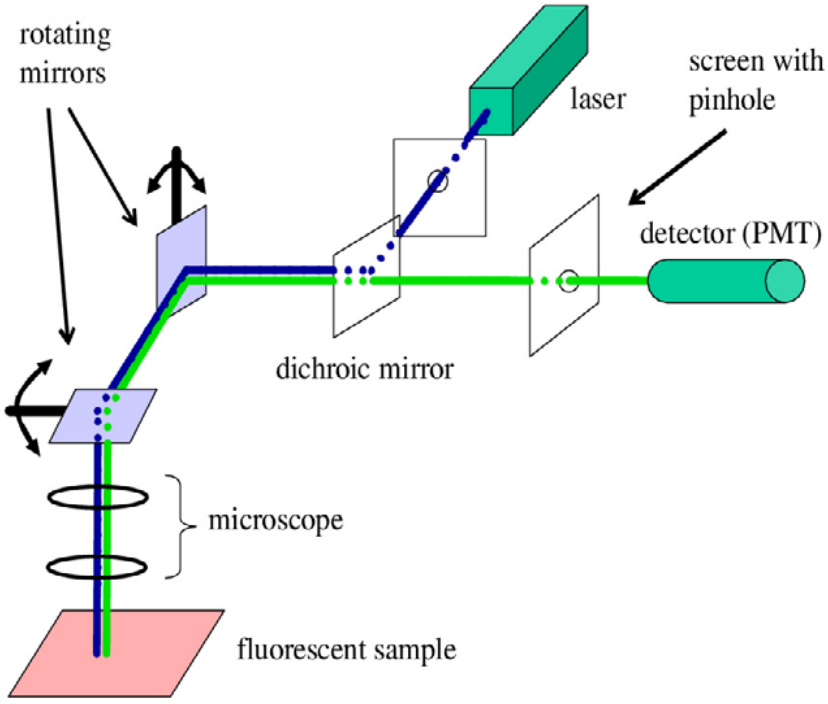

Figure 8.1. Schematic illustration of a confocal microscope. The image is taken from Weeks et al[84].

The light passes through the microscope objective and excites the fluorescent sample. The fluorescent emitted light is reflected by the rotating mirrors; it passes through the dichroic mirror and a pinhole before arriving at the detector. The plane of the pinhole is conjugated with the focal plane of the sample (confocal means conjugated focal plane) in order to reject the out of focus light.

The image is taken point-by-point and a 2D image in constructed at first by scanning the sample in xy-plane. By moving the focal plane along the z axis it is possible to assemble a collection of subsequent 2D images which can be worked out to get the 3D reconstruction of the sample.

Images shown in chapter 7 are taken by a Zeiss LSM 510 confocal scanning laser microscope. A water-immersion objective was used : (C-Aprochomat 40x, NA 1.2). For the image in Figure 7.1b, it was used a HeNe laser (λ=543, LP560 filter for emission). For the image in Figure 7.2, it was used an Argon laser (λ=541, LP 530 filter for emission).
Image 7.5d was obtained with a home-made LSCM with a 100x objective (Olympus UPlanApo PH3, NA 1.35). A reasonable signal to noise ratio was obtained for a laser power of 1μW (solid state laser, 532nm, 25mW) and an integration time of 5μs.

8.1.10 Confocal profilometer

3D profile images of the surfaces are obtained by μSurf® white-light confocal profilometer (Nanofocus AG, Germany). The 160 x 160 μm^2 surface profiles were taken by a 100x magnification objective. The 800 x 800 μm^2 surface profiles were taken by a 20x magnification objective.

8.1.11 Dynamic Light Scattering measurements

The size of the particles used for the determination of the surface charge was measured by Dynamic Light Scattering. DLS measurements were performed by a ALV/CGS3 Compact Goniometric System with He/ne laser (632.8 nm), ALV/LSE-5004 Correlator and ALV5000 Software. The correlation function was fitted by the cumulant data analysis.
The measurements were performed by Christine Rosenauer.

8.2 Experimental procedures

8.2.1 Materials.

Styrene (Acros Organics, 99% extra pure, stabilized), sodium hydroxide (WTL Laborbedarf GmbH, 99%), ammonium persulfate (Acros Organics, 98%), azobisisobutyronitrile (AIBN)(Sigma Aldrich, 98 %), acrylic acid (Acros Organics, 99.5%, stabilized), ethanol absolute (Sigma Aldrich), tetrahydrofuran (THF) (Sigma Aldrich, 99.9 %), poly(allylamine hydrochloride) (PAH) (Aldrich, average M_w ~15,000), polyvinylpyrrolidone (PVP) (Fluka, K 90 M_w ~360,000), Triton X-305 (SERVA Feinbiochemica, Heidelberg/New York), ammonia (Fluka, 25% in water), tetraethoxysilane (TES) (Acros Organics, 98%), (3-Aminopropyl)triethoxysilane (99%, Sigma Aldrich), sodium chloride (NaCl) (Riedel-de Haën,

99.8 %), (tridecafluoro-1, 1, 2, 2-tetrahydrooctyl)-1-trichlorosilane (97%, Sigma Aldrich), Dioctyl sodium sulfonsuccinate (AOT) (Fluka, > 99%). Milli-Q water was obtained from a Millipore purification system operating at 18.2 MΩ. Hellmanex II solution (Hellma GmbH) was used to clean the glass slides used as a basis for the superhydrophobic surfaces.

8.2.2 Synthesis of polystyrene particles by soap-less emulsion polymerization

Here the standard procedure to get polystyrene particles by emulsion polymerization is described. In particular, this is the recipe used to get the polystyrene particles illustrated in Figure 2.5 in chapter 2. The first recipe produces nanometer sized particles and the second one micrometer sized particles using the product of the first reaction as seeds. All the other particles shown in this thesis work are prepared with a similar procedure. In case that the amount of reagents is different, these are specified by means of a table directly within the chapter where the synthesis is discussed.

Removal of the inhibitor. The inhibitor was removed from the styrene by washing with 3 aliquots of 2 M sodium hydroxide solution and 3 aliquots of milli-Q water. The washed styrene was distilled under reduced pressure before use.

First step: synthesis of 600 nm polystyrene particles. A 500 ml three-necked flask was equipped with a condenser, a PTFE stirrer, and a gas inlet. Milli-Q water (300 ml) was put in the reactor and nitrogen was bubbled for 20 minutes. Ammonium persulfate (0.11 g) dissolved in 10 ml water and styrene (25 g) was added. After that, NaCl (0.20 g), acrylic acid (0.15 g) were added subsequently. The system was closed and the mixture heated to 75 ˚C under stirring at 350 rpm. After 1 day the heating was turned off. After the mixture was cooled down to room temperature, particles were cleaned by at least 6 centrifugation steps with fresh milli-Q water. Each centrifugation step was carried out at 6000 rpm for 30 minutes.

Second step: synthesis of 1 µm polystyrene particles. 38 ml of the reaction mixture (without washing) were transferred in a clean 500 ml flask. 300 ml of milli-Q water were added and the apparatus was heated at 75 ˚C under nitrogen flow. Ammonium persulfate (0.4 g) was added. A mixture of acrylic acid (0.042 g) and styrene (7.2 g) are added drop-wise within 1 hour. After 1 day under stirring at 75˚C, particles were washed 6 times with fresh milli-Q water by subsequent centrifugation steps (6000 rpm for 20 minutes) and in the end transferred to ethanol.

Note: The amount of styrene necessary to increase the size of the particles can be roughly estimated by simple geometrical calculation. If R_1 is the radius of the seed particles and R_2 is the desired radius of the particles after the growing step (in cm), then:

$$V_{R_1} = \frac{4}{3}\pi R_1^3 \qquad V_{R_2} = \frac{4}{3}\pi R_2^3$$

are the volumes of the particle before and after the growing step. The change in volume per particles is:

$$\Delta V = V_{R2} - V_{R1} = \frac{4}{3}\pi(R_2^3 - R_1^3)$$

The amount of styrene in grams can be estimated as:

$$Gr(styrene) = \Delta V \cdot N_{seed} \cdot \rho_{PS}$$

where N_{seed} is the number of seed particles and ρ_{PS} is the density of polystyrene (in gr/cm^3).

8.2.3 Synthesis of the polystyrene particles by dispersion polymerization

Here the experimental the procedure to get the 2 μm polystyrene particles used for subsequent silica coating is described (chapter 2 and 3). The first step is a classical dispersion polymerization. As discussed in chapter 2, these particles needed to be functionalized with acrylic acid to be suitable for coating with silica. This functionalization was performed only for this special case. All the other dispersion polymerizations were performed like the first step except for the amount of reagents and type of polymer stabilizer. The differences are highlighted by means of a table within the chapter where the synthesis is discussed.

First step: 2 μm polystyrene particles. In a 250 mL three-necked flask equipped with a condenser, a mixture of poly(acrylic acid) (0.5 g, Mw= 450000), part of the styrene (6.4 g) , ethanol (67 g), and Milli-Q water (5 g) were mixed and flushed with nitrogen for 15 min. Then the system was closed and heated to 70 °C. When the temperature was stable (after about 20 minutes), a mixture of the remaining styrene (2.7 g), azobisisobutyronitrile (0.200 g), and ethanol (2.7 g) was added in one step. The reaction was allowed to proceed for 20 h under stirring rate of about 400 rpm (round per minutes).

Second step: surface functionalization with acrylic acid. PS spheres (6.4 g) from the first step were washed and dispersed in 39.5 g of ethanol. Then 50 g of water were added. A mixture of styrene (1.27 g), azobisisobutyronitrile (0.06 g) and acrylic acid (1.05 g) was added to the dispersion, and the mixture was stirred for 20 h. After being deoxygenated by nitrogen flow for 20 min, the system was closed and heated to 75 °C at kept at this temperature for about 20 h. Particles were cleaned by centrifugation in water (5000 rpm for 15 minutes) and ethanol (4000 rpm for 10 minutes) at least six times.

8.2.4 Synthesis of core-shell polystyrene-silica particles (smooth shells)

Here the recipe to get 15 nm silica shells on 790 nm polystyrene colloids is given (particles shown in Figure 3.6b). All the other particles discussed in chapter 3 are synthesized exactly in the same way except for the final amount of TES added to the reaction mixture. Such amount is listed in Table 3.4 in chapter 3 together with the corresponding shell thicknesses. The amount of TES necessary to get the desired thickness can be predicted by geometrical calculation.

The polystyrene spheres were stored in water (concentration of 68 g/L). A 10 mL solution of PAH dispersed in water and sodium chloride (NaCl) was prepared (c = 1.2 g/L in PAH and 2.8 g/L in NaCl). A 4 mL portion of the colloidal dispersion in water (0.272 g of particles in 4 ml water) was added drop-wise under stirring. This dispersion was stirred for 1 h and then centrifuged, washed twice with fresh water, and finally redispersed in a solution of PVP in ethanol (c = 7 g/L). After another 1 h of stirring, the sample was centrifuged twice and redispersed in 20 mL fresh ethanol. To form the silica shell, ammonia (1.6 mL) and 0.1 ml of TES were added. The spheres were washed three times in fresh ethanol.

In course of this thesis work, it was found that the PVP coating step can be skipped without affecting the shell smoothness. Despite that, here the PVP step is included in the synthesis because it was performed in the case of the samples shown in chapter 3.

8.2.5 Synthesis of raspberry-like particles

The following recipe corresponds to the raspberry-like particles showed in chapter 4 (Figure 4.2b and c for the composite particles and Figure 4.7 for the raspberry particles). All the other particles showed are prepared in the same way except for some reaction parameters which are listed in the tables in chapter 4.

1st step: synthesis of composite particles. Polystyrene particles (1.53 g, diameter = 1 μm) were dispersed in a solution of PVP and ethanol (1.63 g PVP in 80 ml ethanol) and kept under stirring for 1 day. Then ammonia (6.6 ml) and a mixture of TES and ethanol (2 ml TES in 18 ml ethanol) were added in 4 steps (1staddition: 4 ml, 2nd addition: 4 ml after 3 h, 3rd addition: 6 ml after 1 h, 4th addition: 6 ml after 1h). After 1 night, the composite particles were washed in fresh ethanol by 4 consecutive centrifugation steps.

Like in the case of the smooth shell, it was later found out that PVP coating is not necessary in order to grow silica particles on polystyrene surface (discussion in chapter 4).

2nd step: synthesis of raspberry particles. This is the synthesis of a smooth shell on the composite particles. 0.84 g of composite particles from the previous reaction were dispersed

in 13 ml of milli-Q water. This volume is added to a solution of PAH (0.046 g) and NaCl (0.084 g) in water (30 ml). After 1 hour under stirring, particles were washed 2 times in fresh water and in the end dispersed in a solution of PVP (0.294 g) in ethanol (42 ml). After 1 hour under stirring, particles are washed 2 times with fresh ethanol and dispersed in 60 ml fresh ethanol. Immediately after, ammonia (4.8 ml) and TES (0.6 ml) were added. After 1 day the raspberry particles were washed several times with milli-Q water.

8.2.6 Synthesis of silica particles by Stöber method

This is the synthesis of the silica particles shown in chapter 3, Figure 3.2. A 500 ml three-necked flask equipped with a condenser and a PTFE stirrer was filled with ethanol (89 ml) and ammonia (32 ml, 25% w/w) and heated at 60˚C. Then APS (1.9 ml, distilled before use) and TES (6.1 ml) were added and the mixture is kept under stirring for 1 night. After that, the particles are washed by several centrifugation steps with fresh ethanol.

8.2.7 Synthesis of fluorescently labelled polystyrene particles by "two-stage" dispersion polymerization

This is the synthesis of labelled polystyrene particles discussed in par. 7.1.1 and shown in Figure 7.1.

First stage: Ethanol (19 g) and polyvinylpyrrolidone (1.0 g, Mw = 55000 g/mol) were sonicated (Bandelin Sonorex, Bandelin electronic) for 30 minutes and then triton X-305 (0.35 g) was added. Sonication was performed again for 15 minutes. The solution was put in a 250 ml three-neck flask and stirred at 150 rpm (round per minutes). Styrene (2 g) and AIBN (0.25 g) were added and nitrogen was flushed for 30 minutes. The apparatus was closed and heated at 70 ˚C. At the same time a second solution containing styrene (2 g), ethanol (19 g) and Nile Red (6 mg) was put in a 100 ml three-neck flask under nitrogen flow for 20 minutes and then closed and heated at 70˚C.

Second stage: 1 hour after the reaction was started, the second solution was added to the reaction mixture. After 24 hours the reaction was stopped by cooling it down and the mixture was washed 5 times with fresh ethanol by subsequent centrifugation steps and then redispersed in milli-Q water.

8.2.8 Synthesis of fluorescent silica shells on polystyrene particles

Polystyrene cores. The polystyrene cores (diameter: 2 µm) were synthesised by seed-emulsion polymerization according to the procedure described in par. 8.2.2. The amount of reagents is listed in Table 8.1.

Table 8.1. Reagents for the synthesis of polystyrene cores with a diameter of 2 µm.

		Amount in grams					
Reaction	Diameter (nm)	Initiator	Styrene	Acrylic acid	NaCl	Distilled water	Seeds
(a) seed	700	0.11	25	0.15	0.2	300	-
(b) growth	2000	0.2	60	0.36	0.12	300	38 ml reaction mixture (a)

Initiator: Ammonium persulfate; reaction temperature: 75˚C

Step 1: Synthesis of rhodamine-functionalized APS. Rhodamine (0.058 g) was dissolved in ethanol (5 ml) in a 20 ml vessel and stirred under nitrogen flow for 5 minutes. Then 3-Aminopropyl)triethoxysilane (APS, 0.047 g) was added. The apparatus was closed and kept under stirring for 1 day at room temperature.

Step 2: preparation of the polystyrene particles for silica coating. Poly(allylamine hydrochloride) (0.096 g) and sodium chloride (0.240 g) were dissolved in 82 ml of milli-Q water. After that, a dispersion of polystyrene particles synthesized by two-steps emulsion polymerization (2 g particles in 19 ml milli-Q water, diameter = 2 µm) was added drop-wise.
The dispersion was stirred for 30 minutes and then centrifuged two times with fresh water and in the end dispersed in a solution of polyvinylpyrrolidone (0.78 g) in ethanol (112 ml) prepared by ultrasonication for 15 minutes. The dispersion was kept under stirring for 30 minutes and then washed two times with fresh ethanol.

Step 3: Silica coating. After the second wash, the particles were dispersed in ethanol (160 ml). Ammonia (12.8 ml), the mixture obtained in step 1 (0.34 ml) and tetraethoxysilane (0.960 ml). After 1 day under stirring at room temperature, particles were washed with ethanol at for 5 times by subsequent centrifugation steps. This gave rise to a fluorescent silica shell of ~35 nm. This step was repeated one more time and the shell obtained was ~ 80nm (corresponding to the particles shown in Figure 7.4).

8.2.9 Preparation of superhydrophobic monolayer by LbL assembly

Cleaning of the glass slides. Microscope glass slides (Thermo scientific, 76 x 26 mm) were cut in pieces of about 10 x 26 mm with a diamond tip. All glass substrates were sonicated

twice with a 2 % aqueous solution of Hellmanex (Hellma GmbH, Mühlheim, Germany) for 15 minutes and extensively rinsed with milli-Q water.

PAH solution. The PAH-solution in which the glass substrates were dipped was prepared in the following way: 10 mg of PAH, 16 mg NaCl and 10 ml milli-Q water were mixed for 10 minutes in an ultrasonicator until a homogeneous solution is obtained.

Particles dispersions. The dispersion of raspberry particles in water (labelled as RD dispersion) was at a concentration of 60 g/L. The polystyrene particles (slightly crosslinked with divinylbenzene, diameter = 600 nm, labelled as PS dispersion) were suspended in water at a concentration of 17 g/L.

Film with only raspberry particles. A clean glass slide was dipped consecutively in PAH-solution and the dispersion of raspberry particles, 5 minutes per immersion. After each immersion the glass was washed by dipping it three times in fresh milli-Q water. After the last wash, the glass was dried on air.

Film with raspberry particles and polystyrene particles. A clean glass slide was dipped consecutively in the following liquids: PAH-PS-PAH-RD. This sequence was repeated two times. After each immersion the glass was washed by dipping it three times in fresh milli-Q water. After the last wash, the glass is dried on air. The film was heated in an oven at 180 ˚C for 1 hour in order to melt polystyrene particles.

8.2.10 Monolayer by Langmuir-Blodgett technique

Experimental apparatus. The surface tension at the air–water interface (the plots of pressure (π) versus the mean molecular area (mmA)), was measured with a Wilhelmy system using a filter paper (S&S 595 Filter paper Circles, Schleicher&Schuell GmbH, Dassel, Germany) suspended from a strain gauge (Riegler & Kirstein GmbH, Postdam, Germany).The maximum available surface area of the Langmuir trough is 1149.93 cm^2 (compression ratio 8:1). As subphase, distilled water was used. The temperature of the water subphase was maintained at 20 ± 0.5° using a thermostated water circulating system (Thermohaake C25P, Karlsruhe, Germany).

Cleaning of the glass slides. The glass slides (10 x 26 mm) were immersed in a 1:1 solution of concentrated H_2SO_4 and HNO_3 for 24 h. They were then transferred into a solution of 9 parts of H_2O_2 (35 % w/w) and 1 part of aqueous ammonia (25 % w/w) for another 24 h and then rinsed intensively with milli-Q water. Clean glass slides were stored in milli-Q water.

Procedure. Particles were dispersed in ethanol at concentration of 40 g/L; for each monolayer sample, 800 µl of this dispersion were gently deposited on the water interface by a micro-syringe in several steps of about 5 µl. The compression (5 cm^2/min) was started after 10 minutes from the deposition to ensure the evaporation of ethanol.

8.2.11 Superhydrophobic multilayer by particle sedimentation

Multilayers of raspberry particles were prepared by evaporating a 0.36 ml of particles in water in a circular holder (diameter = 1.5 cm) made of a glass floor and Teflon removable walls. The concentration of the particles in water was varied in dependence of the desired number of layers. For the samples described in chapter 6 (paragraph 1.2.2), 0.36 ml of a water dispersion of particles at concentration of 10 g/L was filled and the water was evaporated at different temperatures. After water evaporation, the sample was exposed to THF vapor for 3.5 hours at room temperature and then hydrophobized by CVD of a semi-fluorinated silane as described in par. 8.2.12. The contact angle was measured after annealing the sample at 70 ˚C for 2 hours to ensure complete evaporation of remaining THF. Contact angles measured on not annealed samples showed variability with time. The contact angle was lower immediately after the preparation and improved with time, likely due to evaporation of residual THF.

8.2.12 Chemical vapour deposition (CVD) of trichloro(1*H*,1*H*,2*H*,2*H*-perfluorooctyl)silane

Silica surface can be modified from hydrophilic to hydrophobic by means of silane coupling agent (i.e. chlorosilane)
The process[92] is based essentially on the reaction between the Si-Cl groups and –OH groups:

$$Cl\text{-}SiR_3 + H\text{-}O\text{-}R' \longrightarrow R'\text{-}O\text{-}SiR_3 + HCl$$

If R’ is a silicon oxide surface and R is an alkyl chain or a fluoroalkyl chain, the silica is covered by an apolar organic molecules which confers low-surface tension to the surface. However, chlorosilanes can also quickly react with water (R’ = H). Therefore, the reaction must be carried out in inert environment. This implies anhydrous solvents if the reaction is carried out in solution or nitrogen/argon flow if it is carried out in gas phase. This is especially important when the reaction involves a tri-chlorosilane where water can induce

polymerization. Furthermore, it is important to consider that silica surface normally contains a thin water layer which can be 10-15 Å thick; hence there is always a competition between the hydroxyl groups of water and the ones belonging to silica. All the samples prepared for this study were hydrophobized by CVD of trichloro(1*H*,1*H*,2*H*,2*H*-perfluorooctyl)silane, a semi-fluorinated silane:

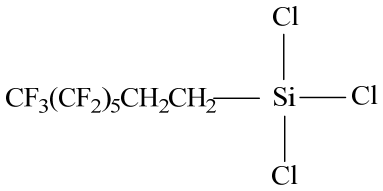

Hydrophobization of the films. All the films were hydrophobized with (tridecafluoro-1, 1, 2, 2-tetrahydrooctyl)-1-trichlorosilane (FS) according to the following procedure: Films and 1 ml of FS are put together in an exsiccator under vacuum for 4 hours. During this time vacuum was not pumped continuously but only for 5 minutes every half an hour. Then the FS is removed from the exsiccator and vacuum is pumped continuously for 1 hour in order to remove residual of unreacted FS.

9 Conclusion and outlook

A new approach for building superhydrophobic surfaces from hybrid raspberry-like particles was developed. The effect of the conditions during synthesis of the particles and the film assembly on the surface roughness and on contact angle towards water was studied in detail. The nanometer-sized roughness, conferred to the polystyrene particles by small silica spheres can be tuned by the reaction conditions. The amount of acrylic acid determines the number of silica particles attached to polystyrene particles. A certain amount of acrylic acid is required to provide sufficient anchoring strength.

Covering these composite particles with a smooth silica shell not only enhances their mechanical stability, but also increases the number of binding sites for the fluorosilane used to hydrophobize the silica surface.

The silica surface of the raspberry particles is hard, chemically inert and can be easily modified. Since the particles disperse in water, mono- or multi-layers can be prepared on substrates by simple drop casting or water evaporation, even on surfaces with grooves and slots. This has the advantage that the suspension can easily take any form, i.e. it is not hindered by edges and can creep into small corners. Evaporation time can be decreased and surface roughness increased by drying well above room temperature. The mechanical stability of assembled raspberry particle films can be improved by polystyrene bridges. These offer the possibility of building thick particle layers. If the amount of leaked-out PS is large, this affects the dual scale roughness and reduces the number of hydroxyl sites on the silica shells available for silane binding. This reduces contact angles. Superhydrophobicity can be recovered by plasma cleaning and successive silanization.

Even after removing particles the surface morphology hardly changes due to its self-similarity. So far thick layers of superhydrophobic surfaces have not been reported yet. The preparation of multi-layers allows going one step further toward the design of “scratch resistant” superhydrophobic surfaces, i.e. surfaces that preserves the superhydrophobic behaviour after scratching of the outer layer.

Understanding the underlying processes leading to the desired structures takes us closer to making thick and mechanically resistant superhydrophobic surfaces.

These promising results open the way to new challenges. First of all, the mechanical stability of the films has to be further improved. Preliminary experiments show that combining the polystyrene leakage with CVD of silica by Stöber method on pre-formed films can further anchor the particles.

Besides of that, so far the improved mechanical resistance was proven only qualitatively by comparing the degree of wear for samples with and without polystyrene leakage (e.g.

continuously depositing water drops or qualitative scratch-tests). A more quantitative method to mechanically characterize the surfaces needs to be developed.

References:

1. Young, T., An Essay on the Cohesion of Fluids. *Philosophical Transactions of the Royal Society of London* **1805,** *95*, 65-87.

2. Butt, H. J.; Graf, K.; Kappl, M., *Physics and chemistry of interfaces*. Wiley-VCH: 2003.

3. Quere, D., Wetting and roughness. *Annual Review of Materials Research* **2008,** *38*, 71-99.

4. Wenzel, R. N., Resistance of solid surfaces to wetting by water. *Industrial and Engineering Chemistry* **1936,** *28*, 988-994.

5. Cassie, A. B. D.; Baxter, S., Wettability of porous surfaces. *Transactions of the Faraday Society* **1944,** *40*, 0546-0550.

6. Shibuichi, S.; Onda, T.; Satoh, N.; Tsujii, K., Super water-repellent surfaces resulting from fractal structure. *Journal of Physical Chemistry* **1996,** *100* (50), 19512-19517.

7. Onda, T.; Shibuichi, S.; Satoh, N.; Tsujii, K., Super-water-repellent fractal surfaces. *Langmuir* **1996,** *12* (9), 2125-2127.

8. Neinhuis, C.; Barthlott, W., Characterization and distribution of water-repellent, self-cleaning plant surfaces. *Annals of Botany* **1997,** *79* (6), 667-677.

9. Barthlott, W.; Neinhuis, C., Purity of the sacred lotus, or escape from contamination in biological surfaces. *Planta* **1997,** *202* (1), 1-8.

10. Oner, D.; McCarthy, T. J., Ultrahydrophobic Surfaces. Effects of Topography Length Scales on Wettability. *Langmuir* **2000,** *16* (20), 7777-7782.

11. Shiu, J. Y.; Kuo, C. W.; Chen, P. L.; Mou, C. Y., Fabrication of tunable superhydrophobic surfaces by nanosphere lithography. *Chemistry of Materials* **2004,** *16* (4), 561-564.

12. Martines, E.; Seunarine, K.; Morgan, H.; Gadegaard, N.; Wilkinson, C. D. W.; Riehle, M. O., Superhydrophobicity and superhydrophilicity of regular nanopatterns. *Nano Letters* **2005,** *5* (10), 2097-2103.

13. Lafuma, A.; Quere, D., Superhydrophobic states. *Nature Materials* **2003,** *2* (7), 457-460.

14. Callies, M.; Quere, D., On water repellency. *Soft Matter* **2005,** *1* (1), 55-61.

15. Barbieri, L.; Wagner, E.; Hoffmann, P., Water wetting transition parameters of perfluorinated substrates with periodically distributed flat-top microscale obstacles. *Langmuir* **2007,** *23* (4), 1723-1734.

16. Gao, L. C.; McCarthy, T. J., How Wenzel and Cassie were wrong. *Langmuir* **2007,** *23* (7), 3762-3765.

17. Gao, L. C.; McCarthy, T. J., Wetting 101 degrees. *Langmuir* **2009,** *25* (24), 14105-14115.

18. Zhang, X.; Shi, F.; Niu, J.; Jiang, Y. G.; Wang, Z. Q., Superhydrophobic surfaces: from structural control to functional application. *Journal of Materials Chemistry* **2008,** *18* (6), 621-633.

19. Roach, P.; Shirtcliffe, N. J.; Newton, M. I., Progess in superhydrophobic surface development. *Soft Matter* **2008,** *4* (2), 224-240.

20. Zhang, X.; Shi, F.; Yu, X.; Liu, H.; Fu, Y.; Wang, Z. Q.; Jiang, L.; Li, X. Y., Polyelectrolyte multilayer as matrix for electrochemical deposition of gold clusters: toward super-hydrophobic surface. *Journal of the American Chemical Society* **2004,** *126* (10), 3064-3065.

21. Shi, F.; Wang, Z. Q.; Zhang, X., Combining a layer-by-layer assembling technique with electrochemical deposition of gold aggregates to mimic the legs of water striders. *Advanced Materials* **2005,** *17* (8), 1005-+.

22. Huang, L.; Lau, S. P.; Yang, H. Y.; Leong, E. S. P.; Yu, S. F.; Prawer, S., Stable superhydrophobic surface via carbon nanotubes coated with a ZnO thin film. *Journal of Physical Chemistry B* **2005,** *109* (16), 7746-7748.

23. Hosono, E.; Fujihara, S.; Honma, I.; Zhou, H. S., Superhydrophobic perpendicular nanopin film by the bottom-up process. *Journal of the American Chemical Society* **2005,** *127* (39), 13458-13459.

24. Morra, M.; Occhiello, E.; Garbassi, F., Contact-angle hysteresis in oxygen plasma treated poly(tetrafluoroethylene) *Langmuir* **1989,** *5* (3), 872-876.

25. Youngblood, J. P.; McCarthy, T. J., Ultrahydrophobic polymer surfaces prepared by simultaneous ablation of polypropylene and sputtering of poly(tetrafluoroethylene) using radio frequency plasma. *Macromolecules* **1999,** *32* (20), 6800-6806.

26. Tadanaga, K.; Katata, N.; Minami, T., Formation process of super-water-repellent Al2O3 coating films with high transparency by the sol-gel method. *Journal of the American Ceramic Society* **1997,** *80* (12), 3213-3216.

27. Shang, H. M.; Wang, Y.; Limmer, S. J.; Chou, T. P.; Takahashi, K.; Cao, G. Z., Optically transparent superhydrophobic silica-based films. *Thin Solid Films* **2005,** *472* (1-2), 37-43.

28. Zhai, L.; Cebeci, F. C.; Cohen, R. E.; Rubner, M. F., Stable superhydrophobic coatings from polyelectrolyte multilayers. *Nano Letters* **2004,** *4* (7), 1349-1353.

29. Bravo, J.; Zhai, L.; Wu, Z. Z.; Cohen, R. E.; Rubner, M. F., Transparent superhydrophobic films based on silica nanoparticles. *Langmuir* **2007,** *23* (13), 7293-7298.

30. Sun, M. H.; Luo, C. X.; Xu, L. P.; Ji, H.; Qi, O. Y.; Yu, D. P.; Chen, Y., Artificial lotus leaf by nanocasting. *Langmuir* **2005,** *21* (19), 8978-8981.

31. Decher, G., Fuzzy nanoassemblies: Toward layered polymeric multicomposites. *Science* **1997,** *277* (5330), 1232-1237.

32. Donath, E.; Sukhorukov, G. B.; Caruso, F.; Davis, S. A.; Moehwald, H., Novel hollow polymer shells by colloid-templated assembly of polyelectolytes. *Angewandte Chemie Int. Ed.* **1998,** *37* (16), 2202-2205.

33. Caruso, F.; Caruso, R. A.; Mohwald, H., Nanoengineering of inorganic and hybrid hollow spheres by colloidal templating. *Science* **1998,** *282* (5391), 1111-1114.

34. Dubreuil, F.; Elsner, N.; Fery, A., Elastic properties of polyelectrolyte capsules studied by atomic-force microscopy and RICM. *European Physical Journal E* **2003,** *12*, 215-221.

35. Ming, W.; Wu, D.; van Benthem, R.; de With, G., Superhydrophobic films from raspberry-like particles. *Nano Letters* **2005,** *5* (11), 2298-2301.

36. Tsai, H. J.; Lee, Y. L., Facile method to fabricate raspberry-like particulate films for superhydrophobic surfaces. *Langmuir* **2007,** *23* (25), 12687-12692.

37. Qian, Z.; Zhang, Z. C.; Song, L. Y.; Liu, H. R., A novel approach to raspberry-like particles for superhydrophobic materials. *Journal of Materials Chemistry* **2009,** *19* (9), 1297-1304.

38. D'Acunzi, M.; Mammen, L.; Singh, M.; Deng, X.; Roth, M.; Auernhammer, G. K.; Butt, H. J.; Vollmer, D., Superhydrophobic surfaces by hybrid raspberry-like particles *Faraday Discussion 146* **2010,** (Accepted).

39. Fery, A.; Weinkamer, R., Mechanical properties of micro- and nanocapsules: Single-capsule measurements. *Polymer* **2007,** *48* (25), 7221-7235.

40. Zoldesi, C. I.; Ivanovska, I. L.; Quilliet, C.; Wuite, G. J. L.; Imhof, A., Elastic properties of hollow colloidal particles. *Physical Review E (Statistical, Nonlinear, and Soft Matter Physics)* **2008,** *78* (5), 051401-8.

41. Zhang, L.; D'Acunzi, M.; Kappl, M.; Auernhammer, G. K.; Vollmer, D.; van Kats, C. M.; van Blaaderen, A., Hollow Silica Spheres: Synthesis and Mechanical Properties. *Langmuir* **2009,** *25* (5), 2711-2717.

42. Zhang, L.; D'Acunzi, M.; Kappl, M.; Imhof, A.; A., v. B.; Butt, H. J.; Graf, R.; Vollmer, D., Tuning the Mechanical Properties of Silica Microcapsules *Submitted* **2010**.

43. Adachi, T.; Sakka, S., Dependence of the elastic-moduli of porous silica-gel prepared by the sol-gel method on heat-treatment. *Journal of Materials Science* **1990,** *25* (11), 4732-4737.

44. Arshady, R., Suspension, emulsion, and dispersion polymerization: A methodological survey. *Colloid and Polymer Science* **1992,** *270* (8), 717-732.

45. Qun, W.; Shoukuan, F.; Tongyin, Y., Emulsion polymerization. *Prog. Polym. Sci.* **1994,** *19* (4), 703-753.

46. Antonietti, M.; Landfester, K., Polyreactions in miniemulsions. *Prog. Polym. Sci.* **2002,** *27* (4), 689-757.

47. Goodwin, J. W.; Hearn, J.; Ho, C. C.; Ottewill, R. H., Studies on the preparation and characterisation of monodisperse polystyrene laticee. *Colloid & Polymer Science* **1974,** *252* (6), 464-471.

48. Furusawa, K.; Norde, W.; Lyklema, J., method for preparing surfactant-free polystyrene latices of high surface charges. *Kolloid-Zeitschrift and Zeitschrift Fur Polymere* **1972,** *250* (9), 908-909.

49. Reynhout, X. E. E.; Hoekstra, L.; Meuldijk, J.; Drinkenburg, A. A. H., Contribution of steric and electrostatic repulsion forces to the stability of styrene latices copolymerized with acrylic acid. *Journal of Polymer Science: Part A: polymer Chemistry* **2003,** *41*, 2985-2995.

50. Reynhout, X. E. E.; Beckers, M.; Meuldijk, A.; Drinkenburg, B. A. H., Electrosteric stability of styrene/acrylic acid copolymer latices under emulsion polymerization reaction conditions. *Journal of Polymer Science Part a-Polymer Chemistry* **2005,** *43* (4), 726-732.

51. Shouldice, G. T. D.; Vandezande, G. A.; Rudin, A., Practical aspects of the emulsifier-free emulsion polymerization of styrene. *European Polymer Journal* **1994,** *30* (2), 179-183.

52. Chung-li Y. , G. J. W., Ottewill R. H., Studies onthe preparation and characterization of monodisperse polystyrene latices. *Progress in Polymer Science* **1976,** *60*, 163-175.

53. Ottewill, R. H.; Shaw, J. N., Studies on preparation and characterization of monodisperse polystyrene latices. I. Preparation. *Kolloid-Zeitschrift and Zeitschrift Fur Polymere* **1967,** *215* (2), 161-&.

54. Holzapfel, V.; Musyanovych, A.; Landfester, K.; Lorenz, M. R.; Mailander, V., Preparation of fluorescent carboxyl and amino functionalized polystyrene particles by miniemulsion polymerization as markers for cells. *Macromolecular Chemistry and Physics* **2005,** *206* (24), 2440-2449.

55. Musyanovych, A.; Rossmanith, R.; Tontsch, C.; Landfester, K., Effect of hydrophilic comonomer and surfactant type on the colloidal stability and size distribution of carboxyl- and amino-functionalized polystyrene particles prepared by miniemulsion polymerization. *Langmuir* **2007,** *23* (10), 5367-5376.

56. Kawaguchi, S.; Ito, K., Dispersion polymerization. *Advancwd polymer science* **2005,** *175*, 299–328.

57. Ober, C. K.; Hair, M. L., The effect of temperature and initiator levels on the dispersion polymerization of polystyrene. *Journal of Polymer Science Part A: Polymer Chemistry* **1987,** *25* (5), 1395-1407.

58. Horák, D.; Scaronvec, F.; Fréchet, J. M. J., Preparation and control of surface properties of monodisperse micrometer size beads by dispersion copolymerization of styrene and butyl methacrylate in polar media. *Journal of Polymer Science Part A: Polymer Chemistry* **1995,** *33* (14), 2329-2338.

59. Uyama, H.; Kobayashi, S., Dispersion polymerization of styrene in aqueous alcohol solution - effects of reaction parameters on the polymer particle formation. *Polymer International* **1994,** *34* (3), 339-344.

60. Stoeber, W.; Fink, A.; Bohn, E., Controlled growth of monodisperse silica spheres in the micron size range. *Journal of Colloid and Interface Science* **1968,** *26*, 62-69.

61. van Blaadeen, A.; Vrij, A., Synthesis and characterization of monodisperse colloidal organo-silica spheres. *Journal of Colloid and Interface Science* **1993,** *156*, 1-18.

62. Verhaegh, N. A. M.; van Blaaderen, A., Dispersions of rhodamine-labeled silica spheres- synthesis, characterization, and fluorescence confocal microscopy. *Langmuir* **1994,** *10* (5), 1427-1438.

63. van Blaaderen, A.; Vrij, A., Synthesis and characterization of colloidal dispersion of fluorescent, monodisperse silica spheres. *Langmuir* **1992,** *8* (12), 2921-2931.

64. van Blaaderen, A.; Wiltzius, P., Real space structure of colloidal hadr-sphere glasses. *Science* **1995,** *270* (5239), 1177-1179.

65. Verhaegh, N. A. M.; Vanduijneveldt, J. S.; van Blaaderen, A.; Lekkerkerker, H. N. W., Direct observation of stacking disorder in a colloidal crystal. *Journal of Chemical Physics* **1995,** *102* (3), 1416-1421.

66. Graf, C.; Vossen, D. L. J.; Imhof, A.; A., v. B., A general method to coat colloidal particles with silica. *Langmuir* **2003,** *19*, 6693-6700.

67. Schmid, A.; Fujii, S.; Armes, S. P., Polystyrene-silica nanocomposite particles via alcoholic dispersion polymerization using a cationic azo initiator. *Langmuir* **2006,** *22* (11), 4923-4927.

68. Lee, J.; Hong, C. K.; Choe, S.; Shim, S. E., Synthesis of polystyrene/silica composite particles by soap-free emulsion polymerization using positively charged colloidal silica. *Journal of Colloid and Interface Science* **2007,** *310* (1), 112-120.

69. Park, I.; Ko, S. H.; An, Y. S.; Choi, K. H.; Chun, H.; Lee, S.; Kim, G., Monodisperse Polystyrene-Silica Core-Shell Particles and Silica Hollow Spheres Prepared by the Stober Method. *Journal of Nanoscience and Nanotechnology* **2009,** *9* (12), 7224-7228.

70. Tuncel, A.; Kahraman, R.; Piskin, E., Monosize polystyrene latices carrying functional groups on their surfaces. *Journal of Applied Polymer Science* **1994,** *51*, 1485-1498

71. Still, T.; D'Acunzi, M.; Vollmer, D.; Fytas, G., Mesospheres in nano-armor: Probing the shape-persistence of molten polymer colloids. *Journal of Colloid and Interface Science* **2009,** *340* (1), 42-45.

72. van Blaaderen, A.; Kentgens, A. P. M., Particle morphology and chemical microstructure of colloidal silica spheres made from alkoxysilanes. *Journal of Non-Crystalline Solids* **1992,** *149* (3), 161-178.

73. Vanhelden, A. K.; Jansen, J. W.; Vrij, A., Preparation and characterization of spherical monodisperse silica dispersions in non-aqueous solvents. *Journal of Colloid and Interface Science* **1981,** *81* (2), 354-368.

74. Badley, R. D.; Ford, W. T.; McEnroe, F. J.; Assink, R. A., Surface modification of colloidal silica. *Langmuir* **1990,** *6* (4), 792-801.

75. Dehaan, J. W.; Vandenbogaert, H. M.; Ponjee, J. J.; Vandeven, L. J. M., Characterization of modified silica powders by Fourier-Transform Infrared-Spectroscopy and Cross-Polarization Magic Angle Spinning NMR. *Journal of Colloid and Interface Science* **1986,** *110* (2), 591-600.

76. Matsuda, A.; Matsuno, Y.; Tatsumisago, M.; Minami, T., Changes in porosity and amounts of adsorbed water in sol-gel derived porous silica films with heat treatment. *Journal of Sol-Gel Science and Technology* **2001,** *20* (2), 129-134.

77. Miguez, H.; Meseguer, F.; Lopez, C.; Blanco, A.; Moya, J. S.; Requena, J.; Mifsud, A.; Fornes, V., Control of the photonic crystal properties of fcc-packed submicrometer SiO2 spheres by sintering. *Advanced Materials* **1998,** *10* (6), 480-+.

78. Kellaway, I. W.; Najib, N. M., The adsorption of hydrophilic polymers at the polystyrene-water interface. *International Journal of Phermaceutics* **1980,** *6*, 285-294.

79. Smith, J. N.; Meadows, J.; Williams, P. A., Adsorption of polyvinylpyrrolidone onto polystyrene latices and the effect on colloidal stability. *Langmuir* **1996,** *12*, 3773-3778.

80. KSV instruments handbook on Langmuir-Blodgett films

81. Bresme, F.; Oettel, M., Nanoparticles at fluid interfaces. *Journal of Physics-Condensed Matter* **2007,** *19* (41), 33.

82. Conchello, J. A.; Lichtman, J. W., Optical sectioning microscopy. *Nature Methods* **2005,** *2* (12), 920-931.

83. van Blaaderen, A., Imaging individual particles in concentrated colloidal dispersions by confocal scanning light microscopy. *Advanced Materials* **1993,** *5* (1), 52-54.

84. Prasad, V.; Semwogerere, D.; Weeks, E. R., Confocal microscopy of colloids. *Journal of Physics-Condensed Matter* **2007,** *19* (11), 25.

85. Song, J. S.; Tronc, F.; Winnik, M. A., Monodisperse, controlled micron-size dye-labeled polystyrene particles by two-stage dispersion polymerization. *Polymer* **2006,** *47* (3), 817-825.

86. Schaertl, W.; Sillescu, H., Dynamics of colloidal hard-spheres in thin aqueous suspension layers - particle tracking by digital image-processing and brownian Dynamics computer-simulations. *Journal of Colloid and Interface Science* **1993,** *155* (2), 313-318.

87. Song, J. S.; Winnik, M. A., Cross-linked, monodisperse, micron-sized polystyrene particles by two-stage dispersion polymerization. *Macromolecules* **2005,** *38* (20), 8300-8307.

88. Greenspan, P.; Fowler, S. D., Spectrofluorometric studies of the lipid probe, Nile Red. *Journal of Lipid Research* **1985,** *26* (7), 781-789.

89. Greenspan, P.; Mayer, E. P.; Fowler, S. D., Nile Red - a selective fluorescent stain for intracellular lipid droplets *Journal of Cell Biology* **1985,** *100* (3), 965-973.

90. Butt, H. J.; Jaschke, M., Calculation of thermal noise in Atomic-Force Microscopy. *Nanotechnology* **1995,** *6* (1), 1-7.

91. Cappella, B.; Butt, H. J.; Kappl, M., Force measurements with the atomic force microscope: Technique, interpretation and applications. *Surface Science Reports* **2005,** *59* (1-6), 1-152.

92. Rye, R. R.; Nelson, G. C.; Dugger, M. T., Mechanistic aspects of alkylchlorosilane coupling reactions. *Langmuir* **1997,** *13* (11), 2965-2972.

Acknowledgements

First, I would like to express my gratitude to my supervisor Dr. Doris Vollmer for her guidance during the three years of this thesis project. She was always open to discussion and encouraged me, especially when things were not going smoothly!!

I thank Prof. Hans-Jürgen Butt for the possibility to work in his group and the scientific support during my stay in MPIP.

I am grateful to Dr. Günter Auernhammer; he was always available to help and the discussions with him were really useful.

I want to thank Prof. Alfons van Blaaderen and Dr. Carlos van Kats for the fruitful collaboration for the synthesis of the hollow silica particles.

I was very happy to collaborate with Dr. Li-Juan Zhang, Dr. Robert Graf, Prof. Georg Fytas and Dr. Tim Still for the characterization of the hollow particles.

Dr. Kathy McNamee taught me how to prepare particle monolayer by Langmuir-Blodgett technique and helped me with the preparation of chapter 5.

A big thank to Gabi Schäfer…. She took most of the SEM images shown in this thesis and her support with the synthesis was incomparable!

Many people helped me during these three years. I hope I will not forget anyone.

Andreas Best gave me instructions for using CSLM and the confocal profilometer and was available to help me with the interpretation of the results. The discussions with Dr. Kaloian Koynov on CLSM imaging were very useful. Maren Müller and Kathrin Kirchhoff were always available to image my samples by SEM and TEM. Christine Rosenauer did the light scattering measurements and Dr. Werner Steffen discussed the results. Dr. Umaporn Paiphansiri introduced me to particle charges measurements and helped with their interpretation.

Thanks to Deng Xu, Maninder Singh, and Lena Mammen….. I learned a lot while trying to supervise you!

All the other people in my sub-group: Dr. Beate Ulrich, Jinyu Zhao, Marcel Roth, Stefan Geiter, Ebie Sam, Danyang Xu, Dr. Mordechai Sokuler, Harsha Paroor, Ying Liu, Daniela Fell, Miao Wang, Tomas Corrales, Dr. Mika Kobayashi. We met regularly once per week to present the state of the art of our work. They patiently listened to my presentations and always gave me good suggestions…. and of course thanks for your company!

My office-mates Maria Lechmann, Marcel Roth, Daniela Fell and Gabi Schäfer made my time in the office always enjoyable. I will miss you a lot! And I will never forget all the help you gave me….. especially when I had difficulties with the German language. Besides of that, my computer is very grateful to Marcel Roth for keeping ‘him’ alive despite me.

Thanks a lot to all the friends I encountered here in Mainz: Mine Memesa, Tiago Rodriguez, Lizandra Castro, Ramon Pericet-Camara, Nikolas Gomopoulos, Despoina Tsapakidou, Karmena Jaskiewicz, Manos Anyfantakis, Ahmad Juhari Azhar, Stoian Yordanov, Sulivan Dias Borges Vianna.

Thanks to the whole AK-Butt for the nice time spent together here in Mainz and during our group seminars!

Grazie a Valentina ed Alessandra per la vostra amicizia e sostegno.... ed anche per aver reso il mio corridoio piu' allegro e meno silenzioso!

I miei genitori e mio fratello, anche se da lontano, mi hanno sempre fatto sentire il loro amore e il loro supporto.... Non finiro' mai di esservi riconoscente!

Un grazie infinito a mio marito Carlo ..... senza il suo continuo sostegno non avrei portato a compimento questo lavoro.

Curriculum Vitae

Personal Data:

Name:	Maria D'Acunzi
Date of birth:	24.03.1976
Place of birth:	Nocera Inferiore (Salerno, Italy)
Nationality:	Italian

Educational background:

May 2007- present:	PhD student at Max Planck Institute for Polymer Research (Mainz, Germany) and Johannes Gutenberg Universität, Mainz, Germany supervised by Dr. Doris Vollmer
November 2006-April 2007:	Scholarship at Max Planck Institute for Polymer Research on *"Solvent mediated forces between polymer particles"*" supervised by Prof. Hans-Jürgen Butt
December 2004- December 2005:	Scholarship at the University of Padova on "*Inorganic-organic hybrid systems as dielectric and electro-active layers for application in microelectronic"* supervised by Prof. Vito Di Noto
March 2004:	Master Degree in Chemistry (110/110) with experimental thesis on polymerization of olefins by Ziegler-Natta catalysts
July 1994:	High School Diploma in Scientific Studies at Liceo scientifico Statale "N. Sensale" (Nocera Inferiore, Italy)

Attended schools, workshops and conferences:

November 2007:	IMPRS school on "Thin films", Oberwesel, Germany
April 2008:	School on "Polymer synthesis", Kirchberg, Germany
September 2008:	16th Wolfgang Ostwald Colloquium, Leipzig, Germany (poster presentation)

March 2009:	5th Zsigmondy Colloquium, Bayreuth, Germany (oral presentation)
September 2009:	44th Meeting of the German Colloidal Society, Hamburg, Germany (poster presentation)

List of publications:

1. Capacchione, C.; **D'Acunzi, M.**; Motta, O.; Oliva, A.; Okuda, J.; Isolated ethylene units in isotactic polystyrene chain: stereocontrol of an isospecific postmetallocene titanium catalyst. *Macromol. Chem. Phys.* **2004**, *205* (3), 370-373.
2. Kaune, G.; Memesa, M.; Meier, R.; Ruderer, M. A.; Diethert, A.; Roth, S. V.; **D'Acunzi, M.**; Gutmann, J. S.; Muller-Buschbaum, P.; Hierarchically structured titania films prepared by polymer/colloidal templating. *ACS Appl. Mater. Intertaces* **2009**, *1* (12), 2862-2869.
3. Still, T.; **D'Acunzi, M.**; Vollmer, D.; Fytas, G.; Mesospheres in nano-armor: probing the shape-persistence of molten polymer colloids. *J. Colloid Interface Sci.* **2009**, *340* (1), 42-45.
4. Zhang, L.; **D'Acunzi, M.**; Kappl, M.; Auernhammer, G. K.; Vollmer, D.; van Kats, C. M.; van Blaaderen, A.; Hollow silica spheres: synthesis and mechanical properties. *Langmuir* **2009**, *25* (5), 2711-2717.
5. Roth, M.; **D'Acunzi, M.**; Vollmer, D.; Auernhammer, G. K.; Viscoelastic rheology of colloid-liquid crystal composites. *J. Chem. Phys.* **2010**, *132*, 124702.
6. **D'Acunzi, M.**; Mammen, L.; Singh, M.; Deng, X.; Roth, M.; Auernhammer, G. K.; Butt, H. J.; Vollmer, D.; Superhydrophobic surfaces by hybrid raspberry-like particles. *Faraday discussion 146* accepted **2010**.
7. Zhang, L.; **D'Acunzi, M.**; Kappl, M.; Imhof, A.; van Blaaderen, A.; Butt, H. J.; Graf, R.; Vollmer, D.; Tuning the mechanical properties of silica microcapsules. ACS Nano submitted **2010**.